Growth and relaxation studies of strained epitaxial layers in the InGaAs/GaAs system

J. te Nijenhuis

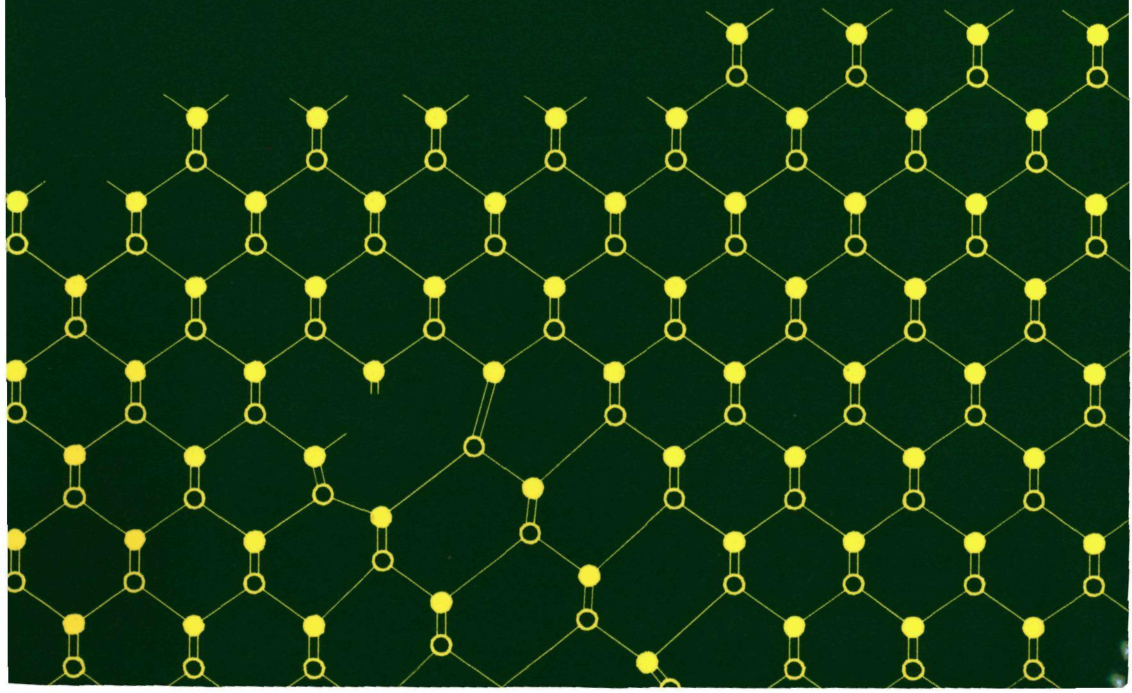

Growth and relaxation studies
of strained epitaxial layers
in the InGaAs/GaAs system

CIP-GEGEVENS KONINKLIJKE BIBLIOTHEEK, DEN HAAG

Nijenhuis, Johannes te

Growth and relaxation studies of strained epitaxial layers
in the InGaAs/GaAs system / Johannes te Nijenhuis. -
[S.l.: s n]. - Ill.
Proefschrift Nijmegen. - Met lit opg - Met samenvatting
in het Nederlands.
ISBN 90-9005700-5
Trefwoorden halfgeleiderepitaxie / spanningsrelaxatie

Growth and relaxation studies of strained epitaxial layers in the InGaAs/GaAs system

een wetenschappelijke proeve op het gebied van
de Natuurwetenschappen

Proefschrift

ter verkrijging van de graad van doctor
aan de Katholieke Universiteit Nijmegen,
volgens besluit van het College van Decanen
in het openbaar te verdedigen op
dinsdag 9 februari 1993
des namiddags te 1.30 uur precies

door

Johannes te Nijenhuis

geboren op 5 april 1964
te 's-Gravenhage

Promotor: Prof. Dr. L.J. Giling

... zolang hij het boek schrijft,
is het het duidelijkst van hem...

Louis Couperus

Aan mijn ouders
Aan Lenneke

The work described in this thesis is part of the research programme of the Stichting voor Fundamenteel Onderzoek der Materie (FOM) and was made possible by financial support from the Nederlandse Organisatie voor Wetenschappelijk Onderzoek (NWO).

Voorwoord

Dit proefschrift vormt de afronding van het wetenschappelijk onderzoek dat ik in de afgelopen jaren heb verricht. Iedereen die op enigerlei wijze een bijdrage, in woord of in daad, geleverd heeft aan de totstandkoming van dit proefschrift wil ik op deze wijze bedanken.

Daarbij denk ik allereerst aan mijn promotor Prof. John Giling, die mij de gelegenheid geboden heeft om mijn promotieonderzoek te verrichten.

Diegenen die betrokken zijn geweest bij de bouw, het onderhoud en de automatisering van de lage-druk-flowreactor wil ik bedanken voor de prettige samenwerking: Piet van Rijsingen, Harry van der Linden, John Schermer, Wilfried van Sark en Wilfred Janssen. Dit werk is technisch ondersteund door de medewerkers van de verschillende facultaire diensten: de instrumentmakerij, de glasinstrumentmakerij en de afdeling elektronica. In dit verband dient met name Willy Corbeek vermeld te worden. Voorts is gedurende de bouwfase veelvuldig gebruik gemaakt van de ervaring van de buren van de pulsereactor Jaap van Suchtelen en Jos Hogenkamp.

Paul van der Wel wil ik bedanken voor de enthousiaste samenwerking op het gebied van de misfitdislocaties.

Xiao Tang, Paul Hageman, Yuan Li, Thijs Bongers, Stef Olsthoorn, Harry Lochs en Frank Driessen dank ik voor de hulp bij het groeien en het karakteriseren van de epitaxiale lagen.

Henk van Well, Ernst van Eck en Ronny van Asten ben ik erkentelijk voor de bijdragen aan de resultaten van dit onderzoek, die zij tijdens hun afstudeerstage op de afdeling hebben geleverd.

Verder wil ik alle medewerkers en studenten van de afdeling Vaste Stof Fysica III bedanken voor de plezierige tijd die ik op de afdeling heb doorgebracht. De "buitenschoolse" activiteiten, het vrijdagmiddagvoetbal en de Beuningen Open, zorgden voor een welkome afleiding van de dagelijkse bezigheden.

Mijn familie, in het bijzonder mijn ouders, dank ik voor de belangstelling die zij de afgelopen jaren voor dit onderzoek hebben getoond.

De steun en het vertrouwen van Lenneke gedurende de afgelopen jaren hebben een belangrijke bijdrage geleverd aan de voltooiing van dit proefschrift.

Hans te Nijenhuis

The work described in the chapters 2, 4 and 5 is based on the following publications:

X. Tang, J. te Nijenhuis, Y. Li and L.J. Giling, Journal of Crystal Growth **107** (1991) 263.

J. te Nijenhuis, P.J. van der Wel, R.W.F. van Asten, P.R. Hageman and L.J. Giling, Journal of Crystal Growth **107** (1991) 496.

P.J. van der Wel, J. te Nijenhuis, E.R.H. van Eck and L.J. Giling, Semiconductor Science and Technology **7** (1992) A63.

Contents

1 General introduction 1

1.1 Metalorganic Vapour Phase Epitaxy 3
1.2 Misfit dislocations 5
1.3 Contents of this thesis 6
References 8

2 The influence of substrate orientation and mis-orientation on the silicon-doping of GaAs grown by metalorganic vapour phase epitaxy 11

2.1 Introduction 12
2.2 Experimental 12
2.3 Results and discussion 13
    2.3.1 Some considerations on silicon-doping 13
    2.3.2 Group (110) 14
    2.3.3 Group (100) 17
    2.3.4 Group (111)A 20
    2.3.5 The influence of the V/III ratio 21
2.4 Summary and conclusions 22
References 23

3 Anisotropic indium incorporation during growth of $In_xGa_{1-x}As$ by metalorganic vapour phase epitaxy 25

3.1 Introduction 26
3.2 Periodic bond chains on $\{100\}$ and $\{111\}$ faces 27
    3.2.1 The (100) surface 27
    3.2.2 The (111)A surface 29
3.3 Experimental details 31
3.4 Results and discussion 32
    3.4.1 Growth on (100) faces 33
    3.4.2 Growth on (111)A faces 34
    3.4.3 Comparison with silicon incorporation experiments 34

3.5 Summary and conclusions 36
3.A Appendix 38
References 41

4 Critical layer thickness of GaAs grown by metalorganic vapour phase epitaxy on $In_xGa_{1-x}As$ 43
4.1 Introduction 44
4.2 Experimental details 45
4.3 Results and discussion 46
  4.3.1 Strain and relaxation 46
  4.3.2 Bandgap energy shifts 48
4.4 Summary and conclusions 51
References 53

5 High spatial resolution photoluminescence studies on misfit dislocations in lattice mismatched III-V heterostructures 55
5.1 Introduction 56
5.2 Experimental details 57
5.3 Results 57
  5.3.1 The system under tensile stress: GaAs on $In_xGa_{1-x}As$ 57
  5.3.2 The system under compressive stress: $In_xGa_{1-x}As$ on GaAs . . . 61
5.4 Discussion 65
  5.4.1 Structural asymmetry 65
  5.4.2 Opto-electronic asymmetry 67
5.5 Summary and conclusions 68
References 69

6 Strain relaxation mechanisms in lattice mismatched III-V heterostructures grown by metalorganic vapour phase epitaxy 71
6.1 Introduction 72
6.2 Experimental details 73
6.3 Results 74
  6.3.1 Morphology of layers under tensile stress 74
  6.3.2 Morphology of layers under compressive stress 75
6.4 Discussion 77
  6.4.1 Nucleation and propagation of misfit dislocations 77
  6.4.2 Relaxation by cross slip of misfit dislocations 79

6.4.3 The energy barrier for the cross-slip process 85
6.4.4 Hillock formation in layers under tensile stress 88
6.4.5 The non-parallel dislocation lines 90
6.5 Summary and conclusions 91
References 93

7 Dissociated V-shaped dislocation model for the relaxation of strained single heterostructures 95
7.1 Introduction 96
7.2 Theory of equilibrium models 97
7.2.1 Mechanical equilibrium model 100
7.2.2 Nucleation model for semicircular dislocation loops 101
7.2.3 Nucleation model for dissociated semicircular dislocations 101
7.2.4 Nucleation model for V-shaped dislocations 104
7.2.5 Nucleation model for dissociated V-shaped dislocations 105
7.3 Discussion 108
7.4 Summary and conclusions 111
7.A Appendix 112
References 114

8 Relaxation slip systems in (110) oriented epitaxial layers in the zincblende structure 117
8.1 Introduction 118
8.2 Slip systems in (110) epitaxial layers. 119
8.2.1 Nucleation of misfit dislocations in (110) epitaxial layers 121
8.2.2 Critical layer thickness model for (110) epitaxial layers 124
8.3 Experimental details 125
8.4 Results and discussion 126
8.4.1 Morphology 126
8.4.2 Critical layer thickness 128
8.4.3 Comparison with strained Ge_xSi_{1-x} and diamond (110) epitaxial layers 131
8.5 Summary and conclusions 132
References 133

General conclusions 135

Summary 137

Samenvatting 140

Chapter 1

General introduction

Already in the nineteenth century semiconductor materials have attracted the attention of physicists, because of their negative coefficient of electrical resistance [1], but the enormous developments in the field of semiconductor science and technology have been started by the realization of the first bipolar, germanium based, transistor [2, 3] in 1947. Nowadays semiconductor materials are used in a wide range of electronic and opto-electronic devices transistors, lasers, wave guides, solar cells, etc The material from which the first devices were made, was germanium, later silicon became the most important semiconducting material Still the majority of the micro-electronic industry is based on silicon technology

A drawback of silicon and germanium is their indirect band gap, which makes these materials unsuitable for use in opto-electronic devices III-V compound semiconductors, like GaAs and InP, have a direct band gap and are efficient photon absorbing and emitting materials With alloys of III-V compounds it is possible to obtain direct band gaps between 0.18 and 2 42 eV III-V semiconductors have found applications as the base material for high-electron mobility transistors, light-emitting diodes and lasers for optical communication and optical recording and reading systems (*e g* CD-players)

Many of the developments in the III-V based device technology have been made possible by the developments in the techniques for both bulk and thin film growth of single crystals of III-V compounds of high crystallographic perfection Important techniques for thin film growth of III-V compounds are liquid phase epitaxy (LPE), metalorganic vapour phase epitaxy (MOVPE) and molecular beam epitaxy (MBE) The good control of the process conditions of the latter two techniques makes it possible to grow heteroepitaxial multilayer systems of small dimensions and with sharp interfaces, like multiple quantum wells Growth of thin epitaxial layers of III-V compounds by metalorganic vapour phase epitaxy is briefly reviewed in section 1 1

The growth of strained layers (*i e* layers with a lattice constant which is different from the lattice constant of the substrate) makes it possible to obtain electronic materials with tailorable properties [4], which were not achievable with lattice-matched III-V materials [5] For example, it has been shown that the presence of strain in the active region in semiconductor lasers results in a higher performance and reliability, compared to lattice-matched structures [6]

A disadvantage of the growth of strained epitaxial layers is the possibility of the introduction of misfit dislocations at the interfaces between the layer and the substrate or between two subsequent layers Generally, these dislocations will degrade the device characteristics [7] and therefore they have to be avoided So it is important to obtain knowledge of the formation processes of these dislocations, in order to predict whether or not the dislocations will appear in strained layers. For this purpose several models for dislocation formation have been developed. An introduction to the relaxation by the formation of misfit dislocations is given in section 1.2.

In this thesis the growth by MOVPE and the relaxation of strained layers in the $In_xGa_{1-x}As$/GaAs system have been investigated. This system (with an effective bandgap between 0.45 and 1.45 eV) is of technological interest for optical fibre communication. The bandgap can be controlled by the indium concentration. The maximum lattice mismatch in this system (between GaAs and InAs) is 7.2%. Misfit dislocation formation and propagation have been studied in GaAs layers under tensile stress grown on $In_xGa_{1-x}As$ substrates and in $In_xGa_{1-x}As$ layers under compressive stress grown on GaAs substrates.

1.1 Metalorganic Vapour Phase Epitaxy

Metalorganic vapour phase epitaxy for the growth of single-crystal GaAs has been introduced in 1968 [8, 9]. For this process a hydride (arsine (AsH_3)) and a metalorganic compound (triethylgallium, TEG) are transported by a carrier gas (H_2) and introduced into a reactor cell. In this cell the gases are heated and homogeneous and heterogeneous reactions take place. As a result a thin film of GaAs is deposited on top of the substrate surface. Alternative names of the same growth process are amongst others: metalorganic chemical vapour deposition (MOCVD) and organometallic pyrolysis (OMP).

In the following years also hydrides of phosporus, antimony and nitrogen, and alkyl compounds of aluminum and indium were used to grow a large variety of binary, ternary and quaternary III-V compounds, like InP, GaSb, AlN, $Al_xGa_{1-x}As$, $In_xGa_{1-x}As$ and $In_xGa_{1-x}As_{1-y}P_y$ [10]. Nowadays the MOVPE process is also widely used to grow compounds like II-VI semiconductors [11, 12] and high-temperature superconductors ($YBa_2Cu_3O_{7-\delta}$) [13]. The great interest of the opto-electronic industry for the MOVPE-process arose in 1977 from the demonstration that with this process it is possibile to grow low-threshold double-heterojunction lasers [14]. At present, MOVPE-process is an important growth technique for the fabrication of semiconductor devices like solid state lasers, solar cells and high-speed transistors, in which complex structures, as multiple quantum wells, with thin layers and sharp interfaces are required.

The various types of MOVPE-reactor systems can be discriminated on the basis of *e.g.* the flow direction of the process gases and the operating pressure. A brief review of reactor types is given by Leys [15]. The MOVPE-reactor systems used for the studies

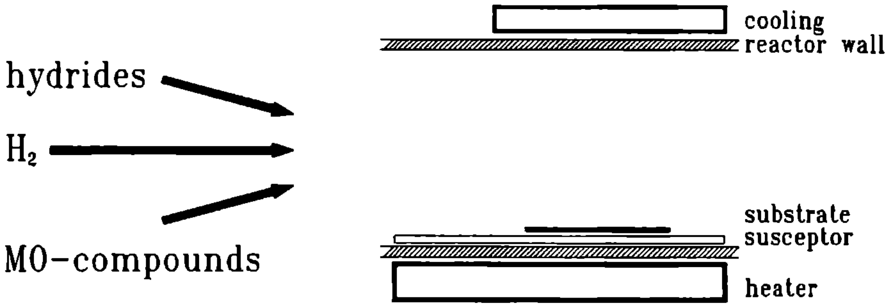

Figure 1.1 Schematic diagram of a horizontal-flow reactor.

described in this thesis were cold-walled horizontal laminar-flow reactors. This reactor type is schematically given in fig. 1.1. The reactor cells are rectangular quartz tubes. The substrates, on which the epitaxial layers are to be deposited, lie on a susceptor (molybdenum or graphite) which is (indirectly) heated at the bottom. The cooling at the top of the reactor cell is optional. In order to get a good control of the growth process (sharp interfaces, homogeneous composition of the layers) it is necessary that the flow in these reactors is laminar and without longitudinal and transversal return flows during the growth process. The flow and temperature profiles have to be completely developed at the position of the substrate [16]. Return flows, caused by free convection due to thermal instabilities in the reactor, can act as memory cells and thus have to be avoided. The process conditions can be characterized by dimensionless numbers, which determine the transition between laminar and turbulent flow (Reynolds, Re) and the occurence of longitudinal (Rayleigh, Ra) and transversal (the ratio of Grashoff and Reynolds, Gr/Re) return flows. For horizontal-flow reactors criteria for these numbers have been derived from flow visualization experiments and theoretical calculations [17]. An important conclusion of these studies is that the gas flow stability is increased by increasing the mass-flow rate of the carrier gas or reducing the reactor pressure. The latter situation is preferred, since the growth gases are more economically used at low operating pressures. Low-pressure MOVPE of III-V compounds is first reported by Duchemin [18] and is nowadays commonly used. The GaAs and $In_xGa_{1-x}As$ layers described in this thesis have been grown by MOVPE in long horizontal-flow reactors in which the flow and temperature profiles were completely developed.

1.2 Misfit dislocations

In an epitaxial heterostructure the orientation of the single-crystal substrate determines the orientation of the single-crystal layer. If the lattice constants of the substrate and the epitaxial layer parallel to the interface are not equal, a certain misfit is present. This misfit will be accomodated by the substrate and the epitaxial layer in order to obtain a low interface configuration. In theories in which the interfacial structure is considered, it is assumed that the substrate thickness and the lateral dimensions of the heterostructure are large, with respect to the thickness of the epitaxial layer. The interface is considered to be flat, with a sharp transition between the layer and the substrate. In this situation the misfit is only accomodated by the epitaxial layer and not by the substrate [19].

Mott and Nabarro [20] were the first to consider the accomodation of the misfit. They have described the elastic deformation of precipitates in order to form coherent lattice planes of the precipitate and the matrix. This deformation is completely elastic until a certain critical precipitate size is reached [21]. This critical size is determined by balancing the release of the elastic energy stored in the precipitate with the rise in interfacial energy, due to the loss of coherence of the lattice planes.

Frank and Van der Merwe [22] have used this concept of a critical size in order to calculate the critical layer thickness, which is the thickness at which epitaxial layers lose their coherence. Above this thickness "regions of bad register" between the substrate and the epitaxial layer are formed, containing the so-called misfit dislocations. In fig. 1.2 a schematic representation is given of a coherent and an incoherent interface between a substrate and an epitaxial layer.

The model of Frank and van der Merwe has been followed by others [23], which determine the optimum strain in the layer, by minimizing the sum of the elastic and the interfacial energy.

In these models the formation process of the misfit dislocations is not taken into account. Therefore another approach of this problem has been reported by Jesser and Matthews [24] and Matthews and Blakeslee [25]. They derive the critical layer thickness from force balance equations on threading dislocations (with their Burgers vectors inclined to the interface). Recently, it has been shown that the critical layer thickness relation may also be derived from energy equilibrium calculations [26]. It is stated that this model yields the minimal thickness at which the misfit dislocations can be formed [27], since no nucleation or kinetic barriers are taken into account. Models have been proposed which do take into account these barriers [28, 29]. The critical layer thickness is increased for short relaxation times. For long relaxation times these kinetic models are reduced to the

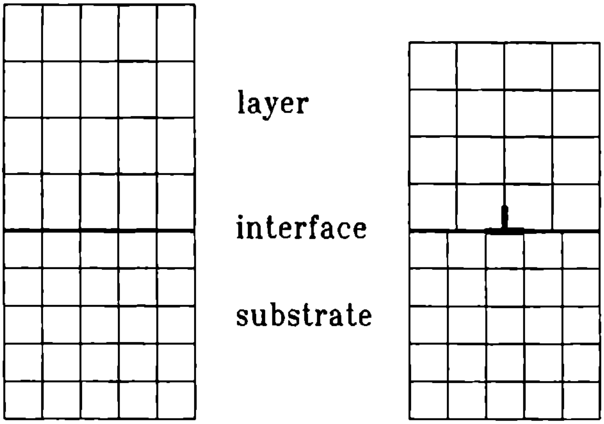

Figure 1.2 Schematic diagram of an epitaxial layer which has formed a coherent and an incoherent interface with the substrate. In the incoherent situation a misfit dislocation is present at the interface.

mechanical equilibrium model.

When the density of threading dislocations in the substrate is insufficient to release the strain in the epitaxial layer, as is the case with substrates of semiconductor materials, like silicon and GaAs, new dislocations have to be formed in the epitaxial layer. These dislocations nucleate at the surface and propagate through the epitaxial layer towards the interface in order to form long, straight misfit dislocations at the interface [30]. This concept of dislocation formation and propagation is refined in other papers [31]-[33] and is used in this thesis to obtain a realistic description of the mechanism for the relaxation of epitaxial layers in the $In_xGa_{1-x}As/GaAs$ system.

1.3 Contents of this thesis

In this thesis studies on growth from the vapour phase of epitaxial layers in the system $In_xGa_{1-x}As/GaAs$ and the relaxation of strained layers in this system are described.

In the chapters 2 and 3 the influence of the direction of the misorientation of the substrate on the incorporation of silicon and of indium during the growth of GaAs by MOVPE is discussed.

The studies on the relaxation of strained layers under tensile as well as under compressive stress are described in the chapters 4 to 8.

In chapter 4 the relaxation of GaAs epitaxial layers grown on $In_xGa_{1-x}As$ substrates with (100) orientation is studied. The residual strain in the layers is measured as a function of the layer thickness and is compared to the critical-strain-thickness relation.

Chapter 5 deals with the opto-electronic behaviour of the misfit dislocations. The asymmetric behaviour of the dislocations in (100) oriented samples along the two ⟨011⟩ directions as found on photoluminescence intensity mappings and on photo-etch patterns is compared to the core types of the dislocations under tensile and compressive stress.

The relaxation mechanism of (100) epitaxial layers is studied more in detail in chapter 6. A model, which assumes that the misfit dislocations nucleate at the surface of the layer and propagate as dissociated V-shaped dislocations toward the interface is proposed. Using this model the asymmetric strain relieve and the formation of hillocks in layers under tensile stress at relatively low growth temperatures is explained.

In chapter 7 a model for the critical layer thickness of (100) oriented epitaxial layers under tensile and under compressive stress is derived. This model is based on the mechanism for relaxation by the formation of dissociated V-shaped dislocations, as is described in chapter 6. A comparison of this model with other critical layer thickness models, described in the literature, and with experimental observations of the formation of misfit dislocations in the $In_xGa_{1-x}As/GaAs$ system is given.

Finally, the relaxation of (110) oriented strained layers is studied in chapter 8. A survey of the possible slip systems which can relieve the misfit strain in these layers is given. The critical layer thickness model as described in chapter 7 is applied to these systems and compared to the experimentally observed dislocation patterns.

References

[1] M Faraday, Experimental Researches on Electricity, 1839 Facsimile reprint by Taylor and Francis, London

[2] J Bardeen and W H Brattain, Phys Rev **74** (1948) 230

[3] W Shockley, Bell Syst Techn J **28** (1949) 435

[4] G C Osbourn, Phys Rev B **27** (1983) 5126

[5] E P O'Reilly, Semicond Sci Technol **4** (1989) 121

[6] K J Beernink, P K York, J J Coleman, Appl Phys Lett **55** (1989) 2585

[7] J M Woodall, G D Pettit, T N Jackson, C Lanza, K L Kavanagh and J W Mayer, Phys Rev Lett **51** (1983) 1783

[8] H M Manasevit, Appl Phys Lett **12** (1968) 156

[9] H M Manasevit and W I Simpson, J Electrochem Soc **116** (1969) 1725

[10] M J Ludowise, J Appl Phys **58** (1985) R31, and references therein

[11] J B Mullin, S J C Irvine and J Tunnicliffe, J Crystal Growth **68** (1984) 214

[12] B Cockayne and P J Wright, J Crystal Growth **68** (1984) 223

[13] T Hirai and H Yamane, J Crystal Growth **107** (1991) 683

[14] R D Dupuis and D Dapkus, Appl Phys Lett **31** (1977) 466

[15] M R Leys, Chemtronics **2** (1987) 155

[16] J van de Ven, G M J Rutten, M J Raaijmakers and L J Giling, J Crystal Growth **76** (1986) 352

[17] E P Visser, C R Kleijn, C A M Govers, C J Hoogendoorn and L J Giling, J Crystal Growth **94** (1989) 929

[18] J P Duchemin, M Bonnet, F Koelsch and D Huyghe, J Electrochem Soc **126** (1979) 1134

[19] J W Matthews and A E Blakeslee, J Vac Sci Technol **14** (1977) 98

[20] N F Mott and F R N Nabarro, Proc Phys Soc **52** (1940) 86

[21] F R N Nabarro, Proc Roy Soc London, Ser **A175** (1940) 519

[22] F C Frank and J H van der Merwe, Proc Roy Soc London, Ser **A198** (1949) 205

[23] See *e g* J W Matthews, in Epitaxial Growth, Part B, Ed J W Matthews (Academic Press, New York, 1975) ch 8, and references therein

[24] W A Jesser and J W Matthews, Phil Mag **15** (1967) 1097

[25] J W Matthews and A E Blakeslee, J Crystal Growth **27** (1974) 118

[26] S M Hu, J Appl Phys **70** (1991) R53

[27] M R Leys, in Low-Dimensional Structures in Semiconductors, Eds A R Peaker and H G Grimmeis (Plenum, New York, 1991)

[28] B W Dodson and J Y Tsao, Appl Phys Lett **51** (1987) 1325

[29] D C Houghton, J Appl Phys **70** (1991) 2136

[30] J.W. Matthews, S. Mader and T.B. Light, J. Appl. Phys. **41** (1970) 3800.

[31] P.M.J. Marée, J.C. Barbour, J.F. van der Veen, K.L. Kavanagh, C.W.T. Bulle-Lieuwma and M.P.A. Viegers, J. Appl. Phys. **62** (1987) 4413.

[32] R.H.M. van de Leur, A.J.G. Schellingerhout, F. Tuinstra and J.E. Mooij, J. Appl. Phys. **64** (1988) 3043.

[33] Y. Fukuda, Y. Kohama and Y. Ohmachi, Jap. J. Appl. Phys. **29** (1990) L20.

Chapter 2

The influence of substrate orientation and mis-orientation on the silicon-doping of GaAs grown by metalorganic vapour phase epitaxy

Abstract

In this investigation the influence of the direction of the mis-orientation of the substrate has been studied (*i*) on the amount of silicon which is incorporated in the GaAs layer during growth by metalorganic vapour phase epitaxy and (*ii*) on the degree of compensation. For this purpose substrates with eleven different orientations have been used. They include the (110) group: (110), (110)2°$(\bar{1}11)$, (110)2°$(1\bar{1}\bar{1})$ and (110)2°(001); the (100) group: (100), (100)2°(011), (100)2°$(01\bar{1})$ and (100)2°(110); and the (111)A group: (111)A, (111)A 2°(001) and (111)A 2°(110). Quite a number of clear trends have been found which can be explained by a careful consideration of the atomic configurations of the various surface, step and kink sites. The results of this study have provided information on the incorporation of silicon on an atomic scale and lead to insight in the most preferable atomic configuration of the GaAs surface during MOVPE growth.

2.1 Introduction

Silicon is the most widely used n-type dopant for GaAs in metalorganic vapour phase epitaxy (MOVPE). In a recent study of silicon-doped GaAs [1] the net carrier concentration for constant silane partial pressure $p_{\mathrm{SiH_4}}$ was found to decrease in the order $n_{(100)2^\circ(110)} > n_{(111)A} > n_{(110)}$, due to a difference in the binding strength and the surface diffusion rate of the adsorbed silicon species on the surface, as well as to steric hindrance. A certain difference in compensation ratio ($N_{\mathrm{A^-}}/N_{\mathrm{D^+}}$), which can be regarded as an approximation for $[\mathrm{Si}_{As}]/[\mathrm{Si}_{Ga}]$, was found to exist among the above orientations. It was proposed that this difference most probably is due to the various step and kink site configurations at the growth front. The initial motivation of the present study was to verify this assumption and to see to what extent the compensation ratio can be changed.

It is known that by changing the substrate misorientation direction from a major flat surface, various steps, *i.e.* various dangling bond configurations at the steps, can be revealed. For this reason substrates with eleven different orientations have been used. They include the (110) group: (110), (110)2°$(\bar{1}11)$, (110)2°$(1\bar{1}\bar{1})$ and (110)2°(001); the (100) group: (100), (100)2°(011), (100)2°$(01\bar{1})$ and (100)2°(110); and the (111)A group: (111)A, (111)A 2°(001) and (111)A 2°(110). The choice of this set of samples is to enable a good comparison among various major steps which can be present on these surfaces.

The discussion of the growth results of the three orientation groups is discussed separately for clarity. At first the configuration of the various surfaces, including the expected or reported step and kink site configurations, is outlined followed by a discussion of the observed results. The influence of the V/III ratio is discussed briefly in the last part.

2.2 Experimental

The silicon doped GaAs layers have been grown by MOVPE at atmospheric pressure using trimethylgallium (TMG) and arsine (AsH_3) as source materials whereas silane (SiH_4, 100 ppm diluted in hydrogen) was used as dopant source. Details about the reactor have been described elsewhere [1, 2]. The growth temperature has been kept constant at 970 ± 5 K for all the MOVPE runs. The ratio between AsH_3 and TMG (the V/III ratio) has been varied between 5 and 50. All the GaAs substrates as obtained from MCP (UK) were chromium-doped, semi-insulating, horizontal Bridgman grown, and chemo-mechanically polished on one face. The accuracy of the (mis-)orientation angle of all the used substrates was better than ±0.5 degrees, as specified by the supplier. During the MOVPE growth, samples belonging to the same orientation group have been placed in the same axial position in the reactor in order to enable a direct comparison of the incorporation results. Due to the large number of samples used in the experiments, samples of a different orientation group have been placed at a different axial position. As a result of the depletion effect along the gas flow direction in the reactor, these samples had slight differences in growth rate and carrier concentration. Therefore a direct comparison between groups must be performed with care. The growth rate for one group was essentially the same. The averaged growth rate was approximately 1.5 nm/s.

The morphology after growth has been observed with an interference-contrast microscope. The thickness of the grown layers has been measured by cleaving and staining. The electrical characterisation was performed by Hall-Van der Pauw measurements using a clover-leaf configuration. The error in the measured carrier concentration values was estimated to be smaller than 10%. The inaccuracy in the results is mainly due to the error in the measurement of the layer thicknesses.

2.3 Results and discussion

2.3.1 Some considerations on silicon-doping

It has been established that doping with silane goes along the following lines: (*i*) the decomposition of SiH_4 into SiH_2, which happens very close to the hot surface of the GaAs substrate, and (*ii*) the adsorption of SiH_2 on the surface followed by diffusion to the step sites which subsequently leads to silicon incorporation [1, 3, 4]. It is well known that silicon is an amphoteric dopant leading to incorporation as a donor (Si_{Ga}) or as an acceptor (Si_{As}) [1],[5]-[7]. The ratio $[Si_{As}]/[Si_{Ga}]$ can be estimated by the compensation ratio, N_{A^-}/N_{D^+}. The compensation ratio can be calculated from the measurements of the carrier concentration and the mobility values [8, 9]. The reliability of the calculated values used in the comparison is quite good for two reasons: (*i*) the carrier concentrations of the grown samples are relatively low which satisfies the requirements of refs. [8, 9] and (*ii*) only the relative change of the compensation ratio is of importance in the discussion. Therefore a systematic error in the calculated values is allowed. It has been reported that the compensation ratios obtained in this way can be overestimated [10, 11], but this does not have any influence on the observed incorporation trends.

After a proper correction for the depletion effect, the general trend of the carrier concentration for the three orientation groups was found to be $n_{(100)} > n_{(111)\mathrm{Ga}} > n_{(110)}$, which is the same as in ref. [1]. This trend might be explained by a difference in bond strengths of the SiH_2 species on the various oriented surfaces, *i.e.* the difference in desorption energy. Adsorption of SiH_2 on the (111)A surface will occur at the gallium sites, thereby forming a Si-Ga bond, while on the arsenic stabilized (100) surface a Si-As bond will be formed. Since the Si-Ga bond strength is smaller than the Si-As bond strength (202 *vs*. 231 kJ/mol), the desorption flux of SiH_2 from an (111)A surface will be somewhat larger than from an (100) surface. As a consequence the silicon incorporation on the (100) surface is higher than on the (111)A surface. The still smaller incorporation rate on the (110) can be explained by steric hindrance caused by the so called zipper way of growth on the (110) surface (for details see ref. [1]). However, adsorption in itself is not decisive, the incorporation of silicon is governed by the surface flux, *i.e.* by the product of the coverage and the diffusion velocity. A lower adsorption strength will also lead to a higher diffusion velocity to the steps, so *a priori* it is not clear which of both effects will dominate. Most likely the electronic configuration at the step itself determines the observed differences.

2.3.2 Group (110)

Surface relaxation is expected for the (110) face. This relaxation causes a slight lowering of the top gallium atoms towards bulk crystal, leaving the top arsenic atoms somewhat raised [12, 13]. On the (110) surface steps exist in six directions, which can be classified in four different types. They are in the $[001]$, $[00\bar{1}]$, $[\bar{1}11]$, $[1\bar{1}\bar{1}]$, $[1\bar{1}1]$ and $[\bar{1}1\bar{1}]$ directions, as shown in fig. 2.1. The steps in the $[1\bar{1}1]$ and the $[\bar{1}1\bar{1}]$ directions are equivalent to those in the $[\bar{1}11]$ and the $[1\bar{1}\bar{1}]$ directions respectively. The direction of the step is defined as the step normal, parallel to the major flat surface. Silicon incorporation at the $[001]$ and $[00\bar{1}]$ steps is expected to be similar, since growth proceeds in a so-called zipper way where alternating group III and group V kink sites are present at both the steps (fig. 2.1b). In this study the $[001]$ step has been examined. The $[\bar{1}11]$ and $[1\bar{1}\bar{1}]$ steps are terminated by arsenic and galliums atoms respectively (fig. 2.1c). As a consequence it is expected that silicon atoms arriving at the $[\bar{1}11]$ step will have a greater chance to be incorporated as Si_{Ga} than in the case of the $[1\bar{1}\bar{1}]$ step, therefore the compensation ratio of the layers grown on $(110)2^\circ(\bar{1}11)$ should be lower than the layers grown on $(110)2^\circ(1\bar{1}\bar{1})$. This is nicely proven by the experimental results (fig. 2.2). For all the examined V/III ratios the incorporation of Si_{Ga} is the highest at the $[\bar{1}11]$ steps. When the V/III ratio is 10, the net carrier concentration is even an order of magnitude higher. This large difference in carrier concentration between the $(110)2^\circ(\bar{1}11)$ and $(110)2^\circ(1\bar{1}\bar{1})$ layers may find potential

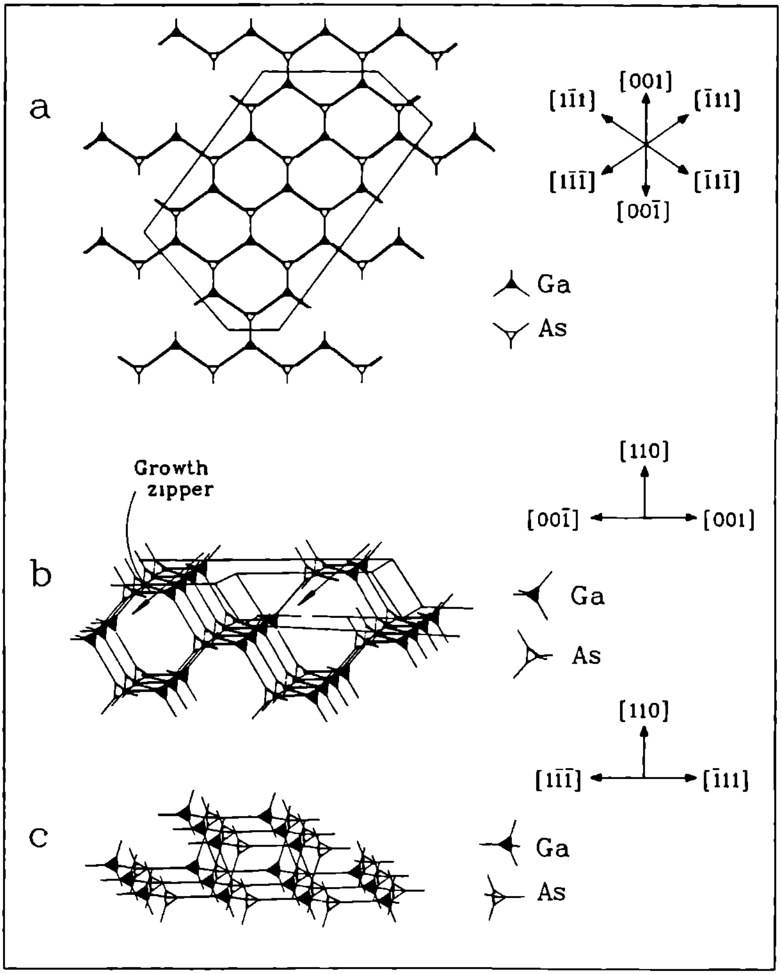

Figure 2.1 a) Schematic top view of the possible steps present on the (110) surface. The middle part can be seen as a plateau bordered by the four types of steps. b) Side view on the [001] step, showing a kink site. c) Side view on the [1̄11] and [11̄1̄] steps showing the arsenic and gallium dangling bonds respectively. Extra lines are drawn to reveal the steps.

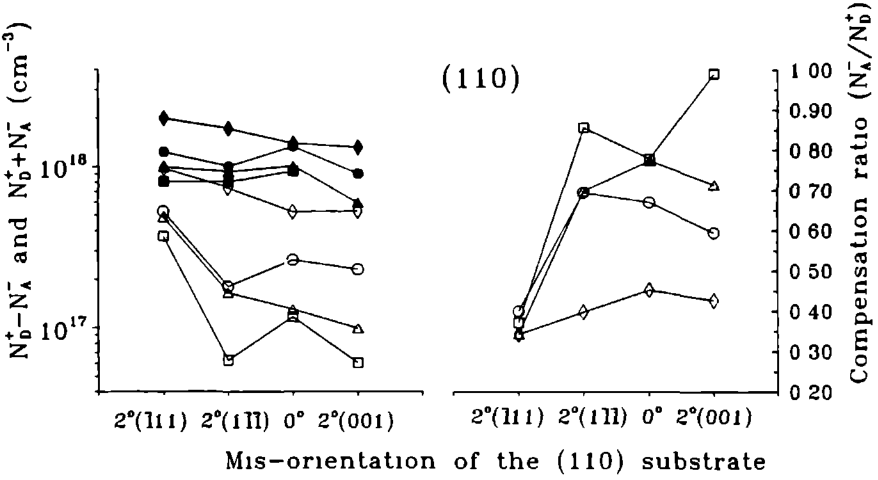

Figure 2.2 Room temperature net carrier concentration ($N_{D^+} - N_{A^-}$), total carrier concentration ($N_{D^+} + N_{A^-}$) and compensation ratio (N_{A^-}/N_{D^+}) of the silicon-doped GaAs layers versus the mis-orientation of the (110) substrate The open symbols in the graph at the left hand side represent the values of the net carrier concentration, the filled symbols the total carrier concentration and the open symbols of the graph at the right hand side the compensation ratio. Four different V/III ratios have been used (5 (circles), 10 (squares), 20 (triangles) and 50 (diamonds)). The lines are guides to the eyes

applications in epitaxial device development, e g a lateral doping superlattice of n^+/n can be made on a patterned surface on which both (110)2°(1̄11) and (110)2°(11̄1̄) orientations are present Since this effect is caused by differences in atomic arrangements, small lateral dimensions should be attainable.

The total carrier concentration does not show much difference for a given V/III ratio. This indicates that the large difference in the carrier concentration is caused by the difference in compensation ratios, as indeed is shown in fig 2.2 The highest compensation ratio, close to 1, was found on a (110)2°(001) sample (V/III =10). At a V/III ratio of *ca.* 10 the surface is expected to have equal coverages of gallium and arsenic atoms. In this case the zipper way of growth on the (110)2°(001) samples gives an equal chance for silicon atoms to be incorporated either at a gallium or at an arsenic site

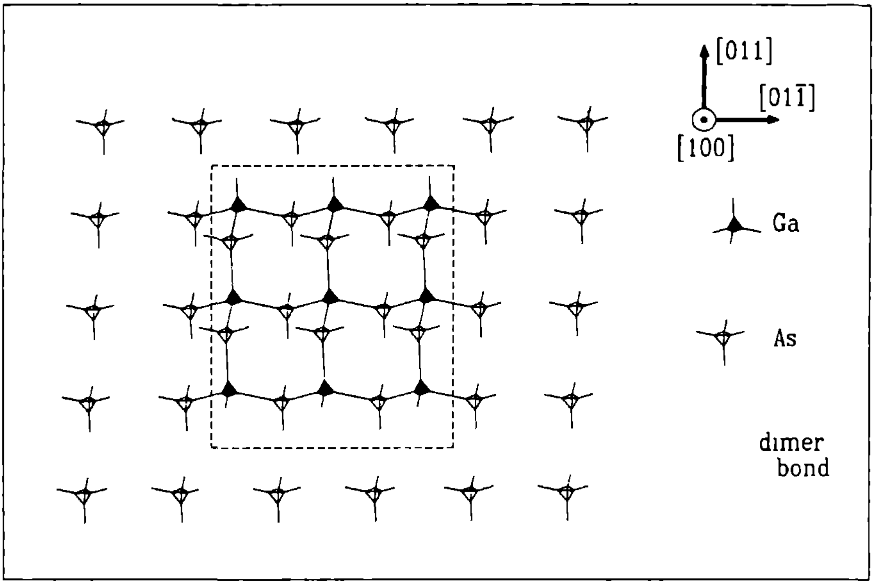

Figure 2.3 Schematic top view of the possible steps present on the (100) surface. The dotted lines show the dimer bonds.

However, if this is true the samples grown on (110)2°(001) with a V/III ratio of 5 should have a higher compensation ratio or even a p-type character, instead of the experimentally observed n-type character. No explanation is known for this result.

2.3.3 Group (100)

The (100) surface is known to reconstruct by the dimerization of the arsenic atoms [14, 15] or of the gallium atoms at the surface [16, 17]. Under arsenic rich conditions (in our case for V/III $\geq$ 10) the dimerization of the arsenic atoms at the surface occurs. At the (100) surface, two major atomic steps are distinguished. They are in the [011] and in the [01$\bar{1}$] directions [18, 19], as is shown in fig. 2.3. The adsorption of growth species at these two steps is similar when the arsenic atoms are unreconstructed [19], but quite different when they are completely dimerized. When the surface is completely covered with dimerized arsenic atoms, an adsorbed species, such as SiH_2, can break one arsenic dimer bond at any place along the [011] step followed by incorporation as Si_{Ga}. At the [01$\bar{1}$] step, however,

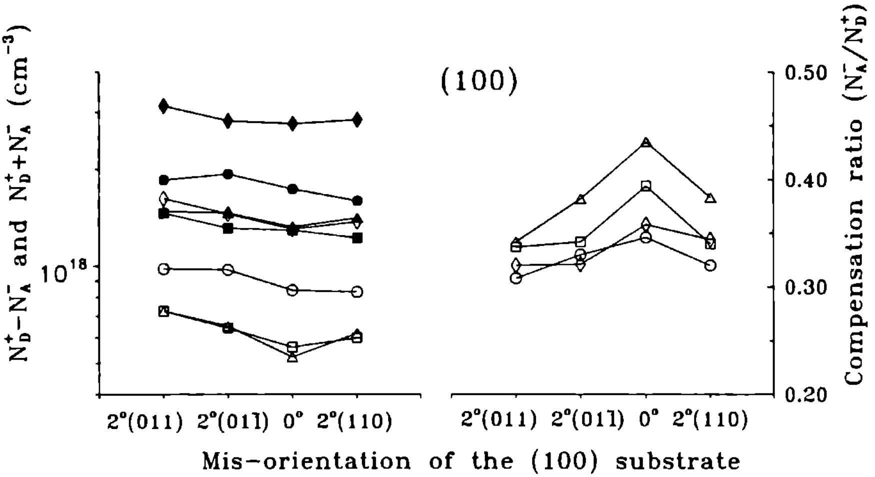

Figure 2.4 Room temperature net carrier concentration ($N_{D^+} - N_{A^-}$), total carrier concentration ($N_{D^+} + N_{A^-}$) and compensation ratio (N_{A^-}/N_{D^+}) of the silicon-doped GaAs layers versus the mis-orientation of the (100) substrate. The open symbols in the graph at the left hand side represent the values of the net carrier concentration, the filled symbols the total carrier concentration and the open symbols in the graph at the right hand side the compensation ratio. The results of four experiments with different V/III ratios (5 (circles), 10 (squares), 20 (triangles) and 50 (diamonds)) are shown. The lines are guides to the eyes.

the adsorbed species arriving at this step cannot directly be trapped at each step site, they only can be incorporated at a specific kink site at the step. During the growth of GaAs this kink site will be a gallium or an arsenic site alternatingly, therefore incorporation as Si_{Ga} or as Si_{As} will be the result. From the above discussion, it can be concluded that an epitaxial layer grown on an (100)2°(011) substrate, which has a large number of [011] steps, has a higher silicon incorporation rate and a lower compensation ratio than an epitaxial layer grown on a (100)2°(01$\bar{1}$) substrate on which the [01$\bar{1}$] step is dominant. The results shown in fig. 2.4 are in agreement with the above expectation for all V/III ratios $\geq$ 10 where dimerization is expected to be present. Only for the case of V/III= 5 the difference in net carrier concentration between the (100)2°(011) and (100)2°(01$\bar{1}$) oriented layers is not really significant. This indeed is an indication that in this case dimerization of the arsenic atoms at the surface is not complete.

It is observed that the compensation ratio for the exact (100) samples consistently is the highest. Although the precise step configuration of the exact (100) samples is not known, this result can be expected. Since the same growth rate as the misoriented samples is maintained, the few steps which are present have to move so fast, that more silicon atoms become trapped at wrong positions. Apparently, this leads to an increased number of silicon at arsenic positions. Further, the exact (100) surface showed a somewhat inferior morphology compared to the misoriented layers, which is most probably due to nucleation difficulties.

An important observation is that the (100)2°(011) samples in all cases show the highest carrier concentration and the lowest compensation ratio. If it is noticed that (100)2°(110) is at present the most widely used substrate orientation for the growth of GaAs, a better choice would be (100)2°(011) when a low compensation ratio is desired.

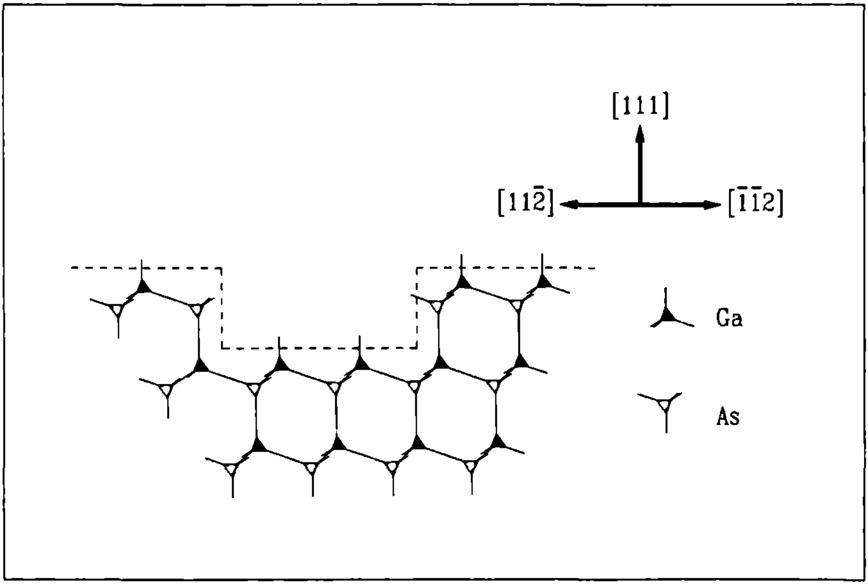

Figure 2.5 Schematic view on the two types of possible steps present on (111)A.

2.3.4 Group (111)A

Based on morphological studies two types of stable steps are distinguished on the (111)A surface, *viz* steps in the $[\bar{1}\bar{1}2]$ and the $[11\bar{2}]$ directions (fig. 2.5). It was proposed that the $[\bar{1}\bar{1}2]$ step, which has an (100) like character, can have step reconstruction forming arsenic dimers [18, 20] The $[11\bar{2}]$ step, which has an (110) like character, will have step relaxation similar to the (110) surface. These two steps have similar configurations as the [011] steps on the (100) surface and the $[1\bar{1}\bar{1}]$ steps on the (110) surface respectively - the atomic configurations at the corner of the steps are similar, although they are rotated These steps are expected to behave in the same way for silicon incorporation as the steps on the (100)2°(011) and $(110)2°(1\bar{1}\bar{1})$ orientations respectively, *i e* the compensation ratio of layers grown on an $(111)A\,2°(\bar{1}\bar{1}2)$ substrate is expected to be lower than that

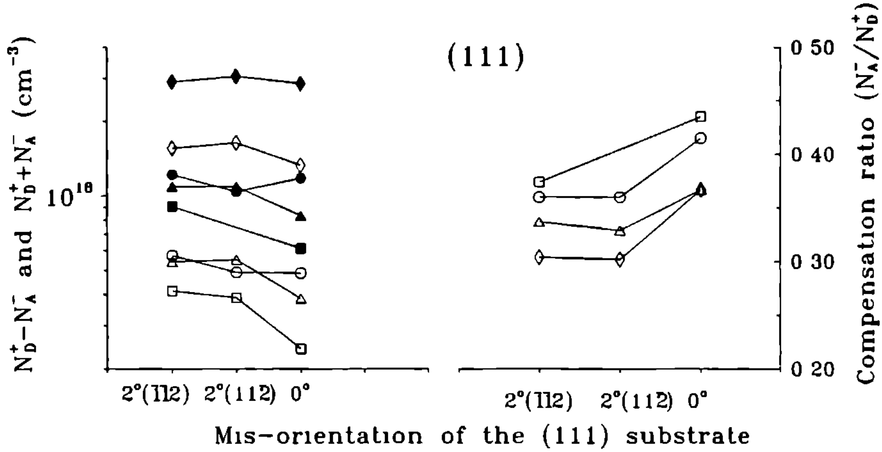

Figure 2.6 Room temperature net carrier concentration ($N_{D^+} - N_{A^-}$), total carrier concentration ($N_{D^+} + N_{A^-}$) and compenation ratio (N_{A^-}/N_{D^+}) of the silicon-doped GaAs layers versus the mis-orientation of the (111)A subastrate The open symbols represent the values of the net carrier concentration (the left hand side graph) and the compensation ratio (the right hand side graph), the filled symbols represent the total carrier concentration The results of four experiments with different V/III ratios (5 (circles), 10 (squares), 20 (triangles) and 50 (diamonds)) The lines are guides to the eyes

of layers grown on an (111)A 2°$(11\bar{2})$ substrate. However, this effect was not observed experimentally (fig. 2.6). Neither the carrier concentration nor the compensation ratio differs much between these two orientations. It appears that the incorporation possibilities for silicon at both the arsenic and the gallium sites are the same, both at the $[11\bar{2}]$ and the $[\bar{1}\bar{1}2]$ steps. A more detailed discussion on incorporation at the steps at the (111)A surface is given in chapter 3, where these results are compared to results of incorporation experiments of indium.

As compared with the mis-oriented samples, the exact (111)A samples have lower values for the carrier concentration and higher values for the compensation ratios. The higher compensation ratios can be explained by the selection difficulties at the step during the fast movement of the step.

2.3.5 The influence of the V/III ratio

The influence of the V/III ratio on the total carrier concentration is shown in fig. 2.7. For the V/III ratio from 5 to 10 the general trend is a decrease of the total carrier concentration. This effect is also reported by Bass [21], but no exact mechanism can be given. For V/III

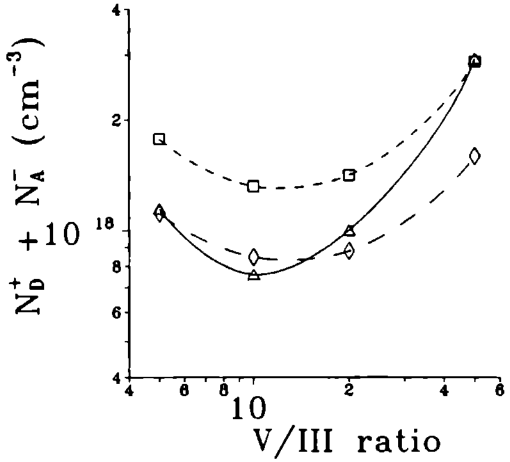

Figure 2.7 Total carrier concentration ($N_{D^+} + N_{A^-}$) versus the V/III ratio for three different groups of samples ((100) (squares), (110) (diamonds) and (111)A (triangles)).

ratios higher than 10, an increase of the total carrier concentration is observed. This effect can be explained by the following argument: with an increase of the arsine partial pressure the concentration of gallium vacancies will be increased which in turn enhances the probability of silicon incorporation on a gallium position. Since the bond strength of Si-As is higher than that of Si-Ga this leads to less desorption of SiH_2 from the surface resulting in a higher total carrier concentration. This argument certainly is the explanation for the relatively stronger increase of the total carrier concentration in the (111)A layers for increasing V/III ratios (fig. 2.7).

2.4 Summary and conclusions

It has been shown that by looking at the silicon doping of GaAs as a function of the substrate orientation and mis-orientation, information of the incorporation of silicon at an atomic scale can be obtained. Quite a number of clear trends have been found in this study. For the (110) group it is observed that the net carrier concentration of the $(110)2^\circ(\bar{1}11)$ oriented layers is larger than that of the $(110)2^\circ(1\bar{1}\bar{1})$ oriented layers and that the compensation ratio is lower. Because this effect is very strong, it may find potential applications in epitaxial devices.

For the group (100) samples, the net carrier concentration decreases in the order $(100)2^\circ(011) > (100)2^\circ(01\bar{1}) > (100)$ and the compensation ratio in the reversed order. This phenomenon has been explained by a consideration of the reconstruction possibilities at the surfaces, and the silicon incorporation possibilities at these different atomic steps. As compared with the commonly used (100)2°(110) substrate, growth on (100)2°(011) oriented substrates gives the highest carrier concentrations and the lowest compensation ratios.

No essential differences have been found between incorporation of silicon at the steps at the (111)A 2°(001) and (111)A 2°(110)surfaces.

References

[1] X. Tang, H.G.M. Lochs, P.R. Hageman, M.H.J.M. de Croon, L.J. Giling and A.J. Bons, J. Crystal Growth **98** (1989) 827.

[2] J. van de Ven, G.M.J. Rutten, M.J. Raaijmakers and L.J. Giling, J. Crystal Growth **76** (1986) 352.

[3] T.F. Kuech, M.A. Tischler, R. Potemski, F. Cardone and G. Scilla, J. Crystal Growth **98** (1989) 174.

[4] P.R. Hageman, X. Tang, M.H.J.M. de Croon and L.J. Giling, J. Crystal Growth **98** (1989) 249.

[5] W.I. Wang, E.E. Mendez, T.S. Kuan and L. Esaki, Appl. Phys. Letters **47** (1985) 826.

[6] S.S. Bose, B. Lee, M.H. Kim, G.E. Stillman and W.I. Wang, J. Appl. Phys. **63** (1988) 743.

[7] J. Maguire, R. Murray, R.C. Newman, R.B. Beall and J.J. Harris, Appl. Phys. Letters **50** (1987) 516.

[8] W. Walukiewicz, L. Lagowski, L. Jastrzebski, M. Lichtensteiger and H.C. Gatos, J. Appl. Phys. **50** (1979) 899.

[9] W. Walukiewicz, L. Lagowski and H.C. Gatos, J. Appl. Phys. **53** (1982) 769.

[10] D. Lancefield, A.R. Adams and M.A. Fisher, J. Appl. Phys. **62** (1987) 2342.

[11] D.A. Anderson, N. Apsley, P. Davies and P.L. Giles, J. Appl. Phys. **58** (1985) 3059.

[12] A. Kahn, Surf. Sci. Reports **3** (1983) 193.

[13] C. Astaldi, L. Sorba, C. Rinaldi, R. Mercuri, S. Nannarone and C. Calandra, Surf. Sci. **162** (1985) 39.

[14] R.Z. Bachrach, R.S. Bauer, P. Chiaradia and G.V. Hansson, J. Vac. Sci. Technol. **18** (1981) 797.

[15] L. Daweritz, Surf. Sci. **160** (1985) 171.

[16] K. Jacobi, Surf. Sci. **132** (1983) 1.

[17] G.X. Qian, R.M. Martin and D.J. Chadi, Phys. Rev. B **38** (1988) 7649.

[18] L.J. Giling and W.J.P. van Enckevort, Surf. Sci. **161** (1985) 567.

[19] J. van de Ven, J.L. Weyher, H. Ikink and L.J. Giling, J. Electrochem. Soc. **134** (1987) 989.

[20] H.H.C. de Moor, Thesis University of Nijmegen, The Netherlands (1986).

[21] S.J. Bass, J. Crystal Growth **47** (1979) 613.

Chapter 3

Anisotropic indium incorporation during growth of $In_xGa_{1-x}As$ by metalorganic vapour phase epitaxy

Abstract

The incorporation of indium during growth of $In_xGa_{1-x}As$ by metalorganic vapour phase epitaxy on GaAs substrates with orientations vicinal to (100) and (111)A has been studied. On the substrates used in this study surface steps are present which are parallel or perpendicular to the periodic bond chains at the surface. During the MOVPE of $In_xGa_{1-x}As$ the incorporation of indium at the group III sublattice sites occurs at monatomic steps at the surface. At the fully kinked steps the growth species can be incorporated at any step site, whereas at stable steps they have to diffuse along the steps towards kink sites to get incorporated. It is shown that the reconstruction possibilities at the step edges under high arsenic partial pressures determine which of these mechanisms is active.

It has been found that under arsenic rich conditions in the gas phase on the (100) as well as on the (111)A surfaces at the kinked steps the incorporation of indium is higher than at the stable steps, due to the lower desorption probability of indium at the kinked steps.

These results have been compared to the studies on the orientation dependence of the incorporation of silicon during GaAs growth. For silicon it is possible to be built in both at group III and group V sites. A comparison of the incorporation possibilities of silicon at the group III and group V sites confirms the results obtained from the $In_xGa_{1-x}As$ experiments.

3.1 Introduction

In the past two decades it has been demonstrated that metalorganic vapour phase epitaxy (MOVPE) is a versatile technique for the epitaxial growth of III-V compound semiconductors [1]. By optimization of the growth conditions, layer structures of high morphological, optical and electric quality can be grown, which have their applications in the opto-electronic industry for the production of devices such as lasers and transistors. In most of these devices, structures as multiple quantum wells (MQW) and strained layer superlattices (SLS) are of great importance for good operating performance [2]. Since the dimensions of these structures are decreasing more and more, a good control of the growth process is needed, including uniformity of composition of ternary and quaternary compounds and extreme sharpness of the interfaces. In order to realize this, a thorough knowledge of the growth mechanisms of the MOVPE process is required.

Crystal growth at $\{100\}$ and $\{111\}$ surfaces of materials with the diamond and the zincblende structure has been described by Giling and Van Enckevort [3]. In their study the periodic bond chain (PBC) theory of Hartman and Perdok [4, 5] has been applied to explain the external morphology of crystals with diamond-like structures. From a PBC-analysis of GaAs and silicon it has been concluded that the PBC-theory does not explain the stability of the $\{100\}$ faces. The step free energy at the surface is zero. Growth can take place at any surface site, resulting in rough surfaces. However, when surface reconstruction is taken into account, the step free energy becomes larger than zero. The growing surfaces are flat, which is in accordance with the observations [3]. A similar reconstruction has been reported for the $\langle\bar{1}\bar{1}2\rangle$ steps at the $\{111\}$ surface [3].

A slight misorientation of the surface parallel or perpendicular to the PBC's reveals the dangling bond configurations at the steps. These configurations determine whether a step is stable or fully kinked during growth. It has been shown that reconstruction at the surface steps has a large influence on the incorporation processes [6] resulting in differences in lateral growth rates [7].

In this study the incorporation processes at different principal steps (parallel or perpendicular to the PBC's) on (100) and (111)A GaAs substrates during growth by metalorganic vapour phase epitaxy of $In_xGa_{1-x}As$ epitaxial layers has been investigated. It was known from $In_xGa_{1-x}As$ growth studies by MOVPE [8], metalorganic molecular beam epitaxy (MOMBE) [9], as well as by molecular beam epitaxy (MBE) [10]-[12], that indium adatoms have a larger desorption probability than gallium adatoms due to the somewhat smaller bond strength In-As (151 kJ/mol) compared to Ga-As (164 kJ/mol). From this it follows that the incorporation efficiency of indium is expected to be lower than that of gallium. The influence of the different step configurations at the steps at the surfaces on the incorporation efficiency of indium are discussed on the basis of the PBC-theory and compared with results of both lateral growth and incorporation studies as described in the literature.

3.2 Periodic bond chains on $\{100\}$ and $\{111\}$ faces

According to the PBC-theory [4], a crystal can be considered as a structure, consisting of interwoven nets of uninterrupted paths of bonds, having the periodicity of the crystal lattice. Depending on the number of different oriented PBC's, present in the surface layer, crystal surfaces can be classified into three categories. The thickness of the surface layer, the slice, is determined by the crystallographic extinction conditions [5]. If in the surface layer no PBC's are present the surface is a K (kinked) face. The surface is rough, an adatom can be trapped at any surface site. In the case of one PBC present in the surface layer, the surface is an S (stepped) face. This means that the surface consists of unidirectional bond chains, which are stable, perpendicular to the PBC, but kinked in the direction of the PBC. A surface, containing two or more different PBC's is called an F (flat) face. These faces are stable and have the lowest growth rates. Usually, on growing crystals only F-faces are observed.

Here a short review of the PBC analysis of the (100) and (111)A surfaces is given and configurations of the major steps at these surfaces on GaAs under arsenic rich conditions in the gas phase are discussed.

3.2.1 The (100) surface

On the (100) surface of GaAs under arsenic poor conditions in the gas phase only one PBC (in the [011] direction) is present within the slice thickness, which is one half of the lattice constant. This shown in fig. 3.1a. Under arsenic rich conditions reconstruction of the surface arsenic atoms is possible, since they can form a σ-bond with the neighbouring atoms [13]. This leads to the formation of a second PBC in the $[01\bar{1}]$ direction (fig. 3.1b). Therefore in this case the (100) face in GaAs may be considered as an F-face [3].

In fig. 3.2 the steps on a reconstructed (100) surface have been drawn. The direction of the step is given by the normal to the step, *i.e.* in the direction a step will move during growth. The steps in the [011] and the $[01\bar{1}]$ directions on the (100) surface behave different under arsenic rich conditions. The step in the [011] direction is fully kinked (fig.

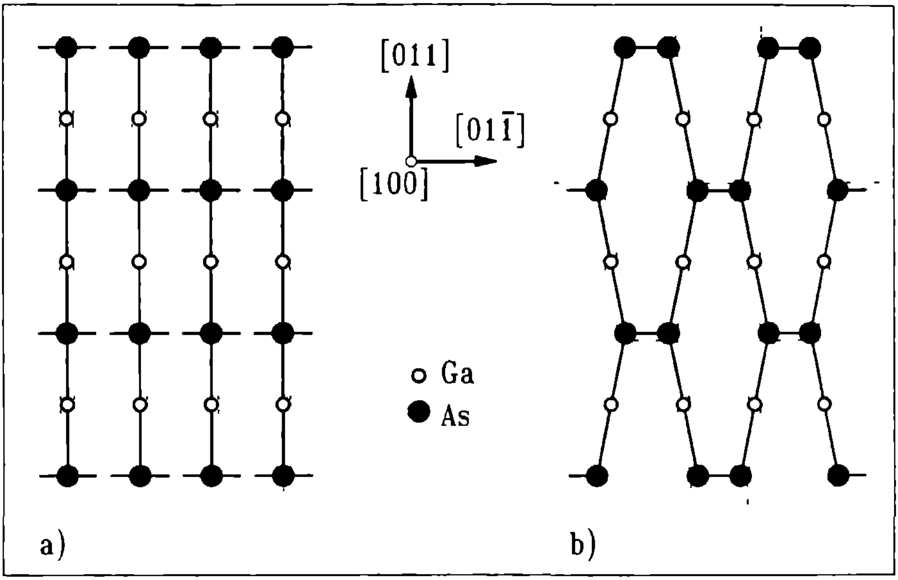

Figure 3.1 Schematic top view on a) an unreconstructed and b) a (2 × 4)As reconstructed (100) GaAs surface The PBC's are indicated on the surfaces by the dashed lines

3.2a) An adsorbed group III (*i e* gallium or indium) species, arriving at this step, can break an arsenic dimer bond and form a triple bond at any step site. Desorption from this position is not possible. The rupture of the arsenic dimer bond forms new kink sites along the step In fig. 3.2a a gallium atom adsorbed at the step is shown.

The [01$\bar{1}$] step is a stable step. Group III species arriving at this step can only adsorb by the formation of a single bond at site S (fig. 3.2b) For a species adsorbed at this site the activation energy for diffusion is lower than for breaking an arsenic dimer bond [14]. So diffusion along the step or to the surface is favoured Incorporation of group III species at the [01$\bar{1}$] step takes place at the specific kink sites (indicated by K in fig 3.2b), where a double bond can be formed to get incorporated. The third bond is formed by breaking the dimer bond next to the step As indium has a lower bond strength with arsenic than gallium it will have a higher desorption probability than gallium as long as it is attached to the step. From this higher desorption probability during the diffusion process along this step, it is expected that the indium incorporation at the stable [01$\bar{1}$] steps is lower than at the kinked [011] steps, where the adatoms can be trapped in at any step site

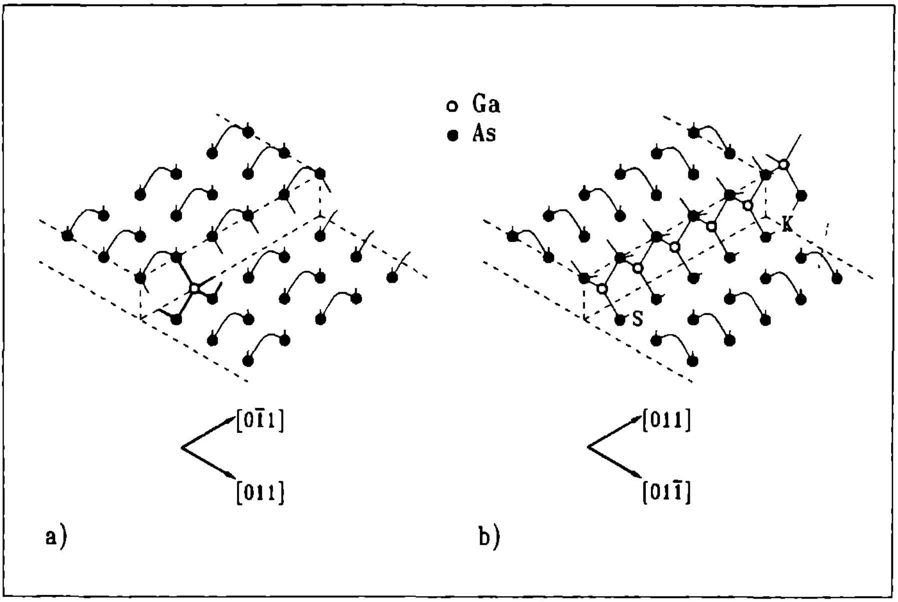

Figure 3.2 Schematic view on the [011] and the [01$\bar{1}$] steps present at the reconstructed (100) surface of GaAs. K and S indicate a kink and a step site respectively. At the [011] step a trapped gallium atom is shown.

3.2.2 The (111)A surface

On the (111)A surface, where the gallium dangling bonds are directed upwards, three different intersecting PBC's are present, as are shown in fig. 3.3. They are parallel to the $\langle 112 \rangle$ directions. The (111)A face is an F-face. The surface consists of gallium atoms, which are relaxed from the bulk (sp^3) to the surface (sp^2) configuration [15]. This means that the dangling bonds at the surface are empty. This is also the case under arsenic rich conditions, since the arsenic coverage of the surface at a temperature of 1000 K is not higher than 8%, as is determined from thermodynamic calculations [14].

Two principal steps, parallel to the PBC's, are present on this surface, they are in the [$\bar{1}\bar{1}$2] (fig. 3.4a) and in the [11$\bar{2}$] directions (fig. 3.4b). At steps in the [$\bar{1}\bar{1}$2] direction (or equivalent directions) the arsenic atoms in the unreconstructed mode contain two dangling bonds (fig. 3.4a). In this case the step is fully kinked. At such a step the group III components can directly be incorporated by the formation of two bonds with

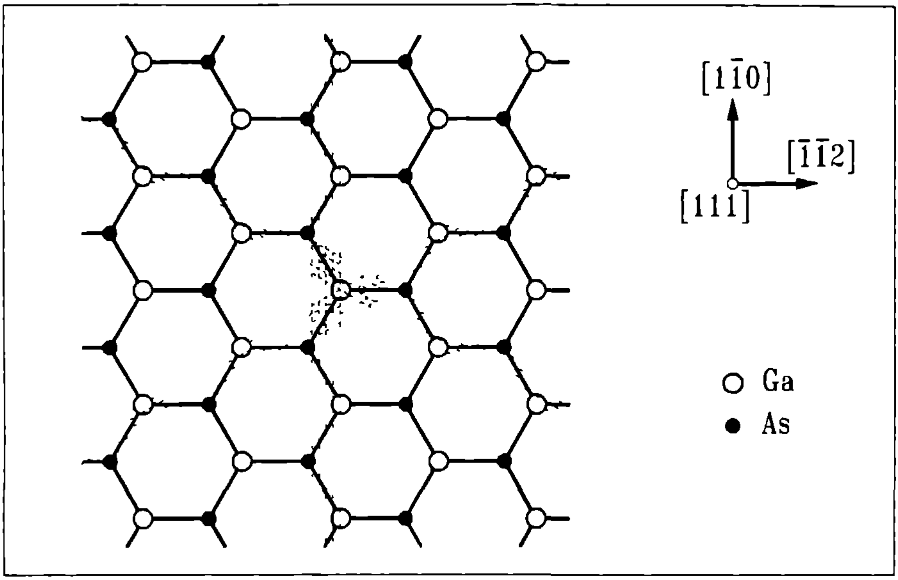

Figure 3.3 Schematic top view on the (111)A GaAs surface. The gallium dangling bonds are directed upward The PBC's along the ⟨110⟩ directions are indicated by the dashed area's

the arsenic atoms, thereby creating a new kink site for arsenic species arriving at the step. From the (100) character of the [$\bar{1}\bar{1}$2] steps it follows that under arsenic rich conditions step reconstruction is possible [16, 17]. The dangling bonds of the arsenic atoms form a dimer bond. This step reconstruction lowers the density of dangling bonds and increases the stability of this step, which is no longer kinked. The incorporation of a gallium component arriving at this step in this case takes place by breaking a dimer bond. In this process no successive new kink sites for group III species are formed, due to the crystallographic structure. Therefore incorporation is expected to take place at any step site. However, the high activation energy needed for each event prevents rapid growth.

At the [11$\bar{2}$] step (fig. 3.4b) the arsenic atoms have one dangling bond. This step is expected to behave as a stable step. The group III components, which can only a form a single bond at the step, have to diffuse to a specific kink site at the step to form a double bond with the arsenic atoms It is therefore expected that the indium incorporation at this step is lower than at the [$\bar{1}\bar{1}$2] step, certainly under arsenic poor conditions where

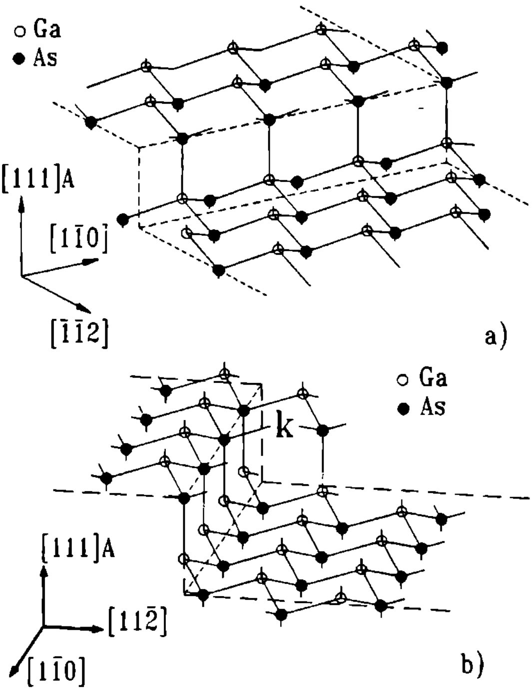

Figure 3.4 Schematic view on a) the $[\bar{1}\bar{1}2]$ and b) the $[11\bar{2}]$ steps present at the (111)A surface. *k* indicates a kink site at the $[11\bar{2}]$ step.

reconstruction of the $[\bar{1}\bar{1}2]$ step is incomplete.

3.3 Experimental details

The incorporation processes at the steps during MOVPE have been investigated by growing $In_xGa_{1-x}As$ epitaxial layers on misoriented (100) and (111)A GaAs substrates. The direction of the misorientations is chosen perpendicular or parallel to the surface PBC's, resulting in kinked and stable step configurations at the growing surface. The misorientation of the surface is indicated by the direction of the step normal, parallel to the (flat) surface. The orientations of the substrates were for the growth experiments on the (100) substrates: (100)2°(011) and (100)2°$(01\bar{1})$; and for the (111)A substrates: (111)A2°$(11\bar{2})$

and (111)A2°($\bar{1}\bar{1}2$). The GaAs substrates were chromium-doped, semi-insulating, horizontal Bridgman (HB) grown and chemo-mechanically polished on one face. The accuracy of the misorientation angle was better than 0.5°, as specified by the supplier.

On these substrates undoped $In_xGa_{1-x}As$ epitaxial layers have been grown by low-pressure-MOVPE. Trimethylgallium (TMG), trimethylindium (TMI) and arsine (AsH_3) have been used as source materials. The growth temperature was 920 K. The ratio of arsine (V) and trimethylgallium and trimethylindium (III), the V/III ratio, at the entrance of the reactor was 125 for the growth on (100) substrates. For the growth on (111)A substrates the V/III ratio has been set to 80, because the anisotropy for growth on these surfaces increases with a decrease of the arsenic partial pressure [18, 19]. Under these conditions the growth hillocks at the surfaces of the epitaxial layers were hexagonally shaped. The samples were placed in the reactor in the area where under the growth conditions as described above the temperature and the flow profiles are fully developed [20] and return flows are present [21]. The vertical growth rate was *ca.* 0.5 nm/s. The total thicknesses of the $In_xGa_{1-x}As$ layers were below the critical layer thickness for the formation of misfit dislocations [22, 23], caused by the difference in lattice constant between the GaAs substrates and the $In_xGa_{1-x}As$ layers.

The indium concentration of completely unrelaxed epitaxial layers can be determined from photoluminescence spectra. The energy bandgap of the $In_xGa_{1-x}As$ layers is shifted with respect to that of GaAs by the indium concentration and by the biaxial stress, generated by the mismatch between $In_xGa_{1-x}As$ and GaAs. From the observed shift and the theoretical relations for the band gap shift, following from the deformation potential theory [24], the indium concentration has been calculated. For the cases of biaxial stresses, parallel to the (100) and (111) planes these relations are given in the appendix. The photoluminescence experiments have been performed at 4 K. The energy resolution of these measurements was better than 0.1 meV around the spectral range of the band gap of GaAs. In order to get a good fit between the measured bandgap shift and the indium concentration, also rocking curves were measured from several samples using high-resolution X-ray diffraction (HRXRD) [25]. From these curves the lattice constant of the epitaxial layer (and thus the indium content) can directly be calculated [26].

3.4 Results and discussion

In this section we discuss the results of the growth experiments on the (100) and (111)A surfaces. The observed incorporation behaviour is compared with studies, reported in the

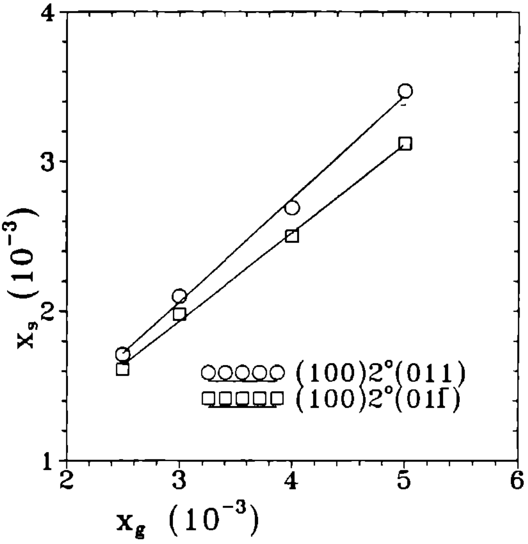

Figure 3.5 Indium concentration x_s in the $In_xGa_{1-x}As$ epitaxial layers grown on (100)2°(011) and (100)2°(01$\bar{1}$) GaAs substrates as a function of the relative gasphase concentration x_g of TMI.

literature, of the lateral growth rate at several step orientations by MOVPE and by MBE. Finally, the results are compared with the results of silicon incorporation experiments.

3.4.1 Growth on (100) faces

The results of the growth experiments on the (100) substrates are given in fig. 3.5. It is shown that the indium incorporation on the (100)2°(011) substrates (with kinked steps) is more efficient than on the (100)2°(01$\bar{1}$) surfaces (with stable steps). These results are in agreement with the expected behaviour discussed in section 3.2.

The results of indium incorporation experiments during growth of $In_xGa_{1-x}As$ on GaAs by MBE [11] have been found to be just opposite to the MOVPE results. During MBE-growth the incorporation of indium on (100)2°(011) is lower than on (100)2°(01$\bar{1}$) surfaces. This can be explained as follows.

Under normal MOVPE conditions the arsenic coverage of the surface steps is expected to be unity as a consequence of the large arsenic partial pressure in the gas phase [7]. The group III species are more easily incorporated at the step sites of the [011] steps than at the $[01\bar{1}]$ steps. This results in a higher lateral growth rate in the [011] direction as is observed by Asai [7] and by Van de Ven *et al.* [27]. The [011] step front is rough, since each growth unit at the step edge is directly incorporated. The $[01\bar{1}]$ step front is straight, only incorporation at kink sites is possible [28]. Decreasing the arsenic partial pressure leads to desorption of arsenic at the step edges. The arsenic coverage becomes less than unity, so the mechanisms as described above are not valid anymore. The arsenic coverage of the steps is strongly dependent on the orientation of the step. The desorption probability for an arsenic atom at the [011] step, where it has only one back bond, is higher than for an arsenic atom at the $[01\bar{1}]$ step, where it has two back bonds. Therefore the lateral growth rate of GaAs at the latter steps is hardly influenced by the arsenic partial pressure [7], in contrast to the [011] steps, which show a strong dependence. These assumptions are confirmed by Pukite *et al.* [29] and Massies *et al.* [30], who conclude from RHEED studies under arsenic poor conditions that surfaces misoriented in the $[01\bar{1}]$ direction have the highest kink density. Therefore the lateral growth rate [31] and the indium incorporation rate during MBE [11] in the $[01\bar{1}]$ direction are larger than in the [011] direction.

3.4.2 Growth on (111)A faces

The results of the $\mathrm{In}_x\mathrm{Ga}_{1-x}\mathrm{As}$ growth experiments on (111)A substrates are shown in fig. 3.6. Again it is observed that the incorporation efficiency of indium at kinked steps (in the $[\bar{1}\bar{1}2]$ direction) is higher than at stable steps (in the $[11\bar{2}]$ direction). These results are also in agreement with the described incorporation behaviour (section 3.2) and the experiments on (100) faces. No conclusion can be drawn whether the $[\bar{1}\bar{1}2]$ steps are reconstructed or not.

In the literature no results of growth experiments on (111)A substrates have been reported, which can directly be compared to the results obtained from the $\mathrm{In}_x\mathrm{Ga}_{1-x}\mathrm{As}$ growth experiments.

3.4.3 Comparison with silicon incorporation experiments

The results of the growth experiments as described in the preceding section have been explained by looking at the incorporation possibilities at the group III sublattice. Since indium is an isoelectronic dopant in GaAs, the indium content in the epitaxial layers was described as the result of a competition between gallium and indium species for

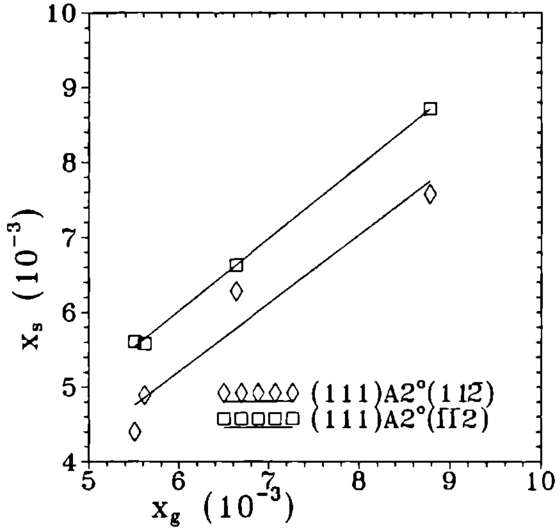

Figure 3.6 Indium concentration x_s in the $In_xGa_{1-x}As$ epitaxial layers grown on (111)A2°(11$\bar{2}$) and (111)A2°($\bar{1}\bar{1}$2) GaAs substrates as a function of the relative gas phase concentration x_g of TMI.

reaching the kink sites. Silicon is an amphoteric dope element in GaAs, which can be built in both at gallium and at arsenic sites. During growth incorporation of silicon takes place at both the sublattices. In chapter 2 it has been shown that the net carrier concentration and the compensation ratio in silicon-doped GaAs is influenced by the direction of the misorientation [6]. An explanation of these results has been given by taking both the incorporation reactions at the group III and at the group V sublattices into consideration. In this section a comparison of the $In_xGa_{1-x}As$ and silicon-doped GaAs growth experiments is given.

Silicon-doped GaAs (100) epilayers have a higher net carrier concentration and a lower compensation ratio for the samples with (100)2°(011) orientation than for the (100)2°(01$\bar{1}$) oriented samples. The steps in the [011] direction on the (100) surface are kinked for the group III lattice sites, but when they are saturated with gallium they are stable. Also in this situation the observed higher incorporation of silicon on gallium sites is due to the trapping-like incorporation behaviour on this sublattice. The growth at the [01$\bar{1}$] steps takes place at the few kink sites along the steps. To get incorporated silicon growth species have to diffuse along the steps to the kink sites, which belong alternatingly to the group III and the group V sublattice. Therefore the incorporation of silicon at the gallium sites at this step is lower than at the [011] step, which is in accordance with the observations These results support the In$_x$Ga$_{1-x}$As experiments, where only the differences on the group III sites have been considered.

For the (111)A surfaces no clear influence of the step direction on the carrier concentration was observed in the silicon experiments, even in the case of a low V/III ratio. Apparently, for silicon the incorporation possibilities at the group III and the group V sites under these conditions were the same, at the kinked as well as at the stable steps At the sites of the fully kinked steps at the (111)A2°$(\bar{1}\bar{1}2)$ samples a double bond can be formed at both the sublattices. At the $[11\bar{2}]$ (stable) steps only at a specific kink site on the group III sublattice along the step a double bond can be formed. The newly incorporated atom forms a new kink site on the group V sublattice. This site is the only possibility for an arsenic or silicon species to be trapped at this sublattice, since it is assumed that the other arsenic-sites are occupied. Due to the higher bond strength of Si-Ga (202 kJ/mol) and of Si-As (231 kJ/mol) with respect to Ga-As (164 kJ/mol) no difference in silicon incorporation at stable and kinked steps could be observed, as it was possible for indium.

3.5 Summary and conclusions

It has been shown that the incorporation process of indium during MOVPE of In$_x$Ga$_{1-x}$As on vicinal surfaces can be described by considering the steps as stable or kinked. At kinked steps the growth components can be incorporated at any step site, whereas at stable steps this is only possible at specific kink sites at the steps. It was found for (100) surfaces that the atomic step configurations under high arsenic partial pressures determine which of these mechanisms is active. The results of the growth experiments on (100) and on (111)A vicinal surfaces indicate that the indium incorporation efficiency is higher at kinked steps than at stable steps.

A comparison of indium incorporation with silicon has been made Since it is possible for silicon to be built in both at group III and at group V sites, the results of the In$_x$Ga$_{1-x}$As and the silicon-doped GaAs growth experiments complement each other For the (100) surface similar results have been obtained with silicon and indium. The silicon incorporation on (111)A differs from the results obtained with indium. It appears that during MOVPE growth the incorporation possibilities for silicon at both the sublattices are the same, both at the fully kinked as well as at the stable steps.

Acknowledgements

The authors would like to thank S.M. Olsthoorn for performing the photoluminescence experiments and Dr. A.J. Kinneging (Philips Research Laboratories, Eindhoven) and A.H. Goemans (Philips Semiconductors, Nijmegen) for the HRXRD-results.

3.A Appendix

In order to determine the shift of the PL-spectrum of biaxially strained $In_xGa_{1-x}As$ epilayers with respect to that of GaAs as a function of the indium concentration x two effects have to be taken into account. Firstly, the bandgap of $In_xGa_{1-x}As$ with respect to that of GaAs changes as a function of x. At a temperature of 4 K this change is given by [32]:

$$\Delta E_g(x) = -1.5837x + 0.475x^2. \tag{3.A.1}$$

Secondly, the energy bandgap in semiconductor materials is changed by elastic strains. A biaxial strain in an epitaxial layer, resulting from the lattice mismatch with the substrate, breaks up the degeneracy of the valence band. The relation between the elastic strain and the indium content is given by:

$$\epsilon = \frac{a_e - a_x}{a_x}, \tag{3.A.2}$$

in which a_e is the lattice constant of the strained epilayer parallel to the substrate and a_x is the lattice constant of the completely relaxed $In_xGa_{1-x}As$ epilayer. Using Vegard's law a_x can be calculated as a function of x:

$$a_x = (1-x)a_{\mathrm{GaAs}} + x a_{\mathrm{InAs}}. \tag{3.A.3}$$

In the case of coherently strained epitaxial layers a_e equals the lattice constant of the substrate a_s.

The bandgap shift is described by the deformation potential theory [33, 34]. The relations for the transition between the conduction band and the heavy-hole and the light-hole valence band at $\vec{k} = 0$ as a function of the strain ϵ are given in a first order approximation by [24]:

$$\Delta(E_c - E_{\mathrm{lh}}) = \delta E_{\mathrm{H,n}} - \delta E_{\mathrm{S,n}}, \tag{3.A.4}$$

$$\Delta(E_c - E_{\mathrm{hh}}) = \delta E_{\mathrm{H,n}} + \delta E_{\mathrm{S,n}}, \tag{3.A.5}$$

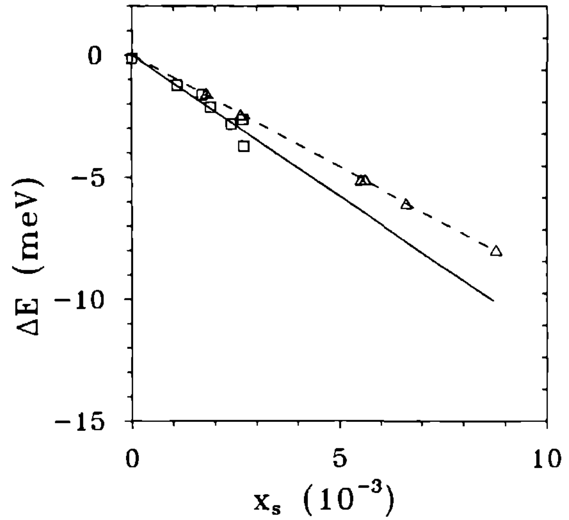

Figure 3.A.1 Shift of the PL-spectrum of biaxially strained $\mathrm{In}_x\mathrm{Ga}_{1-x}\mathrm{As}$ epilayers as a function of the indium content, measured with HRXRD. The (100) oriented samples are indicated by squares, the (111)A oriented samples by triangles.

in which:

$$\delta E_{\mathrm{H,n}} = a(2-\lambda_{\mathrm{n}})\epsilon, \tag{3.A.6}$$

$$\delta E_{\mathrm{S,100}} = b(1+\lambda_{100})\epsilon, \tag{3.A.7}$$

$$\delta E_{\mathrm{S,111}} = (d/2\sqrt{3})(1+\lambda_{111})\epsilon, \tag{3.A.8}$$

(3.A.9)

with

$$\lambda_{100} = \frac{2c_{12}}{c_{11}}, \tag{3.A.10}$$

$$\lambda_{111} = \frac{2(c_{11}+2c_{12}-2c_{44})}{(c_{11}+2c_{12}+4c_{44})}, \tag{3.A.11}$$

a, b and d are the deformation potentials and c_{ij} are the elastic stifness constants. In the case of compressively strained layers, where ϵ is negative, the bandgap is given by the transition between the conduction band and the light hole valence band. In fig. 3.A.1 the shifts of the PL-spectra with respect to that of GaAs as a function of the indium content x_s in the epilayer, determined from HRXRD-data, are shown. From these results we obtain for bandgap shift:

$$\Delta(E_c - E_{hh})_{100} = -1.16 \times 10^{-3} x \text{ (meV)} \tag{3.A.12}$$

$$\Delta(E_c - E_{hh})_{111} = -0.92 \times 10^{-3} x \text{ (meV)}, \tag{3.A.13}$$

which is in fairly good agreement with the literature data [32, 35]:

$$\Delta(E_c - E_{hh})_{100} = -1.17 \times 10^{-3} x \text{ (meV)} \tag{3.A.14}$$

$$\Delta(E_c - E_{hh})_{111} = -0.84 \times 10^{-3} x \text{ (meV)}. \tag{3.A.15}$$

References

[1] M.J. Ludowise, J. Appl. Phys. **58** (1985) R31, and references therein.

[2] P.J.A. Thijs, E.A. Montie and T. van Dongen, J. Crystal Growth **107** (1991) 731.

[3] L.J. Giling and W.J.P. van Enckevort, Surface Sci. **161** (1985) 567.

[4] P. Hartman and W.G. Perdok, Acta Cryst. **8** (1955) 49, 521; Proc. Koninkl. Ned. Acad. Wetenschap. **B60** (1952) 134.

[5] P. Hartman, in: Crystal Growth: An Introduction, Ed. P. Hartman (North-Holland, Amsterdam, 1973) pp. 358-402.

[6] X. Tang, J. te Nijenhuis, Y. Li and L.J. Giling, J. Crystal Growth **107** (1991) 263, this thesis, chapter 2.

[7] H. Asai, J. Crystal Growth **80** (1987) 425.

[8] T. Dosluoglu, U. Sudarsanand and R. Solanki, J. Crystal Growth **106** (1990) 643.

[9] N. Kobayashi, J.L. Benchimol, F. Alexandre and Y. Gao, in: Proc. Int. Symp. GaAs and Related Compounds, Heraklion, Greece, 1987, Inst. Phys. Conf. Ser. **91**, Ed. A. Christou and H.S. Rupprecht (Inst. Phys., London-Bristol, 1988) p. 175.

[10] J.-P. Reithmaier, H. Reichert, H. Schlötterer and G. Weimann, J. Crystal Growth **111** (1991) 407.

[11] T. Suzuki and T. Nishinaga, J. Crystal Growth **111** (1991) 173.

[12] M.T. Emeny, L.K. Howard, K.P. Homewood, J.D. Lambkin and C.R. Whitehouse, J. Crystal Growth **111** (1991) 413.

[13] R.Z. Bachrach, R.S. Bauer, P. Chiaradia and G.V. Hansson, J. Vacuum Sci. Technol. **18** (1981) 797.

[14] L.J. Giling and M.H.J.M. de Croon, J. Crystal Growth **107** (1991) 56.

[15] S.Y. Tong, W.N. Mei and G. Xu, J. Vacuum Sci. Technol. **B2** (1984) 393.

[16] H.H.C. de Moor, Ph.D. thesis, University of Nijmegen, The Netherlands (1987), ch. 7.

[17] W.J.P. van Enckevort and L.J. Giling, J. Crystal Growth **45** (1978) 90.

[18] S. Fuke, M. Umemura, N. Yamada, K. Kuwahara and T. Imai, J. Appl. Phys. **68** (1990) 97.

[19] T. Nishizawa and M. Kimura, J. Crystal Growth **74** (1986) 331.

[20] J. van de Ven, G.M.J. Rutten, M.J. Raaijmakers and L.J. Giling, J. Crystal Growth **76** (1986) 352.

[21] E.P. Visser, C.R. Kleijn, C.A.M. Govers, C.J. Hoogendoorn and L.J. Giling, J. Crystal Growth **94** (1989) 929.

[22] J.W. Matthews and A.E. Blakeslee, J. Crystal Growth **27** (1974) 118.

[23] J. te Nijenhuis, H.F.J.M. van Well, M.M.G. Bongers and L.J. Giling, J. Appl. Phys. (submitted), this thesis, chapter 7.

[24] F.H. Pollak, in: Semiconductors and Semimetals, Eds. R.K. Willardson and A.C. Beer, Vol. 32 Strained-Layer Superlattices Physics, Vol. Ed. T.P. Pearsall (Academic Press, New York,

1990) ch. 2.

[25] W.J. Bartels, J. Vacuum Sci. Technol. **B1** (1983) 338.

[26] J. Hornstra and W.J Bartels, J. Crystal Growth **44** (1978) 513.

[27] J. van de Ven, J.L. Weyher, H. Ikink and L.J. Giling, J. Electrochem. Soc. **134** (1987) 989.

[28] T. Fukui and H. Saito, J. Vacuum Sci. Technol. **B6** (1988) 1373.

[29] P.R. Pukite, G.S. Petrich, S. Batra and P.I. Cohen, J. Crystal Growth **95** (1989) 269.

[30] J. Massies, C. Deparis, C. Neri, G. Neu, Y. Chen, B. Gil, P. Auvray and A. Regreny, Appl. Phys. Letters **55** (1989) 2605.

[31] M. Kawabe and T. Sugaya, Japan. J. Appl. Phys. **28** (1989) L1077.

[32] Landolt-Börnstein, Group III, Vol. 22a, Physics of the group IV Elements and III-V Compounds (Springer, Berlin, 1982).

[33] G.E. Pikus and G.L. Bir, Sov. Phys. Solid State **1** (1959) 136.

[34] G.E. Pikus and G.L. Bir, Sov. Phys. Solid State **1** (1960) 1502.

[35] A.R. Goñi, K. Strössner, K. Syassen and M. Cardona, Phys. Rev. B **36** (1987) 1581.

Chapter 4

Critical layer thickness of GaAs grown by metalorganic vapour phase epitaxy on $In_xGa_{1-x}As$

Abstract

In this chapter a study of strain and relaxation in GaAs layers grown by metalorganic vapour phase epitaxy on indium-alloyed GaAs substrates with indium contents between 0.1 % and 1.15 % is reported. The experimentally determined critical layer thickness for the formation of misfit dislocations in the GaAs layers are compared with theoretical calculations of the change of the Gibbs free energy of the epilayer, containing a half loop dislocation, which has released a certain amount of elastic energy. A good matching between theory and experiments has been obtained, even in the region of very small misfits. The shift of the bandgap energy as induced by the strain in the epilayer is given by the deformation potential theory. These shifts have been measured using photoluminescence at liquid helium temperatures. It appears from these measurements that for layers grown beyond the critical thickness the amount of relaxation is determined by the theoretical equilibrium between elastic deformation and the formation of misfit dislocations.

4.1 Introduction

Strained semiconductor heterostructures, *e.g.* GaAs/$In_xGa_{1-x}As$ and $Si_{1-x}Ge_x$/Si, are important from a fundamental as well as a technological point of view. Such structures offer new electrical and optical properties compared with lattice matched devices [1]-[3]. It is even possible to take advantage of the misfit dislocations, created by the strain, for the operation of field effect transistors [3].

The strain in these structures is a result of the lattice mismatch f between the substrate (lattice constant a_s) and the growing epitaxial layer (lattice constant a_o).

$$f = \frac{a_s - a_o}{a_o}, \tag{4.1}$$

The strain can be either tensile ($a_s > a_o$, like in GaAs on $In_xGa_{1-x}As$) or compressive ($a_s < a_o$, like in $In_xGa_{1-x}As$ on GaAs). In thin layers the misfit will be accommodated by elastic deformation of the epilayer. The growth of the layer is pseudomorphic, the lattice of the epilayer parallel to the interface will be strained in order to fit the substrate lattice. When the thickness of the layer is larger than a certain critical layer thickness, the growth ceases to be pseudomorphic and the strained layer will relax by the formation of misfit dislocations at the interface. Both the strain and the misfit dislocations have a strong influence on the electric and optical material properties [4]-[7].

To study the effect of strain and relaxation one usually uses a substrate with a fixed lattice constant and epilayers with varying chemical compositions and lattice constants. For instance, in the systems $In_xGa_{1-x}P$ grown on GaAs by vapour phase epitaxy (VPE) [4] and liquid phase epitaxy (LPE) [5] and $In_xGa_{1-x}As$ on InP [6] the variation of the electro-optical properties is caused by the changed chemical composition as well as by the strain. However, in these systems there are two intrinsic disadvantages: (*i*) one has to know the composition of the grown layer exactly in order to separate the contribution of the strain and of the misfit dislocations to the change of the material properties from the contribution of the alloy and (*ii*) the physical and mechanical parameters of the totally relaxed alloys are not always known. Therefore, approximate values obtained from interpolation by assuming linear behaviour have to be used for comparison between theory and experiment.

In this chapter on heteroepitaxial systems, these difficulties have been avoided by using (100) $In_xGa_{1-x}As$ substrates with known amounts of indium upon which a layer of undoped GaAs is grown. In this system the uncertainty of the chemical composition of the epilayer is eliminated, because a binary compound semiconductor is grown instead of a ternary or even a quaternary alloy. Therefore the chemical composition of the epilayer is known exactly. Changes in morphology and electro-optical properties of the epilayer compared to one grown by conventional GaAs-homoepitaxy are now only a consequence of the strain and the misfit dislocations in the epilayer and not of the changed chemical composition.

In the literature the growth of GaAs by molecular beam epitaxy (MBE) and MOVPE on indium-alloyed GaAs [8]-[13] is mentioned. However, a precise determination of the critical layer thickness of epitaxially grown GaAs has not been given. The aim of this chapter is to compare the experimental strain in the epitaxial layer and the critical layer thickness for GaAs on $In_xGa_{1-x}As$ with that determined by several models.

4.2 Experimental details

In this study (100) $In_xGa_{1-x}As$ liquid encapsulated Czochralski-grown (LEC) substrates [14], as obtained from LETI, Grenoble, France, have been used. The amounts of indium in the substrates have been measured by inductively-coupled plasma atomic emission spectroscopy (ICPAES) [15]. The indium concentrations ranged from 0.1% to 1.15% and have been determined with an accuracy of 10^{-4}. These concentrations lead to lattice mismatches up to 8×10^{-4}. The local variation in indium content in these substrates was *ca.* 1-2% [14]. The dislocation density is $\leq 10^4$ cm^{-2} [16]. The epitaxial GaAs layers have been grown in a low-pressure MOVPE reactor system. Trimethylgallium (TMG) and arsine (AsH_3) have been used as precursors. The ratio of the arsine and TMG (the V/III ratio) at the entrance of the reactor was 125. The growth temperature was 913 K. The growth rate was *ca.* 0.44 nm/s. For a comparison with GaAs homoepitaxy (100)2°(110) horizontal Bridgman (HB) GaAs substrates, were also placed in the reactor in the same growth experiments.

The morphology of the grown layers has been observed with an interference-contrast (IC) microscope. The thickness of the layers has been measured in a scanning electron microscope (SEM) after cleaving and etching. The thicknesses ranged from 0.4 μm to 6 μm.

To determine the band gap energy, photoluminescence (PL) spectra have been recorded at liquid helium temperatures (4 K) with an energy resolution better than 0.1 meV around the spectral range of the band gap of GaAs. Shifts of the exciton spectrum have been

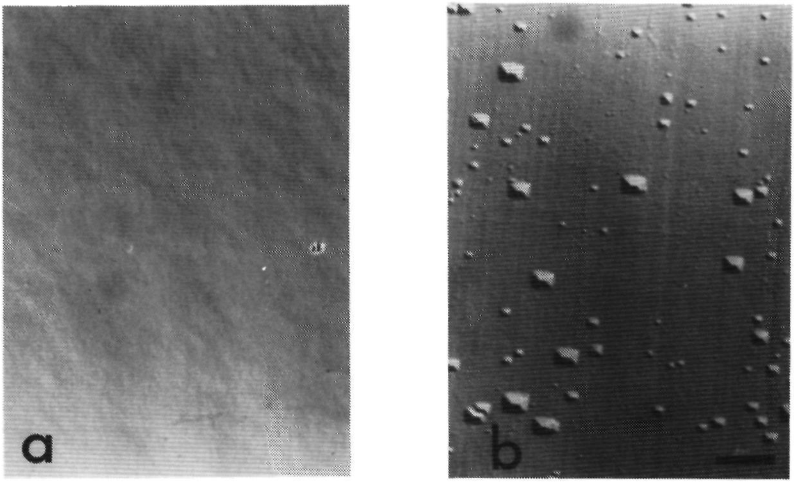

Figure 4.1 Surface morphologies of as-grown GaAs epilayers of a) 0.4 μm and b) 4.4 μm thickness on $In_{0.008}Ga_{0.992}As$. The bar indicates 20 μm.

measured by comparing spectra with the (unstrained) GaAs spectrum.

4.3 Results and discussion

4.3.1 Strain and relaxation

The relative strain in the epilayer ϵ is defined in the same way as the lattice mismatch f (eq. 4.1):

$$\epsilon = \frac{a_e - a_o}{a_o}, \tag{4.2}$$

in which a_e is the lattice constant of the strained epilayer parallel to the substrate. From this definition it follows that the strain is positive for a system which is under tensile stress and negative for compressively stressed systems. In the case the misfit is accommodated only by elastic deformation a_e equals a_s, and therefore $f = \epsilon$. Samples grown under this condition show a specular surface (fig. 4.1a). When the layers are grown beyond a certain critical layer thickness the misfit is also accommodated by dislocations at the interface.

The relation between the mismatch and the strain is now given by $f = \epsilon + \delta$, in which δ is the amount of plastic deformation. On the surface of these layers a cross-hatched pattern is observed, as shown in fig. 4.1b. These patterns are attributed to the presence of misfit dislocations at the interface [17]. Compressively stressed layers show similar surfaces. A more detailed discussion on surface morphologies of both layers under tensile and under compressive stress is given in chapter 6 [18].

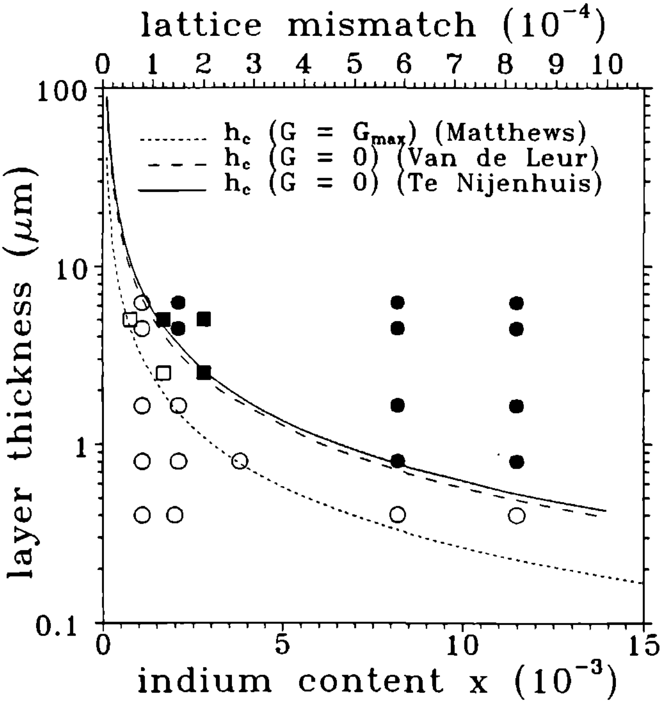

Figure 4.2 The tensile stress system: Calculated critical layer thickness as a function of the indium content x in the $In_xGa_{1-x}As$ substrates (lower scale) and the mismatch f (upper scale), according to refs. [19]-[21]. Filled and open symbols indicate samples with and without misfit dislocations . Circles are samples as described in this work. Squares are data obtained from ref. [8].

To compare the observed critical layer thickness with theory, we have assumed spontaneous nucleation of half loop dislocations in the epilayer. From calculations of the change of the Gibbs free energy ΔG of a layer containing a half loop dislocation, which has released a certain amount of elastic energy, the critical layer thickness is determined as a function of the lattice mismatch. This theory assumes that the misfit dislocations are 60° dislocations along the $\langle 110 \rangle$ directions in a $\{111\}$ glide plane in diamond-like crystals. Originally this theory was developed by Matthews [19] who defined the critical layer thickness as that thickness for which ΔG is at a maximum. Van de Leur *et al.* [20] introduced the energy balance model. In this theory the thickness for which $\Delta G = 0$ is defined as the critical layer thickness. A more realistic relaxation model for both epilayers under tensile and under compressive stress in which extended V-shaped dislocations nucleate, is proposed in chapter 7 [21]. The results of the calculations of the critical layer thickness predicted by these theories are shown in fig. 4.2. In this figure also the results of the growth experiments are given, together with the results from Inoue *et al.* [8]. However, in the latter paper no growth conditions of the epilayer are mentioned, nor are the layer thicknesses measured precisely. It appears that layers containing misfit dislocations lie above the theoretical curves, obtained from refs. [20, 21], while the unrelaxed layers lie under it. The energy balance models [20, 21] give a very good match between theory and experiment, even in the region of very small misfits in which the elastic energy, *i.e.* "the driving force" for the formation of misfit dislocations is very small.

4.3.2 Bandgap energy shifts

The biaxial stress generated by the lattice mismatch breaks up the degeneracy of the valence band [5], which shifts the effective bandgap energy. This shift can clearly be observed in PL spectra taken on various samples with increasing indium content in their substrates (fig. 4.3). The calculated bandgap energy shifts for the light hole and the heavy hole valence band at $\vec{k} = 0$ induced by strain are given by:

$$\Delta(E_c - E_{lh}) = \left\{ 2a\left(\frac{c_{11} - c_{12}}{c_{11}}\right) - b\left(\frac{c_{11} + c_{12}}{c_{11}}\right)\right\}\epsilon, \tag{4.3}$$

$$\Delta(E_c - E_{hh}) = \left\{ 2a\left(\frac{c_{11} - c_{12}}{c_{11}}\right) + b\left(\frac{c_{11} + c_{12}}{c_{11}}\right)\right\}\epsilon, \tag{4.4}$$

where c_{ij} are the elastic stiffness coefficients, and a and b are constants obtained from the deformation potential theory [22, 23]. Using the values as given in refs. [24, 25] it follows for GaAs:

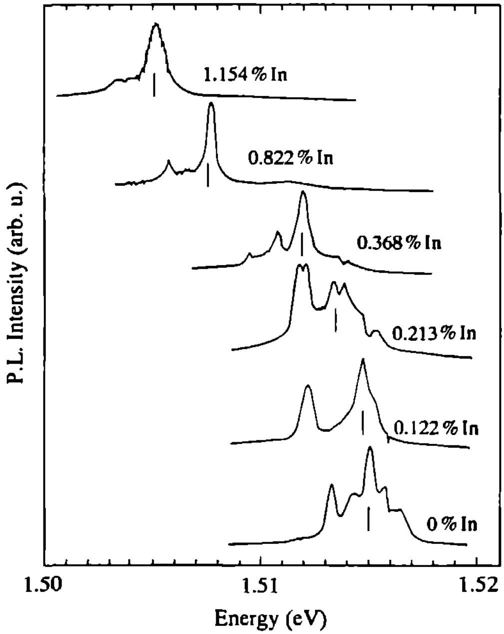

Figure 4.3 PL spectra of GaAs grown on $In_xGa_{1-x}As$ substrates with various indium contents x. The layer thickness of all samples is below the critical layer thickness. The vertical bars indicate the position of the neutral donor-bound exciton transitions.

$$\Delta(E_c - E_{lh}) = -5.84\epsilon \ (eV), \tag{4.5}$$

$$\Delta(E_c - E_{hh}) = -12.35\epsilon \ (eV). \tag{4.6}$$

It follows that $\Delta(E_c - E_{hh})$ has a stronger shift than $\Delta(E_c - E_{lh})$. For systems which are under tensile stress, *i.e.* in the case that ϵ is positive, the bandgap will be between the conduction band and the heavy hole valence band and decreases with increasing strain (see fig. 4.3). Because the bandgap energy is not directly measured in PL experiments, it is assumed that the shift of the exciton spectrum gives a good approximation for the shift of the band gap. This assumption is justified since the change of the exciton binding energy with strain is expected to be very small. Fig. 4.4 shows PL spectra as a function of layer thickness. An increasing layer thickness induces an increase of the misfit dislocation density and thus a decrease of strain in the layers. This explains the shift of the PL spectra

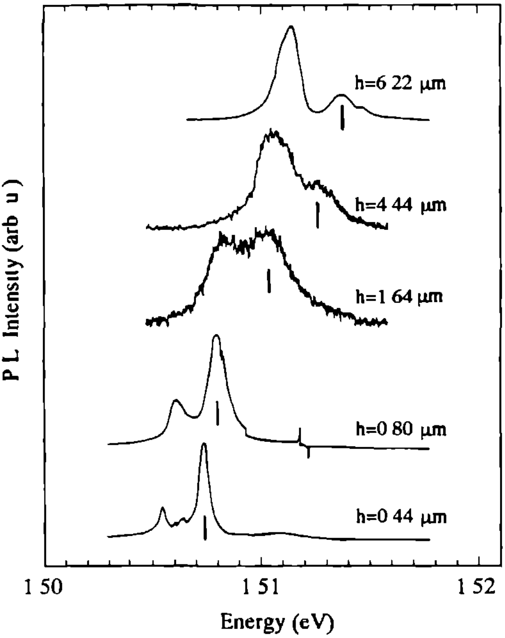

Figure 4.4 PL spectra of GaAs grown on $In_xGa_{1-x}As$ as a function of layer thickness h The indium content x of all substrates is 0 82% The vertical bars indicate the position of the neutral donor-bound exciton transitions

in fig 4 4 towards higher energy. From fig. 4.4 and eq (4 6) it is possible to determine the amount of relaxation in the epilayer. The resulting strain as measured from these PL experiments as a function of layer thickness is shown in fig 4.5. For thin layers the strain ϵ is equal to the lattice mismatch f. For layers with thicknesses larger than the critical value, the strain has only been relieved partially The residual strain of the layer equals the value of the mismatch for which the layer thickness is critical Fig 4 5 again illustrates that both models [20, 21] give a good agreement with the experiments. Since the theories are developed for the formation of the first misfit dislocation, it is concluded that in the observed region of very small misfits the nucleation process is not influenced by the presence of already extant misfit dislocations Post-growth annealing for 200 minutes at 973 K under arsenic pressure does hardly change the amount of relaxation. These results indicate that the GaAs layers already reach the predicted equilibrium during growth, which is in agreement with results on $In_xGa_{1-x}As$ samples grown by MBE on GaAs [26, 27]

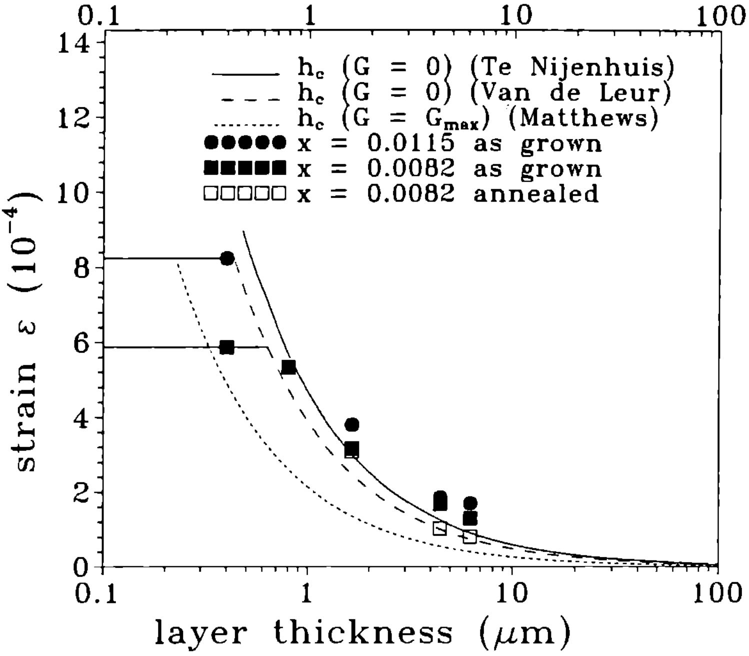

Figure 4.5 Strain in the epilayer as a function of layer thickness *h*. For thin layers, which are not relaxed by misfit dislocations, the strain is equal to the lattice mismatch *f*. When the layer thickness is larger than the critical value h_c, the misfit dislocations release the strain until it has reached the value of the mismatch for which the layer thickness is critical.

4.4 Summary and conclusions

It has been shown that the epilayer-substrate system with a fixed layer composition indeed is a good system to observe the effects of strain and relaxation on the electro-optical properties without any influence of change in chemical composition. The experimentally determined critical layer thickness for the formation of misfit dislocations in GaAs under tensile stress is in good agreement with the energy balance model in the region of very small misfit. No complete relaxation has been found, neither after growth nor after annealing. The remaining strain in the layers is also described by the equilibrium between elastic deformation and the formation of misfit dislocations. The nucleation of misfit dislocations is not influenced by the presence of extant dislocations.

Acknowledgements

Dr. A. Chabli from LETI is acknowledged for kindfully supplying the InGaAs substrates as are S.M. Olsthoorn and F.A.J.M. Driessen for performing the photoluminescence experiments.

References

[1] G C. Osbourn, Phys. Rev. B **27** (1983) 5126.

[2] R. People, IEEE J. Quantum Electron. **QE-22** (1986) 1696.

[3] P. Chau, K. Mirchandani and S. Mil'shtein, Proceedings of the 20th International Conference on the Physics of Semiconductors, Thessaloniki, 1990, Eds. E.M. Anastassakis and J D. Joannopoulos (World Scientific, Singapore, 1990), p. 1665.

[4] G.H. Olsen, C.J. Nuese and R.T. Smith, J. Appl. Phys. **49** (1978) 5523.

[5] H. Asai and K. Oe, J. Appl. Phys. **54** (1983) 2052.

[6] C.P. Kuo, S.K. Vong, R.M. Cohen and G.B Stringfellow, J. Appl Phys. **57** (1985) 5428, and references therein.

[7] J.M. Woodall, G.D. Pettit, T.N. Jackson, C. Lanza, K.L. Kavanagh and J.W Mayer, Phys. Rev. Lett **51** (1983) 1783.

[8] T. Inoue, S. Nishine, M. Shibata, T. Matsutomo, S. Yoshitake, Y. Sato, T. Shimoda and K. Fujita, Inst. Phys. Conf. Ser. **79** (1986) 7.

[9] M. Morioka, T Mishima, K. Hiruma, Y. Katayama and Y. Shiraki, Inst. Phys Conf Ser. **79** (1986) 121.

[10] M. Shinohara, T. Ito and Y. Imamura, J. Appl. Phys. **58** (1985) 3449.

[11] M Shinohara, T. Ito, K. Yamada and Y. Imamura, Jpn. J. Appl. Phys. **24** (1985) L711.

[12] H. Takeuchi, M. Shinohara and K. Oe, Jpn. J. Appl. Phys **25** (1986) L303.

[13] T. Imai, S Fuke, K. Mori and K. Kuwahara, Appl. Phys. Lett. **54** (1989) 816.

[14] E. Molva, Ph. Bunod, F. Roturier, A. Chabli, F. Bertin, J P Leludec and P. Larnaudie, Semi-Insulating III-V Materials, Malmo, 1988, Eds. G. Grossmann and L. Ledebo (Hilger, Bristol, 1988), p. 565.

[15] See *e.g.* Inductively coupled plasma in analytical atomic spectrometry, Eds A. Monpaser and D W. Golightly (VCH Publishers, Weinheim, 1987).

[16] A. Chabli, E. Molva, A.George, F. Bertin, P. Bunod and J. Blétry, Proceedings of the Electronic Materials Research Society Meeting, Strasbourg, 1986

[17] M.S. Abrahams, J. Blanc and C.J. Buiocchi, Appl Phys. Lett. **21** (1972) 185.

[18] J. te Nijenhuis, P.J. van der Wel, E.R.H. van Eck and L.J Giling, submitted to J. Appl. Phys., this thesis, chapter 6.

[19] J.W. Matthews, in: Epitaxial Growth, Part B, Ed. J.W. Matthews, (Academic Press, New York, 1975).

[20] R.H.M. van de Leur, A.J.G. Schellingerhout, F. Tuinstra and J.E. Mooij, J. Appl Phys. **64** (1988) 3043.

[21] J. te Nijenhuis, H.F J.M van Well, M M.G. Bongers and L.J. Giling, submitted to J. Appl. Phys., this thesis, chapter 7.

[22] F H. Pollak and M. Cardona, Phys. Rev. **172** (1968) 816.

[23] A. Gavini and M. Cardona, Phys Rev B **1** (1970) 672.

[24] Landolt-Bornstein, Group III, Vol 17a, Physics of the Group IV Elements and III-V Compounds (Springer, Berlin, 1982).

[25] A R. Goñi, K. Strossner, K. Syassen and M. Cardona, Phys. Rev. B **36** (1987) 1581.

[26] A.V. Drigo, A. Aydinli, A. Carnera, F. Genova, C. Rigo, C. Ferrari, P. Franzosi and G. Salviati, J. Appl. Phys. **66** (1989) 1975

[27] P M J. Marée, J.C Barbour, J.F. van der Veen, K.L. Kavanagh, C.W.T. Bulle-Lieuwma and M.P A Viegers, J. Appl. Phys. **62** (1987) 4413

Chapter 5

High spatial resolution photoluminescence studies on misfit dislocations in lattice mismatched III-V heterostructures

Abstract

The effect of misfit dislocations on the electro-optical behaviour of strained III-V heterostructures has been studied by high-resolution spatially resolved photoluminescence imaging. Epitaxial layers under tensile stress (in this study GaAs on $In_xGa_{1-x}As$) as well as layers under compressive stress ($In_xGa_{1-x}As$ on GaAs) have been examined. Dislocation lines in both $\langle 011 \rangle$ directions have been observed in both systems. In contrast to the compressively strained layers, where no as-grown asymmetry is observed, the dislocations in the layers under tensile stress have been preferably formed in the $[01\bar{1}]$ direction. This is explained by assuming (*i*) that the relaxation of the strained layer is initiated by the nucleation of the most mobile dislocation in GaAs, which is the arsenic glide As(g) dislocation, and (*ii*) that cross slip of these As(g) dislocations is only possible in compressively strained layers. Photoluminescence imaging reveals the presence of many non-radiative deep levels around the dislocation lines and also shows an opto-electronic asymmetry of the two $\langle 011 \rangle$ directions for both systems, in contrast to the as-grown morphology. For the layers under compressive stress this is explained by the difference in depletion between the dislocation lines along the $[011]$ direction, of which the core is believed to consist of gallium atoms, and those along the $[01\bar{1}]$ direction, formed with arsenic atoms. For layers under tensile stress, just the opposite holds. Diluted Sirtl-like etching with the use of light confirms the results obtained with photoluminescence imaging.

5.1 Introduction

The relaxation of layers under tensile stress by the formation of misfit dislocations and the critical layer thickness for GaAs/$In_xGa_{1-x}As$ system have been discussed in chapter 4. This chapter deals with the microscopic effect of misfit dislocations on the opto-electronic properties of layers both under tensile and compressive stress.

In (100) oriented layers of III(A)-V(B) compounds the misfit dislocations are distributed in the two orthogonal $\langle 011 \rangle$ directions [1, 2]. They are expected to be 60° dislocations in $\{111\}$ planes with their Burgers vectors along the $\langle 110 \rangle$ directions. They belong to the glide set (g) if their motion leads to shear within the $\{111\}$ slice, or to the shuffle set (s) if the shear is between two (widely spaced) $\{111\}$ slices [3]. The dislocations are of type A or B depending on whether the A or B atoms are in the most distorted core positions [4]. In the zincblende structure this means that this dislocation core consists of a line of vacancies of A or B atoms respectively. The atoms of which there is an excess in the core contain the dangling bonds. The short notations of the four possible dislocation types are A(s) and B(s) for the dislocations of the shuffle set and A(g) and B(g) for those belonging to the glide set.

The microscopic effect of misfit dislocations in semiconductors can be analysed by several spatially resolved techniques such as diluted Sirtl-like etching with the use of light (DSL), electron beam induced current (EBIC), optical beam induced current (OBIC), transmission electron microscopy (TEM), X-ray topography (XRT), laser scattering tomography (LST), cathodoluminescence (CL) and photoluminescence (PL) [5]-[7]. Spatially resolved photoluminescence (PL) is used in these studies to examine misfit dislocations. A review of the usefulness of PL imaging is given in ref. [8].

Both the GaAs on $In_xGa_{1-x}As$ system (with a lattice mismatch between 1.5×10^{-4} and 8.3×10^{-4}) as well as the $In_xGa_{1-x}As$ on GaAs system (with a lattice mismatch between -3.8×10^{-4} and -13×10^{-4}) have been studied by spatially resolved high resolution PL imaging before and after DSL etching. A different PL behaviour for the dislocations in the two possible orthogonal directions is reported. To our knowledge this is the first time that PL imaging has been used to observe microscopic influences of misfit dislocations on the opto-electronic behaviour of the epitaxial layer. An explanation in terms of the different cores of the dislocations is given.

5.2 Experimental details

The growth of the layers under tensile stress on $In_xGa_{1-x}As$ substrates, has already been described in chapter 4. The compressively strained undoped $In_xGa_{1-x}As$ layers have been grown in a low-pressure metalorganic vapour phase epitaxy (LP-MOVPE) reactor system on semi-insulating (100) GaAs horizontal Bridgman (HB) substrates from MCP, UK. The indium concentrations in the $In_xGa_{1-x}As$ epilayers varied from 0.5% to 2.5% and the thicknesses ranged from 1.2 μm to 6 μm. Both the samples under tensile and compressive stress were n-type due to the residual impurities.

The spatially resolved PL experiments have been performed in a liquid-helium bath cryostat. Both the translation mechanism and the focusing microscope objective operate in the cryostat at 4.2 K. The lateral resolution of the PL imaging was determined experimentally to be 1 μm [9]. Details of the apparatus have been described in ref. [9].

Five samples of each system, *i.e.* under tensile and compressive stress, have been examined by PL imaging. Some of the samples have been investigated as-grown, in order to rule out the effects of the etch process on the PL results. As there appeared to be no differences between the PL results before and after etching, the samples have been DSL photo-etched [10] before the PL imaging has been performed in order to reveal the misfit dislocations more clearly. The morphology of the samples has been investigated with an interference-contrast microscope. Some of the sample surfaces have been examined with a phase-shifting interferometer in order to measure the height differences. The PL mappings have been recorded at the wavelength corresponding to the P-band transition. This transition is a result of exciton-exciton scattering processes and is characteristic of the high excitation density used in our experiments (typically 150 kW/cm^2) [11]. The band-acceptor and donor-acceptor transitions have also been observed in the PL spectra. However, the intensities of these peaks were too weak and therefore too noisy to observe spectral differences due to the misfit dislocations.

5.3 Results

5.3.1 The system under tensile stress: GaAs on $In_xGa_{1-x}As$

The as-grown morphology in the system under tensile stress shows the quite well known asymmetry [2, 12, 13]. The dislocations are preferentially formed in the $[01\bar{1}]$ direction [13]. Fig. 5.1a shows an interference-contrast micrograph of a DSL etched GaAs layer grown on an $In_xGa_{1-x}As$ substrate with x = 0.0021. The thickness of the layer

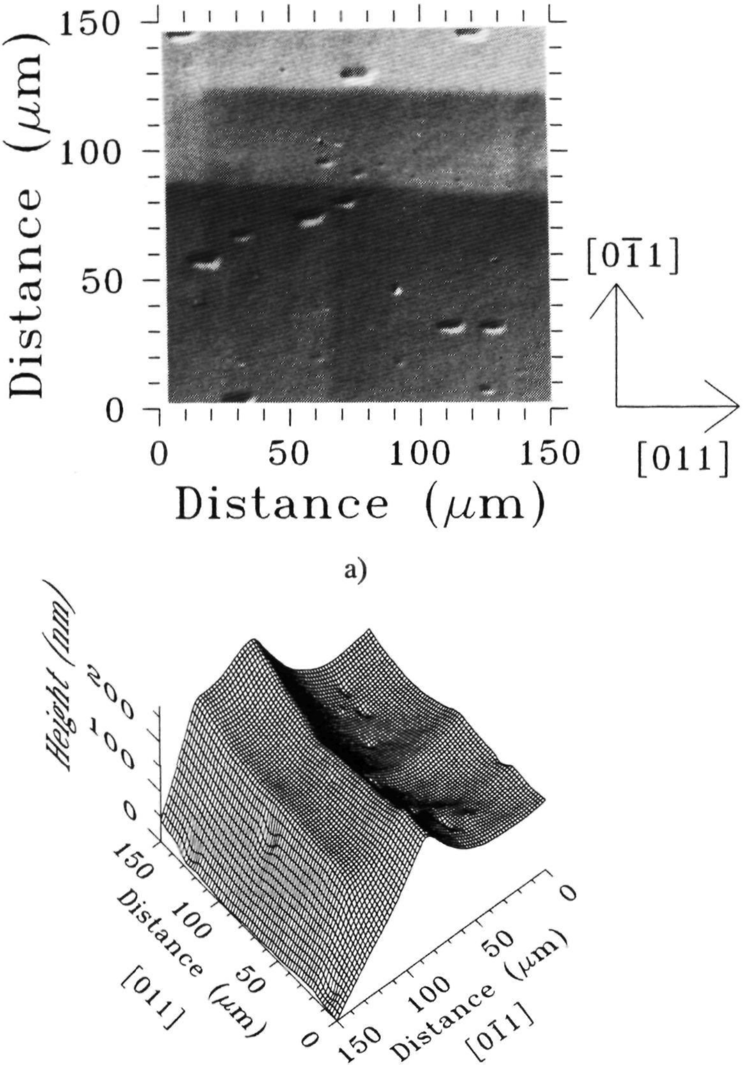
150
100
50
0
Distance (μm)
0
50
100
150
Distance (μm)
[0$\bar{1}$1]
[011]
Height (nm)
200
100
0
150
100
50
0
Distance (μm)
[011]
0
50
100
150
Distance (μm)
[0$\bar{1}$1]

a)

b)

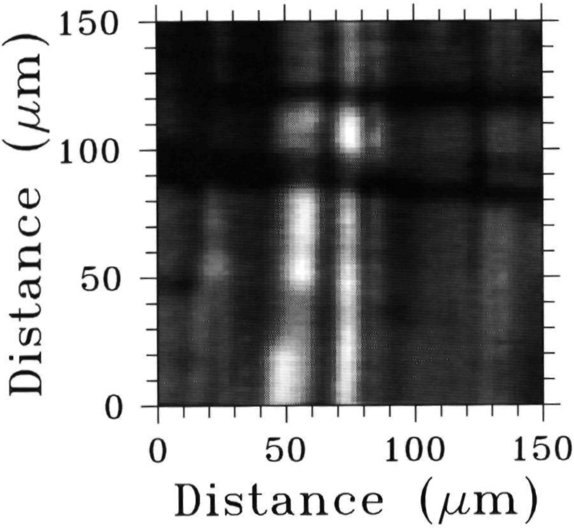

c)

Figure 5.1 a) Interference-contrast microphotograph, b) surface profile and c) PL intensity mapping of the same area of a GaAs epilayer with a thickness of 4.4 μm on $In_{0.002}Ga_{0.998}As$ after DSL etching. The PL mapping was recorded at an energy of 1.513 eV. The laser power was 150 kW/cm^2. The step size of the laser beam was 2 μm. The dislocation lines are not exactly perpendicular to the axes due to misalignment of the sample.

is 4.4 μm, which is above the critical layer thickness. The dislocation pattern is clearly visible. The corresponding 3D surface profile of the same area is shown in fig. 5.1b. This profile shows that the dislocation lines in the [011] direction are more clearly distinguishable because of a rather low DSL etch rate compared to that of the matrix. The etch rate at the dislocations in the orthogonal direction $[01\bar{1}]$ appears not to differ much from that of the matrix. The overall difference in height, as can be seen from fig. 5.1b, is smaller than 0.25 μm which is much smaller than the depth of field of the laser beam (3.5-7.2 μm [9]). Therefore, the focus does not need to be readjusted when the laser beam scans across a dislocation line. Fig. 5.1c shows the PL intensity mapping of the same area as figs. 5.1a and 5.1b.

The misfit dislocation lines in both the [011] and $[01\bar{1}]$ direction show up as dark lines.

The electro-optical effect of the dislocation is much larger (a few μm, see fig. 5.1a-b) than the plastically deformed core of the dislocation itself (10 nm [14]) The lines in the $[01\bar{1}]$ direction are accompanied by bright regions either side of them and appear to show a sharper PL contrast with the matrix than the [011] lines. On the other hand, the facets which are observed on the microphotograph (fig. 5.1a) cannot be distinguished by PL (fig. 5.1a) due to their crystalline character. The formation of the facets is discussed in chapter 6 [15].

From the low density of dislocation lines in figs. 5.1a-c (*ca.* 10^2 cm^{-1}) it can be concluded that only a small part of the misfit is relaxed by the misfit dislocations. This means that the thickness of this layer is very close to the critical layer thickness (see fig. 4.2). In the case of complete relaxation the average value of the distance between the dislocations in this epilayer should be 2 μm. When the density of misfit dislocations increases, the dark regions on the PL mapping overlap each other.

In fig. 5.2 a PL mapping of an as-grown layer under tensile stress from a sample grown at 970 K. On this sample misfit dislocations are observed in the two $\langle 011 \rangle$ directions, parallel to the the surface. In both directions these dislocations are surrounded by bright regions.

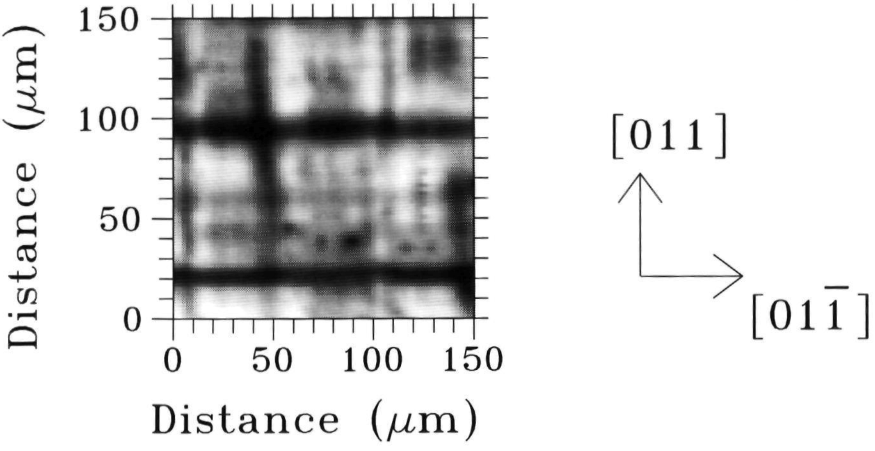

Figure 5.2 PL intensity mapping of a GaAs epilayer with a thickness of 1.6 μm, grown on a $In_{0.008}Ga_{0.992}As$ substrate at 970 K.

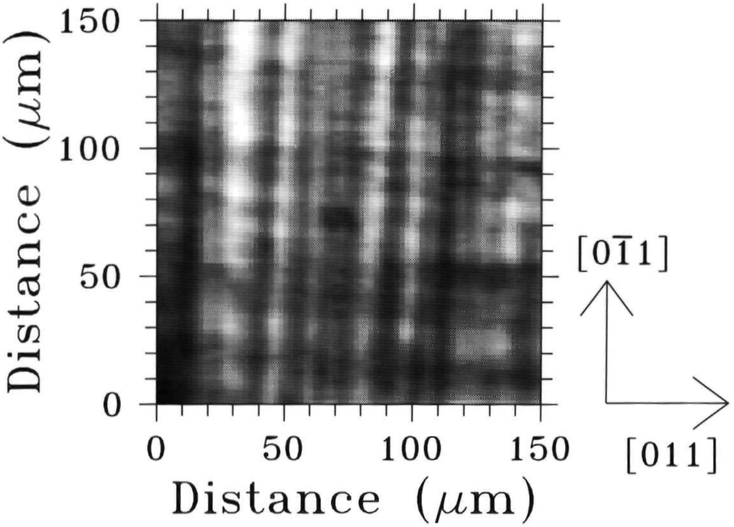

Figure 5.3 PL intensity mapping an as-grown GaAs epilayer with a thickness of 1.64 μm on $In_{0.011}Ga_{0.989}As$. The PL mapping has been recorded at an energy of 1.515 eV. The laser power was 150 kW/cm^2. The step size of the laser beam was 2 μm. The dislocation lines are not exactly perpendicular to the axes due to misalignment of the sample.

Fig. 5.3 shows an example of an as-grown layer under tensile stress and proves that the etch process has no influence on the PL results. In fig. 5.4 a typical PL spectrum taken at a dislocation line is compared with that of the matrix. A slight shift of 1 meV toward higher energy is observed for the PL spectrum from the dislocation. There is no consistent dependence of the shift on the direction of the dislocations. It is most likely caused by a small band gap widening due to a decrease of elastic strain around the dislocation. For sake of clarity, both spectra in fig. 5.4 are shown with their maximum intensities having the same value. In fact, the absolute intensities of the spectra taken at the dislocations are lower (see fig. 5.1c) due to the presence of non-radiative deep levels.

5.3.2 The system under compressive stress: $In_xGa_{1-x}As$ on GaAs

In the system under compressive stress the misfit dislocations do not show any asymmetry in the as-grown morphology [15]. The misfit dislocations were also made clearly visible by DSL etching. Fig. 5.5a shows a typical interference-contrast micrograph of a DSL etched

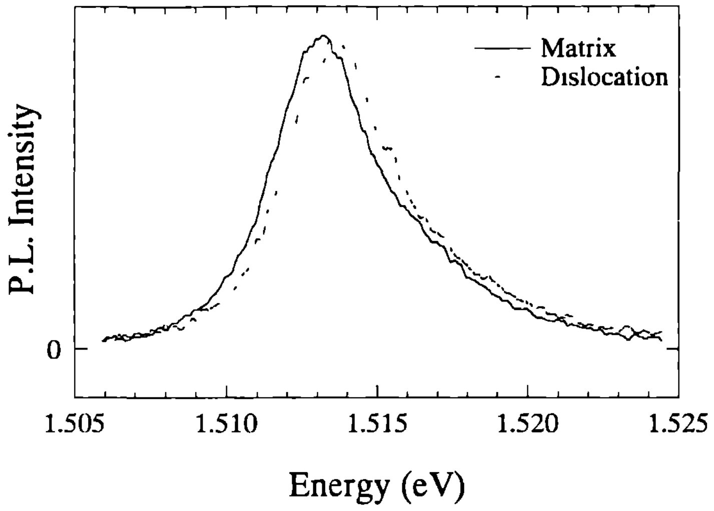

Figure 5.4 PL spectra recorded at the matrix (solid line) and at a dislocation line (dashed line) of the same sample as in fig. 5.1. The excitation density was 150 kW/cm^2 The intensities of both spectra have been normalised in order to have a good comparison of the peak positions.

In$_x$Ga$_{1-x}$As layer (x = 0 023, thickness 2.1 μm, *i e* above the critical layer thickness) on a GaAs substrate. Because the (100) substrate orientation is 2° misoriented in the [110] direction, the lines in the cross-hatched pattern of fig. 5.5a are not parallel. The difference in the DSL etch rate between the two orthogonal dislocation directions is not visible due to the high dislocation density. In fig. 5 5b the corresponding PL intensity mapping with a spatial resolution of 2 μm is shown. Again the misfit dislocations are found to yield lower PL intensities than the surrounding dislocation free areas. Fig. 5.6 shows a PL image of an as-grown layer. No effect of the DSL etch process on the PL results is observed. From figs. 5 5b and 5.1c it appears that the layers under compressive stress show two differences in comparison to those under tensile stress: (*i*) the lines in the [01$\bar{1}$] direction are more diffuse than those in the [011] direction, just opposite to the system under tensile stress and (*ii*) bright regions around the dislocation lines are now present in both directions.

Typical PL spectra taken at a dislocation and in the matrix are shown in fig. 5.7. The spectrum taken at the dislocation is now shifted over 1.5 meV toward lower energy indicating that the compressive strain is partly relaxed around the dislocation area Again

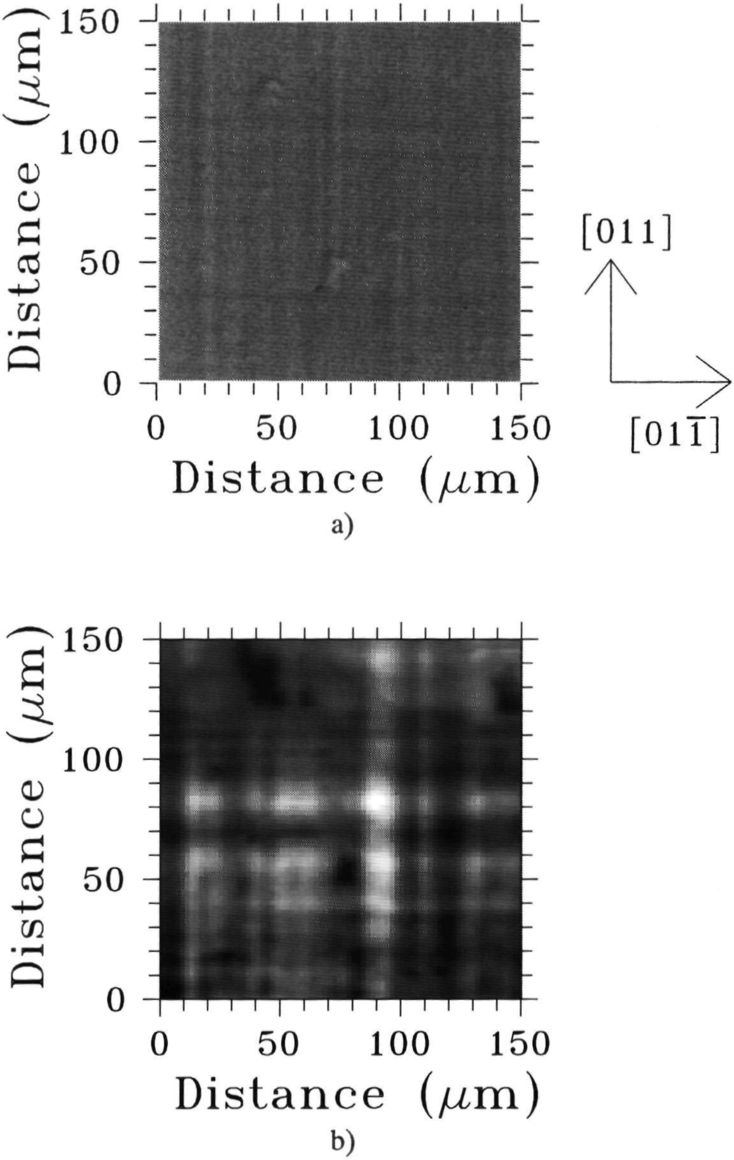

Figure 5.5 a) Interference-contrast microphotograph and b) PL intensity mapping of the same area of an $In_{0.023}Ga_{0.977}As$ epilayer with a thickness of 2.1 μm on GaAs after DSL etching. The PL mapping was recorded at an energy of 1.474 eV. The laser power was 150 kW/cm^2. The step size of the laser beam was 2 μm. The dislocation lines are not exactly perpendicular to the axes due to misalignment of the sample.

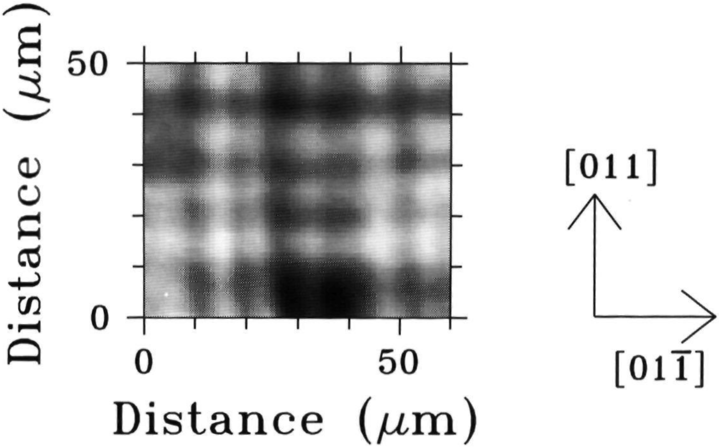

Figure 5.6 PL intensity mapping of an as-grown $In_{0.022}Ga_{0.978}As$ epilayer with a thickness of 2.1 μm on GaAs. The PL mapping was recorded at an energy of 1.474 eV. The laser power was 150 kW/cm^2. The step size of the laser beam was 1 μm. The dislocation lines are not exactly perpendicular to the axes due to misalignment of the sample.

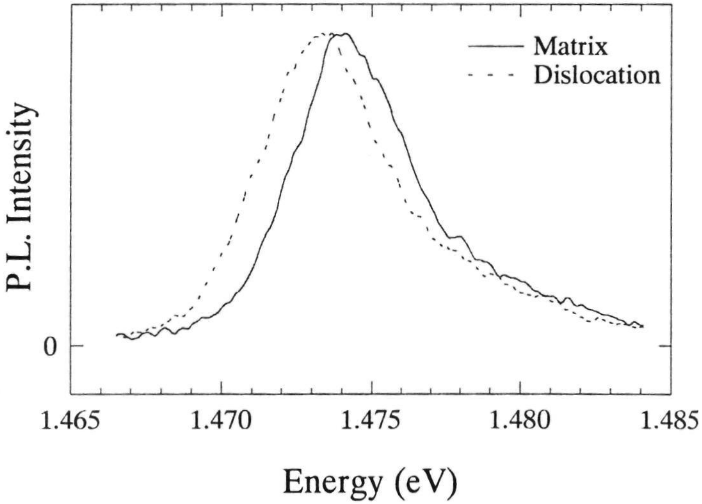

Figure 5.7 PL spectra recorded at the matrix (solid line) and at a dislocation line (dashed line) of the same sample as in fig. 5.5. The excitation density was 150 kW/cm^2. The intensities of both spectra have been normalised in order to give a good comparison between the peak positions.

both spectra have been normalised.

5.4 Discussion

5.4.1 Structural asymmetry

It is generally believed that the glide set, compared to the shuffle set is the energetically more favourable set for the misfit dislocations in GaAs and other III-V compounds with a zincblende structure [16]. The majority of the dislocations are of 60° type and can be dissociated into 30° and 90° partials [17]-[19]. From fig. 5.8 it can be seen that in the system under compressive stress, the As(g) (with gallium dangling bonds) and the Ga(g) (with arsenic dangling bonds) dislocations lie in the [011] and $[01\bar{1}]$ direction respectively. In the system under tensile stress these directions are reversed. Data on the cores of the dislocations together with the experimental results of the PL imaging and of the DSL etching are listed in table 5.1. The as-grown morphological asymmetry as observed in the system under tensile stress can be explained by the difference in mobilities between the As(g) and Ga(g) dislocations. In both systems both types of dislocations are created. Because the As(g) is known to be the more mobile dislocation [16], its dislocation loop expands more easily as far as the interface. However, in the system under tensile stress the As(g) dislocation is extended by the separation of the 30° and the 90° partials [15, 19].

The As(g) dislocation in the system under compressive stress, where no as-grown

Table 5.1 Summary of the dislocation core type and direction and of PL results for the system under compressive and tensile stress. In addition, the dislocation core types and the directions of the misfit dislocations are given.

Dislocation type	Strain type	Direction	PL contrast	Bright regions	DSL etch rate
As(g)	compressive	[011]	sharp	present	-
As(g)	tensile	$[01\bar{1}]$	sharp	present	normal
Ga(g)	compressive	$[01\bar{1}]$	diffuse	present	-
Ga(g)	tensile	[011]	diffuse	absent	low

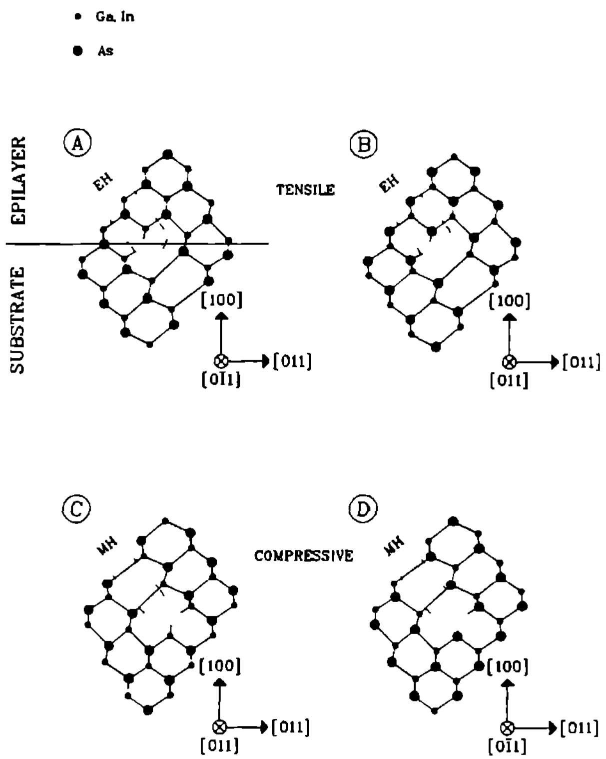

Figure 5.8 Atomic configurations for the dislocations of the glide set in GaAs (growth direction [100]) for the system under tensile stress (a and b) and for the system under compressive stress (c and d) The projection planes and dislocation types are a) $(0\bar{1}1)$, As(g) b) (011), Ga(g) c) (011), As(g) and d) $(0\bar{1}1)$, Ga(g) respectively In all cases the dislocations point perpendicular into the paper The positions of the extra half planes (EH) and missing half planes (MH) are shown by the dotted lines The interface between substrate and epilayer as indicated in a) is also valid for b), c) and d) For sake of clarity the In atoms are represented by the same symbol as the Ga atoms

morphological asymmetry is observed, is less dissociated. Therefore, cross slip is more likely to occur in the system under compressive stress than in the system under tensile stress [15, 19]

This difference in kinetics can also explain the bright PL regions close to the dislocations in the $[01\bar{1}]$ direction on the sample grown at 910 K (see fig 5 1c) which are probably due to the strong and long lasting interaction between dislocation and lattice. These dislocations are formed in an early stage of growth and thus have more time to interact with the defects in the surrounding lattice than the dislocations in the orthogonal direction which are scarcely formed due to the low cross-slip probability [15]. Therefore, the bright regions are absent in the [011] direction.

On the PL mapping of the sample in the system under tensile stress grown at 970 K (fig. 5.2) in both the ⟨011⟩ directions the dark lines are accompanied with bright regions. It is believed that at higher growth temperatures the Ga(g) dislocations are formed by nucleation at the surface and propagation towards the interface [15]. Therefore in this case also the Ga(g) dislocations could act as a sink for impurities and point defects, leaving a region of pure material around them.

In the system under compressive stress, the bright regions are present in both directions, also at the lower growth temperatures (fig. 5.5b). This is consistent with the idea of cross slip in the system under compressive stress which enables the creation of dislocations in both directions in an early stage of the growth process.

5.4.2 Opto-electronic asymmetry

The idea of depletion around the dislocations due to the electronic states associated with the cores of the dislocation is used to explain the results. Jones *et al.* [20] have shown that the arsenic dangling bonds on a Ga(g) dislocation lead to several energy bands centred around the valence band edge E_v. This dislocation acts as a strong acceptor. The As(g) is shown to give rise to a band spread out over the centre of the gap to the conduction band edge. This dislocation acts as a donor. Jones *et al.* [20] also showed that both the Ga(g) and the As(g) dislocation cores can be highly charged negatively and positively, depending on the position of the Fermi level. In our undoped n-type samples the Fermi level lies close to the shallow donor level so that the Ga(g) dislocation will be highly charged negatively whereas the As(g) dislocation is only partly positively ionised. This means that due to the stronger electric field excitons will less likely be formed in the region around the Ga(g) dislocation, explaining the diffuse character of the PL signal. Due to the donor-like character of the As(g) dislocation, the electric field around it will be much smaller than that around the Ga(g) dislocation.

The influence of the Fermi level on the opto-electronic asymmetry can be investigated by varying the dopant concentration in n-type and p-type layers. The observed decrease in PL intensity at the dislocations themselves is commonly ascribed to the presence of deep non-radiative levels [21].

The DSL etch patterns of the samples under tensile stress support the idea about the presence of a depletion region. The rather low etch velocity at the dislocations in the [011] direction can be explained by the higher recombination rate of the photogenerated holes due to the negatively charged core. This decrease of the number of holes slows down the DSL etch process [22, 23]. The etch rate at the dislocations in the $[01\bar{1}]$ direction is only reduced by recombination by deep non-radiative levels. Although the epilayers under compressive stress show the same tendency, the dislocation densities in these layers are too high to draw conclusions from the DSL etch patterns. Furthermore, the influence of indium in GaAs on the DSL etch rate is not very well known yet.

5.5 Summary and conclusions

It has been shown for the first time that PL imaging is a suitable technique for revealing misfit dislocations on a micron scale. The misfit dislocations, which belong to the glide set, have been investigated in both systems under tensile stress (GaAs on $In_xGa_{1-x}As$) and compressive stress ($In_xGa_{1-x}As$ on GaAs). Beside the partial relaxation of the strain around dislocations, it is shown that the effect of the kinetics of the formation of the misfit dislocations during growth on the opto-electronic quality of the sample may be observed by PL imaging. This observation agrees with the higher mobility of the As(g) dislocation in the system under tensile stress and the possibility of cross slip in the system under compressive stress.

PL imaging also reveals an opto-electronic asymmetry for the two orthogonal dislocation directions. This asymmetry has been explained by assuming a difference in core between the dislocations in both directions. DSL photo-etch patterns are shown to support this explanation.

Acknowledgements

Dr. M.R. Leys of the Eindhoven University of Technology and Dr. P.W. Schmidt are gratefully acknowledged for helpful discussions.

References

[1] M.S. Abrahams, J. Blanc and C.J. Buiocchi, Appl. Phys. Lett. **21** (1972) 185.

[2] G.H. Olsen, M.S. Abrahams and T.J. Zamerowski, J. Electrochem. Soc. **121** (1974) 1650.

[3] H. Alexander and P. Haasen, in Solid State Physics, Eds. H. Ehrenreich, F. Seitz and D. Turnbull (Academic Press, New York, 1968), vol.22.

[4] See the convention made at the International Symposium on Dislocations in Tetrahedrally Coordinated Semiconductors, Hünfeld, J. Phys. **40** (1979) Colloque C6, Introduction.

[5] M.E. Pistol, A. Gustafsson, M. Gerling, L. Samuelson and H. Titze, J. Crystal Growth **107** (1991) 458.

[6] A. Gustafsson, M.E. Pistol, M. Gerling, L. Samuelson, M.R. Leys and H. Titze, J. Appl. Phys. **70** (1991) 1660.

[7] S.J. Barnett, A.M. Keir and M. Emeny, Semicond. Sci. Technol. **7** (1992) A158.

[8] H.J. Hovel, Semicond. Sci. Technol. **7**, (1992) A1.

[9] E.P. Visser and L.J. Giling, Rev. of Sci. Instr. **61** (1990) 1490.

[10] J.L. Weyher and J. van de Ven, J. Crystal Growth **63** (1983) 285.

[11] T. Moriya and T. Kushida, J. Phys. Soc. Jpn. **41** (1976) 849.

[12] W.J. Bartels and W. Nijman, J. Crystal Growth **37** (1977) 204.

[13] B.A. Fox and W.A. Jesser, J. Appl. Phys. **68** (1990) 2739.

[14] K. Rajan, J. Appl. Phys. **71** (1991) 5853.

[15] J. te Nijenhuis, P.J. van der Wel, E.R.H. van Eck and L.J. Giling, submitted to J. Appl. Phys., this thesis, chapter 6.

[16] I. Yonenaga and K. Sumino, J. Appl. Phys. **62** (1987) 1212.

[17] J. Hornstra, J. Phys. Chem. Solids **5** (1958) 129.

[18] D.B. Holt, J. Phys. Chem. Solids **23** (1962) 1353.

[19] P.M.J. Marée, J.C. Barbour, J.F. van der Veen, K.L. Kavanagh, C.W.T. Bulle-Lieuwma and M.P.A. Viegers, J. Appl. Phys. **62** (1987) 4413.

[20] R. Jones, S. Öberg and S. Marklund, Phil. Mag. B **43** (1981) 839.

[21] W. Heinke and H.J. Queissner, Phys. Rev. Lett. **33** (1974) 1082.

[22] J.L. Weyher and J. van de Ven, J. Crystal Growth **78** (1986) 191.

[23] J. van de Ven, J.L. Weyher, J.E.A.M. van den Meerakker and J.J. Kelly, J. Electrochem. Soc. **133** (1986) 799.

Chapter 6

Strain relaxation mechanisms in lattice mismatched III-V heterostructures grown by metalorganic vapour phase epitaxy

Abstract

Strain relaxation mechanisms in III-V heterostructures both under tensile and under compressive stress have been studied. Layers of GaAs under tensile stress have been grown by metalorganic vapour phase epitaxy on $In_xGa_{1-x}As$ substrates with indium concentrations between 0.1% and 1.1%. Compressively strained $In_xGa_{1-x}As$ layers with indium concentrations between 0.5% and 2.5% have been grown on GaAs substrates. A description of the relaxation process by the formation of dissociated half loop dislocations is given. A difference in the Peierls barrier between the two possible misfit dislocation types is found to be the origin of asymmetric strain relief at low growth temperatures. In layers under tensile stress the cross slip of screw dislocations is counteracted by the shear stress, leading to relaxation in only one direction. In layers under compressive stress the nucleated misfit dislocations can cross slip, resulting in a cross-hatched pattern at the surface. It appears that the cross-slip process proceeds by means of the formation of a stair-rod dislocation. The formation of hillocks in layers under tensile stress is strongly coupled to the absence of strain relaxation in one direction. This is explained by a mechanism, in which the leading Shockley partial of a 60° dislocation cross slips and the trailing partial reacts with the stair-rod dislocation to form a Frank partial. At higher growth temperatures the dislocation patterns become more symmetric due to the higher dislocation mobilities. It is also shown that the (mis)orientation of the substrate is revealed by non parallel groups of dislocation lines observed at the surface of a relaxed epilayer.

6.1 Introduction

A typical defect in strained layer epitaxy is the misfit dislocation, which is formed when the thickness of the epitaxial layer exceeds a certain, strain dependent, critical layer thickness [1]. Several theoretical models for the calculation of this thickness, where the transition takes place from pseudomorphic (misfit dislocation free) to incoherent growth, have been proposed in the literature [1]-[8]. In the thermodynamic model of Matthews and Blakeslee [1], known as the mechanical equilibrium model, the critical layer thickness is calculated by balancing the elastic strain energy with the energy of a square grid of misfit dislocations. The strain is released by the movement of pre-existing dislocations along the interface between two layers with different lattice constants. However, in semiconductor films the density of grown-in dislocations is not high enough to relieve the strain energy completely. Therefore it is assumed [2]-[8] that new dislocations have to nucleate homogeneously at the surface and propagate as half loop dislocations towards the interface. In order to choose from these models the most realistic one, it is necessary to have a good knowledge of the relaxation processes.

The stress in the epilayer can be either tensile or compressive. In layers under tensile stress the lattice constant of the relaxed epitaxial layer a_0 is smaller than that of the substrate a_s, whereas in compressively stressed layers the lattice constant of the epilayer is larger than the lattice constant of the substrate. It has been shown [9] that in the zincblende structure the surface nucleated misfit dislocations, lying in each of the two $\langle 011 \rangle$ directions in the (100) plane, have different Peierls barriers, leading to asymmetric relaxation patterns [10]-[15]. In chapter 5 the opto-electronic behaviour of the misfit dislocations in layers under tensile and compressive stress in the GaAs/$\mathrm{In}_x\mathrm{Ga}_{1-x}\mathrm{As}$ system has been examined by spatially resolved photoluminescence and defect revealing etch experiments [16]. In these experiments two different dislocation core types have been observed in each of the two $\langle 011 \rangle$ directions.

In this chapter the relaxation processes in lattice mismatched III-V single heterostructures are discussed on the basis of the dislocation cores in layers under tensile and compressive stress. It is shown that the cross-slip possibilities of the dissociated dislocations, which are determined by the direction of the shear stress on the dislocations, play an important rôle in the relaxation processes. It follows from these considerations that in layers under tensile stress the absence of cross slip leads to asymmetric strain relief and hillock formation at low growth temperatures.

6.2 Experimental details

Layers under tensile (GaAs on $In_xGa_{1-x}As$) and compressive ($In_xGa_{1-x}As$ on GaAs) stress have been grown by low pressure metalorganic vapour phase epitaxy (LP-MOVPE). The GaAs layers have been deposited on liquid encapsuled Czochralski-grown (LEC) (100) oriented substrates [17], as obtained from LETI, Grenoble, France. The indium content in these substrates was between 0.1% and 1.15%. The $In_xGa_{1-x}As$ layers have been grown on semi-insulating (SI) horizontal Bridgman (HB) (100) GaAs substrates with different mis-orientations:(100), (100)2°(011), (100)2°(01$\bar{1}$) and (100)2°(110).

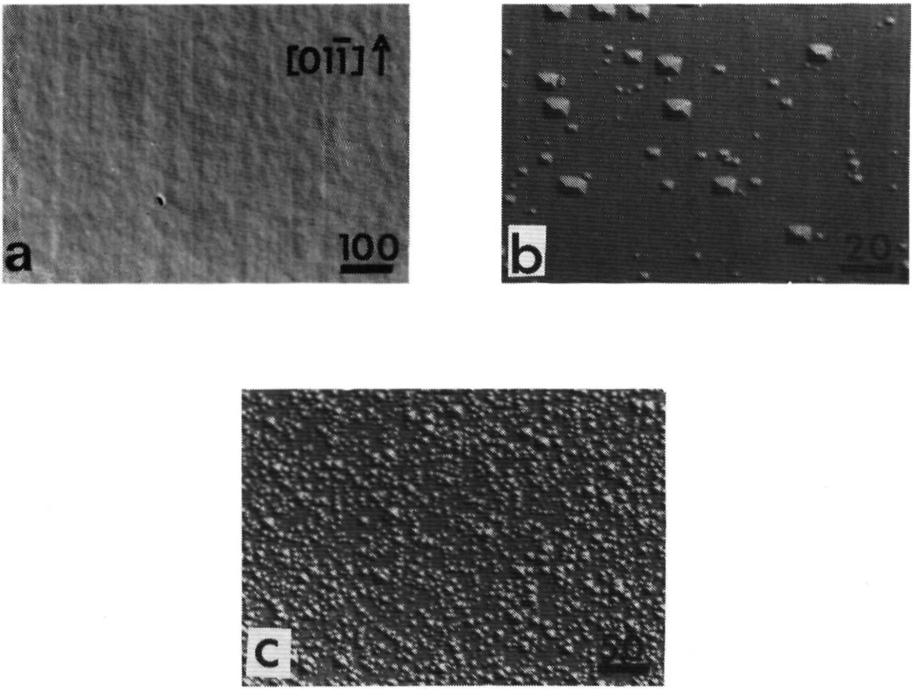

Figure 6.1 Interference contrast micrographs of surface morphologies of GaAs (100) epitaxial layers with thicknesses of a) 1.6 μm, b) 4.4 μm and c) 6.2 μm grown on $In_{0.008}Ga_{0.992}$ As substrates. The growth temperature was 910 K. The bars indicate distances in micrometers. The vertical direction is the [01$\bar{1}$] for all the micrographs.

For the growth of the undoped GaAs epitaxial layers on the $In_xGa_{1-x}As$ substrates arsine (AsH_3) and trimethylgallium (TMG) have been used as starting materials. In this system the lattice mismatch f between the epitaxial layers and the substrate was between -1.5×10^{-4} and -8.3×10^{-4}. During the growth of the $In_xGa_{1-x}As$ epilayers on GaAs, with indium concentrations between 0.5% and 2.5%, trimethylindium (TMI) was added to the gas phase. Here the lattice mismatch varied between 3.8×10^{-4} and 13×10^{-4}. The thicknesses of the epilayers ranged from 1.2 μm to 6.2 μm. The growth was performed at temperatures between 873 K and 973 K. At these temperatures homoepitaxial GaAs can be grown with specular surfaces without defects. Therefore defects, observed in strained layers, can be attributed to the relaxation. In order to reveal the dislocation patterns more clearly several samples have been photo-etched using the diluted Sirtl-like etchant with the use of light (DSL) [18]. The morphology of the epilayers was examined by optical microscopy.

6.3 Results

6.3.1 Morphology of layers under tensile stress

Layers grown under tensile stress show an asymmetric relaxation pattern. In fig. 6.1 IC-micrographs are shown of partially relaxed GaAs epitaxial layers with three different thicknesses grown on $In_{0.008}Ga_{0.992}As$ at 910 K. On the sample with an epilayer thickness of 1.6 μm dislocation lines are present in the $[01\bar{1}]$ direction (fig. 6.1a). In samples with larger thicknesses also hillocks are formed at the surface (figs. 6.1b and 6.1c). The density increases with thickness. The hillocks are not of equal sizes, indicating that they are formed at various stages of the growth process and not only at the start of the process.

The effect of the growth temperature on the relaxation pattern is demonstrated in fig. 6.2. Three micrographs are shown of GaAs epitaxial layers with the same thickness (1.6 μm) grown on $In_{0.011}Ga_{0.989}As$ at three different temperatures. On the sample grown at a temperature of 870 K a high density of hillocks is found and again only dislocation lines in the $[01\bar{1}]$ direction are present (fig. 6.2a). At the surface of the sample grown at 910 K the hillock density is remarkably lower (fig. 6.2b). At the sample grown at 970 K a cross-hatched pattern without hillocks is observed (fig. 6.2c).

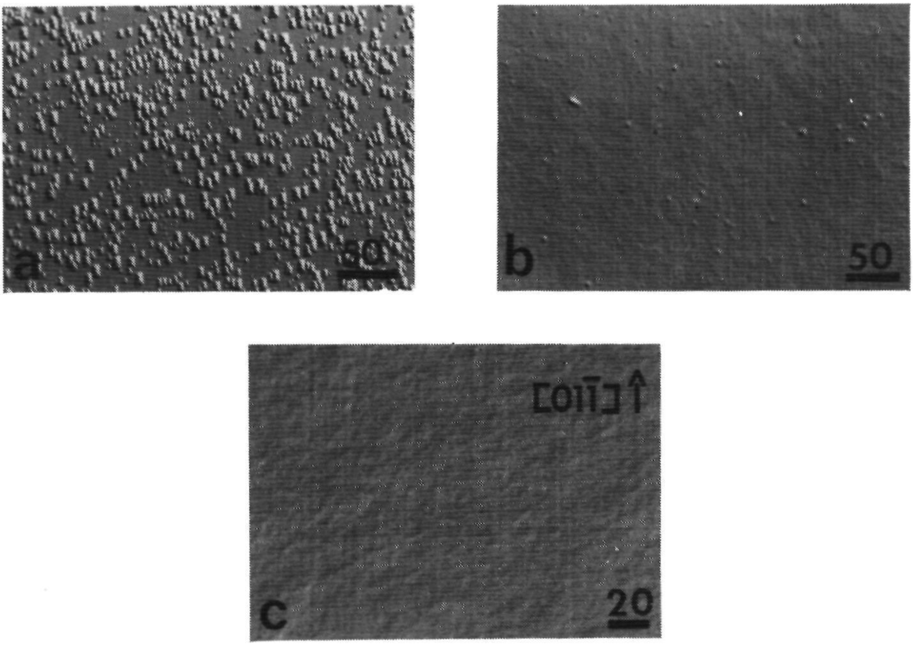

Figure 6.2 Interference contrast micrographs of surface morphologies of GaAs (100) epitaxial layers with thicknesses of 1.6 μm grown on $In_{0.011}Ga_{0.989}As$ substrates. The growth temperatures were a) 870 K, b) 910 K and c) 970 K. The bars indicate distances in micrometers. The vertical direction is $[01\bar{1}]$ for all the micrographs.

6.3.2 Morphology of layers under compressive stress

A cross-hatched relaxation pattern is shown clearly on layers grown under compressive stress beyond the critical layer thickness. No asymmetric distribution of dislocations is observed, even at low growth temperatures. In fig. 6.3 four micrographs are shown of $In_{0.02}Ga_{0.98}As$ epitaxial layers with the same thickness grown on (100) GaAs substrates with different (mis-)orientations. On the surface of the exact (100) sample (fig. 6.3a) it can be seen that the dislocation lines in the [011] and in the $[01\bar{1}]$ directions cross each other at right angles. The sample with orientation (100)2°(011) (fig. 6.3b) also shows a cross-hatched pattern. However, only in the $[01\bar{1}]$ direction all the dislocation lines are parallel to each other. In the [011] direction two groups of parallel dislocations can be observed, making a slight angle of *ca.* 3° with each other. The non-parallel dislocation groups on the (100)2°(01$\bar{1}$) sample (fig. 6.3c) are in the [01$\bar{1}$] direction. On the (100)2°(110) surface (fig. 6.3d) the non-parallel dislocation groups can be seen both in the [011] and in the [01$\bar{1}$] direction. No temperature dependence of the morphology in the range from 873 K to 973 K has been found, which is in contrast to the results obtained from the layers under tensile stress.

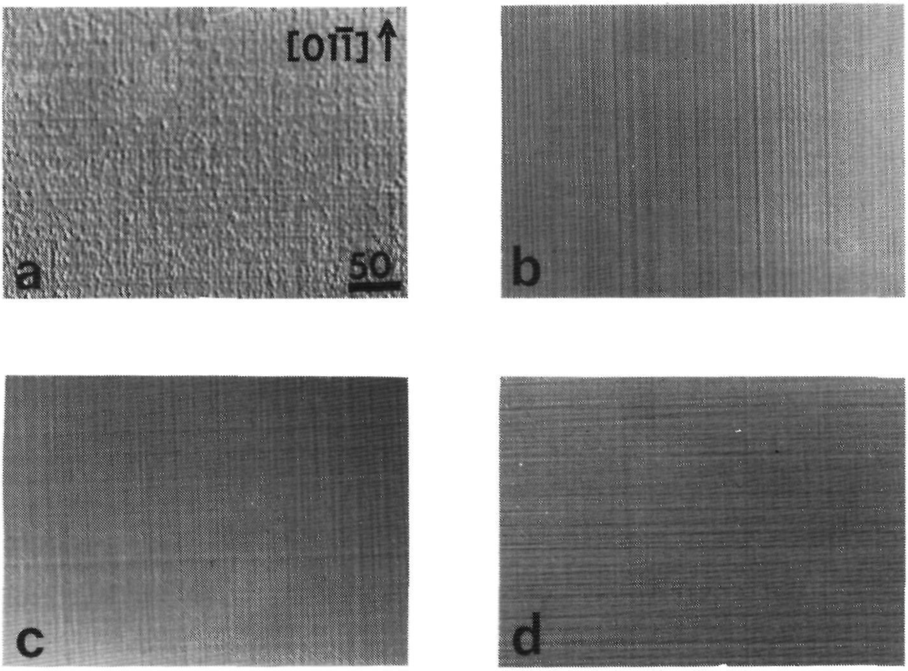

Figure 6.3 Interference contrast micrographs of surface morphologies of $In_{0.02}Ga_{0.98}As$ epitaxial layers with thicknesses of 2.1 μm grown on GaAs substrates. The growth temperature was 910 K. The orientations of the substrates were a) (100), b) (100)2°(011), c) (100)2°(01$\bar{1}$) and d) (100)2°(110). The bar indicates 50 μm and the vertical direction is [01$\bar{1}$] for all the micrographs.

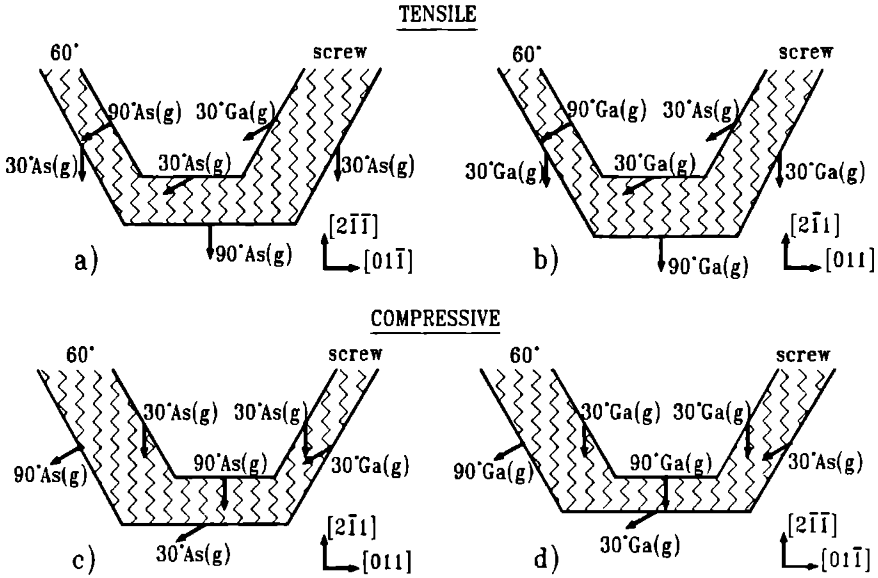

Figure 6.4 Projections of hexagonal dissociated dislocation half loops on the {111} planes, propagating from the surface to the interface, for layers under tensile stress (a,b) and under compressive stress (c,d). The dislocation types are a) As(g), b) Ga(g), c) As(g) and d) Ga(g) respectively. The shaded areas contain a stacking fault.

6.4 Discussion

6.4.1 Nucleation and propagation of misfit dislocations

In the zincblende structure misfit dislocations are mainly of the 60° type [19]. The glide planes are the {111} planes. The dislocation line and the Burgers vector are both along the ⟨110⟩ directions making an angle of 60° with each other [20, 21]. Four distinct types of 60° dislocations can be discriminated on account of (*i*) the nature of the dislocation motion [22] and (*ii*) the atom which is in the most distorted core position [23]. The dislocation motion is either between two (widely spaced) {111} slices or within a (closely spaced) {111} slice. The first kind of dislocations are called shuffle set dislocations, the latter kind glide set dislocations. These two sets can be transferred into each other by

Table 6.1 Overview of the relation between line direction parallel to the (100) surface and the dislocation core as a function of the stress type

Line direction	Stress type	
	Tensile	Compressive
[011]	Ga(g)	As(g)
$[01\bar{1}]$	As(g)	Ga(g)

dislocation climb. The atoms in the dislocation core in III(A)-V(B) compounds can be of element A or B The four types are indicated by the terms A(g) and B(g) for the glide set dislocations and A(s) and B(s) for the shuffle set dislocations. Only screw dislocations do not contain A- or B-characters.

It is well known that the 60° dislocations are dissociated into a 30° and a 90° Shockley partial, containing a stacking fault area inbetween them Since the movement of extended dislocations in the shuffle set is unlikely, due to a high energy stacking fault [24], it is generally believed that the mobile 60° dislocations in GaAs are of the glide set This assumption is in agreement with the calculated [25] and the observed [16] electric behaviour of the dislocation cores. Hence the discussions are limited to the glide set dislocations.

The misfit dislocations nucleate at the surface and propagate as half loop dislocations towards the interface [2]. The configurations of the dissociated hexagonal half-loop dislocations [26] are shown in a projection on the $\{111\}$ planes in fig 6 4 A hexagonal half loop dislocation exists of two 60° dislocations and one screw dislocation. The dissociated screw dislocation differs from the 60° dislocation since it consists of two 30° Shockley partials, instead of one 30° and one 90° partial. The individual parts of this dislocation loop lie in the Peierls valleys along the $\langle 011 \rangle$ directions The two 60° parts are of the same dislocation type, either As(g) or Ga(g), only the orientations of the Burgers vectors of the leading and the trailing Shockley partials with respect to the orientation of the line are reversed. Four different loops are shown, two in layers under tensile stress and two in layers under compressive stress In each of the two cases the horizontal (bottom) lines are in the, mutual perpendicular, [011] and $[01\bar{1}]$ directions An overview of the relation between stress type, line orientation and dislocation type is given in table 6 1.

It is stated by Fox and Jesser [9] that a difference in the energy barrier for the homogeneous nucleation of misfit dislocations at the surface of both glide set types cannot be the origin of the asymmetric relaxation pattern of fig 6.1a. Only the Peierls barrier for dislocation motion is important in the relaxation process. The As(g) dislocation is the most mobile one of the two possible glide set dislocations [27]. Hence in layers under tensile stress the relaxation will start in the $[01\bar{1}]$ direction and along the $[011]$ in layers under compressive stress. In fig. 6.1a it can be seen that in the layers under tensile stress the relaxation indeed has started in the $[01\bar{1}]$ direction. The dislocations are more prominently present in this direction, which is in agreement with the model. However, at the higher growth temperatures the dislocations are observed in both the $\langle 110 \rangle$ directions (fig. 6.2c). The mobility of the Ga(g) dislocation has become sufficiently high to move through the epitaxial layer to release the strain. On the other hand, in layers under compressive stress both the As(g) dislocation in the $[011]$ direction and the Ga(g) dislocation in the perpendicular $[01\bar{1}]$ direction are already present, even at the lower growth temperatures. So it is concluded that the above description of the relaxation process certainly is not complete. It still has to be explained why the formation and propagation of the Ga(g) dislocations is easier in the layers under compressive stress than under tensile stress. In order to do this the motion of dislocations, which are dissociated into Shockley partials, has to be considered.

6.4.2 Relaxation by cross slip of misfit dislocations

In the previous section relaxation is only described in terms of perfect dislocations. It was not explained why the Ga(g) dislocations are present in the layers under compressive stress, whereas they are not observed in the layers under tensile stress at low growth temperatures. In this section the influence of the Shockley partials together with the cross-slip process on the relaxation behaviour is studied.

Cross slip is the process, during which a dislocation changes the slip direction from one glide plane to another. Strain relaxation by means of cross slipped misfit dislocations is typical for materials in the zincblende structure, since in crystals in the diamond structure, like silicon, only one type of 60° glide set dislocations exists [20], and therefore no differences in Peierls barriers in the two $\langle 011 \rangle$ directions are present.

The relaxation mechanism in III-V compounds is described in the literature [3] for both layers under tensile and compressive stress in terms of semicircular loops. It is assumed that the relaxation is initiated by the nucleation of Shockley partial dislocations, which expand to form a semicircular dissociated dislocation loop. In layers under tensile stress the leading partial in this case is the 90° As(g), whereas in compressively strained layers the 30° As(g) is the first partial to move. This is shown in fig. 6.5 and summarized in the first column of table 6.2. The width of the stacking fault area depends on the stress

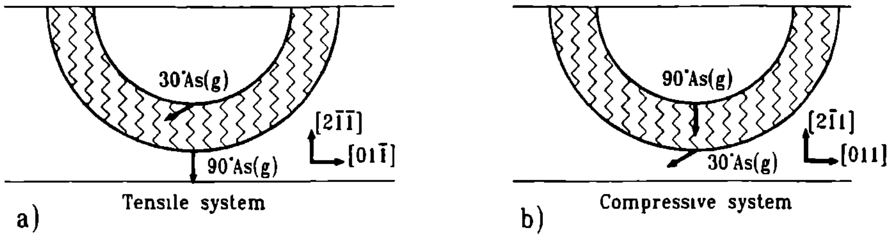

a) Tensile system

b) Compressive system

Figure 6.5 Projections of dissociated semicircular half loop dislocations on the {111} planes. The leading Shockley partials are a) the 90° As(g) in the layer under tensile stress and b) the 30° As(g) partial in the layer under compressive stress.

direction. Since the shear stress, exerted on the 90° partial, is twice the one on the 30° partial, the dissociation distance is large when the 90° Shockley partial is the leading one. This is the case in the layers under tensile stress where the dislocation loop is widely extended, because here the 90° partial is the first to nucleate. The dissociation distance is small when the 90° Shockley partial is the trailing one, as is the case in layers under compressive stress. From this it has been concluded that the cross slip is easier in layers under compressive stress, where the 60° dislocation are (almost) perfect, whereas the large distance between the loops in the layers under tensile stress explains why the cross slip does not occur.

On this model two serious remarks can be made. Firstly, since the dislocation is

Table 6.2 Overview of the relation between the stress and the leading Shockley partial of the As(g) type, according to the models for the relaxation by extended semicircular [3] and V-shaped dislocation loops.

Stress type (line direction)	Semicircular loops	V-shaped loops
Tensile ([01$\bar{1}$])	90°	30°
Compressive ([011])	30°	90°

not a straight line, the character of the dislocation depends on the position on the line. Consequently, the dissociation distance of the Shockley partials changes too. In the second place, only screw (0°) dislocations are known to posses the cross-slip possibility [22]. Therefore a model is presented, which deals with the changing dislocation character along the half loop and in which only the screw dislocation part is supposed to be able to cross slip. However, first the 60° dislocations are considered, since these dislocations are able to release the misfit strain.

In a recent relaxation model [28], Fukuda *et al.* proposed that V-shaped misfit dislocations will propagate through the layer from the surface towards the interface instead of semicircular loops. These dislocations can be divided into two parts, as is shown in fig. 6.6. One is a screw dislocation, whereas the other is a 60° dislocation. When the V-shaped dislocation has reached the interface between the epilayer and the substrate, it will expand along the interface forming a hexagonal half loop (fig. 6.4). This is a realistic model, since in layers with a very low mismatch the dislocations are long and tend to form straight lines along the Peierls valleys in the $\langle 011 \rangle$ directions. Here this model is extended by assuming that in this case the dislocations are also moving in a dissociated state. The leading partial of the 60° As(g) part of the V-shaped loop, which is the first partial to nucleate, is the 30° As(g) in layers under tensile strain (see fig. 6.6 and the second column of table 6.2). According to this model, the dissociation distance of the dislocation is smaller in layers under tensile stress than in the stress-free situation. In compressively strained layers the 90° As(g) now is the leading partial and the dislocation is wider dissociated. From these considerations it follows, that, even if the 60° part of the dislocation loop would posses cross-slip possibilities, no asymmetric strain release would be observed in layers under tensile stress, due to the decreased dissociation distance of the 60° dislocation. This is in contrast with the observations (figs. 6.1 and 6.3). Therefore here the motion of the screw dislocation, which can cross slip in a perfect state, is discussed more in detail.

In case of tensile stress the Burgers vectors along the dislocation half loop, parallel to the $\{111\}$ planes, are shown (fig. 6.6a). The arrows of the screw dislocation point outward in opposite directions. The shear stress along the $\{111\}$ plane increases the dissociation distance. This means that under tensile stress the screw dislocations cannot rejoin and consequently no cross slip is possible. Relaxation in layers under tensile stress is therefore asymmetric. In the case of compressive stress the arrows of the screw dislocation are pointing inward to each other (fig. 6.6b). The shear stress, generated by the mismatch, now pushes the Shockley partials together. Cross slip, in order to relieve the strain in the other direction, is possible. When this process is active a symmetric cross-hatched pattern is observed (fig. 6.3). This latter model seems to be consistent with

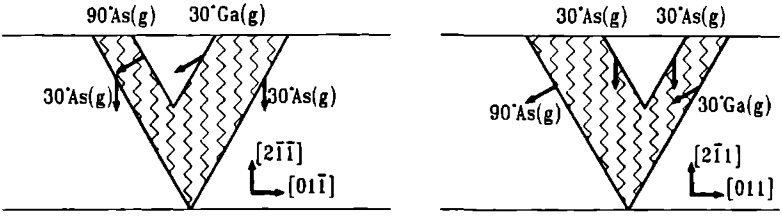

a) Tensile system

b) Compressive system

Figure 6.6 Projections of the dissociated V-shaped dislocations on the $\{111\}$ planes. The leading partials of the 60° parts are a) the 30° As(g) in the layers under tensile stress and b) the 90° As(g) partial in the layers under compressive stress.

all observations and theoretical considerations.

These considerations about contraction and dissociation of misfit dislocations can be made more quantitatively by the following relations. In a stress free crystal the equilibrium dissociation width of an extended dislocation d_0 is determined by (i) the repulsive interaction of the partials [22] A/d, which is inversely proportional to the dissociation distance d, and (ii) the attractive force γ, caused by the stacking fault area, bounded by the Shockley partials. The equilibrium dissociation width in an anisotropic crystal is found from the expression:

$$\gamma = \frac{A}{d_0}. \tag{6.1}$$

In strained layers also misfit stresses F_i act on the partials, causing dislocation motion. This motion is impeded by the presence of frictional forces R_i. In fig. 6.7 these forces are indicated. For 60° dislocations in strained crystals the dissociation distance is given by [29]:

$$d = \frac{d_0}{1 + (g - \rho)b\tau/2\gamma}, \tag{6.2}$$

in which g is a geometrical factor, determined by the relation $F_t - F_l = gb\tau$ (subscripts l and t refer to the leading and the trailing partials), b is the Burgers vector of the perfect

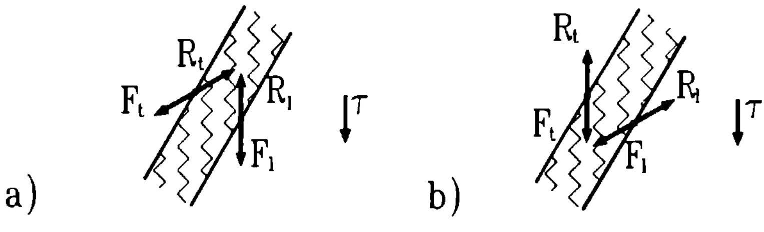

Figure 6.7 Forces acting on Shockley partials of screw dislocations in layers under a) tensile stress and b) compressive stress.

dislocation, τ is the shear stress on the perfect dislocation parallel to the Burgers vector and ρ is given by $\rho = (R_t - R_l)/(R_t + R_l)$.

In the case of screw dislocations the Burgers vectors of both the Shockley partials either point outward (tensile stress) or inward (compressive stress), as is shown in fig. 6.6. For these cases the above relation needs to be modified. At first the derivation will be given for the case of tensile stress, from which the relation for the case of compressive stress is deduced easily. The total force on the perfect dislocation in the stationary state of steady motion is:

$$F_l + F_t = b\tau. \tag{6.3}$$

On each partial the force balance is given by (fig. 6.7a):

$$F_l = -\frac{\gamma d_0}{d} + \gamma + R_l, \tag{6.4}$$

$$F_t = -\frac{\gamma d_0}{d} + \gamma + R_t, \tag{6.5}$$

in which for the repulsive force eq. (6.1) is used. Adding eqs. (6.4) and (6.5) leads to the relation for d:

$$d = \frac{d_0}{1 - (F_l + F_t - R_l - R_t)/2\gamma}, \tag{6.6}$$

while substraction together with the definition of g yields:

$$F_l - F_t = R_l - R_t = -gb\tau. \tag{6.7}$$

Substituting eq. (6.3) and $R_l + R_t = (R_t - R_l)/\rho = gb\tau/\rho$ in eq. (6.6) results in the equation for the dissociation width of the screw dislocations under tensile stress:

$$d = \frac{d_o}{1 - (1 - g/\rho)b\tau/2\gamma}. \tag{6.8}$$

In a similar way with the aid of fig. 6.7b the derivation can be made for the screw dislocation dissociation width in the case of compressive stress, resulting in:

$$d = \frac{d_o}{1 + (1 - g/\rho)b\tau/2\gamma}. \tag{6.9}$$

No exact data are known for the frictional forces R_t in GaAs; for semi-insulating GaAs they are only classified [30]:

$$R_{30^\circ Ga(g)} > R_{30^\circ As(g)} > R_{90^\circ} \tag{6.10}$$

A crude estimate for $R_{90^\circ}/R_{30^\circ As(g)}$ is *ca.* 0.4 [30]. Using this value and data of the dislocation velocities for 60° As(g) and Ga(g) dislocations [31] the value of $R_{90^\circ}/R_{30^\circ Ga(g)}$ is estimated to be 14×10^{-3}. The results of the calculations of the dissociation distances are given in table 6.3.

It is demonstrated that exerting a shear stress τ on the screw dislocation in the case of tensile stress leads to an increase of the dissociation width, preventing cross slip. In the case of compressive stress (eq. (6.9)) the dissociation width of screw dislocations is decreased, which makes it possible for the dislocation to cross slip, resulting in relaxation in both the $\langle 011 \rangle$ directions. A cross-hatched pattern is observed on compressively strained layers (fig. 6.3).

Table 6.3 Calculated dissociation widths of extended dislocations in $\{111\}$-planes, as shown in fig 6.4., according to eqs. (6.6), (6.8) and (6.9). The values of b, γ and τ are taken resp. 0.4 nm, 45 mJ/m^2 [30] and 42 MPa. The equilibrium distances d_0 are 3.1 nm for screw and 5.4 nm for 60° dislocations.

Dislocation type	leading/trailing partial	g	p	d/d_0	d (nm)
Tensile					
0°	30°As(g)/30°Ga(g)	-1/3	0.93	1.34	4.1
60°	90°As(g)/30°As(g)	-1/3	0.43	1.17	6.3
60°	30°As(g)/90°As(g)	-1/3	-0.43	0.98	5.3
0°	30°Ga(g)/30°As(g)	-1/3	-0.93	1.14	3.5
60°	90°Ga(g)/30°Ga(g)	-1/3	0.97	1.33	7.2
60°	30°Ga(g)/90°Ga(g)	-1/3	-0.97	0.89	4.8
Compressive					
0°	30°Ga(g)/30°As(g)	1/3	-0.93	0.80	2.4
60°	30°As(g)/90°As(g)	1/3	-0.43	0.87	4.7
60°	90°As(g)/30°As(g)	1/3	0.43	1.02	5.5
0°	30°As(g)/30°Ga(g)	1/3	0.93	0.89	2.7
60°	30°Ga(g)/90°Ga(g)	1/3	-0.97	0.80	4.3
60°	90°Ga(g)/30°Ga(g)	1/3	0.97	1.14	6.2

It further appears from these calculations that even in the layers under compressive stress the dislocations move in an extended state, which is in contrast to the assumption that in this case the dissociation width is negligible [32]. Therefore even in the compressively strained layers an energy barrier is present, which has to be overcome before the cross slip can take place.

6.4.3 The energy barrier for the cross-slip process

Thus far it has been demonstrated that cross slip under misfit stress by contraction of dissociated screw dislocations is only possible in compressively strained layers. A closer analysis of the cross-slip process has been given by several authors [33]-[36]. Hartley and Blachon [33] have given theoretical descriptions of energy barriers of possible dislocation

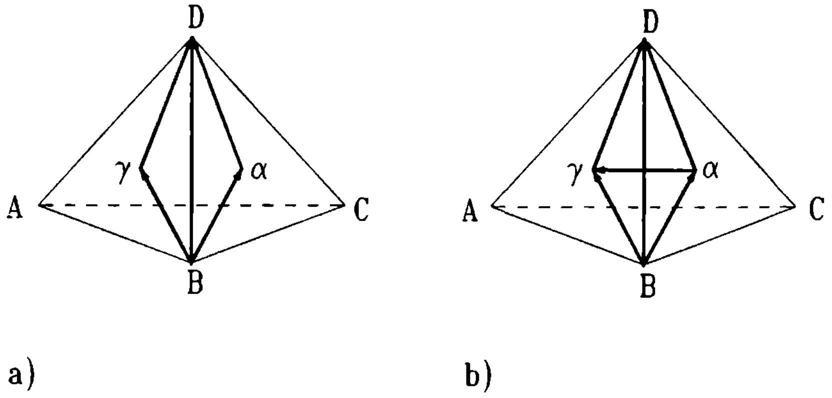

Figure 6.8 Schematic representations in a Thompson tetrahedron of the cross-slip process via a) the formation of a perfect screw dislocation BD (eq. (6.11)), and b) via the formation of an $\frac{a}{6}\langle 110\rangle$ stair-rod dislocation $\alpha\gamma$ (eq. (6.12)).

reactions in the face-centred-cubic lattice. Cross slip is also considered as the initial process for the formation of mechanical twins [34, 35]. Here two basic cross-slip processes are mentioned.

In the first process the extended screw dislocation constricts under the applied stress and becomes glissile in the other slip plane. In the Thompson notation [22] this process for the originally in the γ-plane dissociated dislocation BD, cross slipping to the α-plane, is given by:

$$B\gamma + \gamma D \rightarrow BD \rightarrow B\alpha + \alpha D. \tag{6.11}$$

This process is schematically given in fig. 6.8a.

In the second possible process a sessile stair-rod dislocation of the type $\frac{a}{6}\langle 011\rangle$ is formed during the cross slip of the leading Shockley partial. This reaction is followed by a reaction between the newly formed stair-rod dislocation and the trailing Shockley partial in order to form a second partial, which is glissile in the cross-slip plane. The Thompson notation of this process, given in fig. 6.8b, is:

$$B\gamma + \gamma D \rightarrow B\alpha + \alpha\gamma + \gamma D \rightarrow B\alpha + \alpha D. \tag{6.12}$$

The second process is the most favourable process [37], because the energy barrier to overcome is lower than that of the first process. The energy, required for the formation of the new dislocations, can be calculated by the method, described by Gleichmann *et al.* [38]. The core energy per unit length of a dislocation is given by:

$$\frac{W_c}{L} = kK_t b_t^2, \tag{6.13}$$

in which K_t is the shear modulus of an anisotropic crystal [22] and b_t is the Burgers vector of the specific dislocation type t. k is a parameter depending on the dislocation type. For a 30° Shockley partial and an $\frac{a}{6}\langle 011\rangle$ stair-rod dislocation the values of k are estimated to be respectively 0.047 and 0.0185 [38]. The energy barrier per unit length for the formation of the stair-rod dislocation and the leading cross slipped Shockley partial according to the second cross-slip process is 1.31×10^{-10} J/m (0.82 eV/nm). This energy has to be supplied by the increase in the core energy of the extended dislocation by reducing the distance between the Shockley partials to a critical dissociation width d_c. When the dissociation distance is smaller than the critical distance the core energy of the dislocation is high enough to overcome the energy barrier. The increase in the energy of the dislocation is given by [38]:

$$\frac{W_B}{L} = \frac{W_t(d_c)}{L} - \frac{W_t(d_0)}{L} = \gamma d_0 \left(\ln\left(\frac{d_0}{d_c}\right) + \frac{d_c}{d_0} - 1\right), \tag{6.14}$$

where $W_t(d)/L$ is the total energy per unit length of a straight infinitely long dissociated dislocation. With $K_s = 4.08\times 10^{10}$ Pa [39] for a screw dislocation in the $\langle 110\rangle$ direction, d_0 = 3.1 nm and γ = 45 mJ/m^{-2}, the calculated critical dissociation width is 0.5 nm. For the first process the dissociation width has to be reduced to *ca.* 0.2 nm, which is the length of the Burgers vector of the Shockley partial. The corresponding value of the energy barrier (eq. (6.14)) is 2.33×10^{-10} J/m (1.46 eV/nm), which is nearly twice the energy barrier of the process during which a stair-rod dislocation is formed.

Compared to the activation energy for motion of dislocations in GaAs [40], the energy barrier for cross slip is sufficiently low to assume that strain relaxation in the $[01\bar{1}]$

direction is indeed possible by means of the proposed stair-rod dislocation mechanism Once a cross slipped misfit dislocation is formed, other dislocation reactions, reported in literature [41]-[43], can become active to relieve the strain.

6.4.4 Hillock formation in layers under tensile stress

It has been demonstrated that in layers under tensile stress no cross slip of screw dislocations can occur The tensile stress pushes the partials of these dislocations away from each other On the other hand, as can be seen from fig 6 4a and table 6 3, the dissociation width of the 60° part of the left side of the V-shaped dislocations is reduced by the tensile stress The leading partial of these dislocations is of the 30° As(g) type As the stress is relieved in only one direction, the force on the dislocation in the perpendicular direction becomes higher than in the original direction. Therefore the leading partial can react in the same way as the 30° partial of the screw dislocation in the layers under compressive stress does, *i e.* by the formation of an $\frac{a}{6}\langle 011\rangle$ stair-rod dislocation The energy, required for this process, is supplied by the increase in the core energy, due to the constriction of the 60° dislocation The reaction between the trailing 90° partial and the stair-rod dislocation yields a sessile Frank partial dislocation. If the dislocation is taken along the line BD, which is the intersecting line of the α- and the γ-slip planes, and the Burgers vector of the 60° dislocation is in the direction BA, the dislocation reaction in this process, shown in fig 6 9, is described in the Thompson notation by

$$B\gamma + \gamma A \rightarrow B\alpha + \alpha\gamma + \gamma A \rightarrow B\alpha + \alpha A, \tag{6 15}$$

in which αA is the $\frac{a}{3}\langle 111\rangle$ Frank partial.

The lattice between the cross slipped Shockley partial and the Frank partial contains a stacking fault Gleichmann *et al* [38] have proposed that especially sessile stacking faults can act as strong obstacles to the dislocation motion When in the region of the stacking fault the dislocations are pinned, a locally higher concentration of dislocations is formed At the epilayer surface the dislocations introduce new steps, which can be the origin of a local increase of the growth rate [44, 45] When the concentration of the pinned dislocations is sufficiently high, and therewith the concentration of newly formed surface steps, growth hillocks are formed [38] These hillocks are observed on surfaces of GaAs samples, grown under tensile stress (fig 6 1) It is shown that the hillock growth

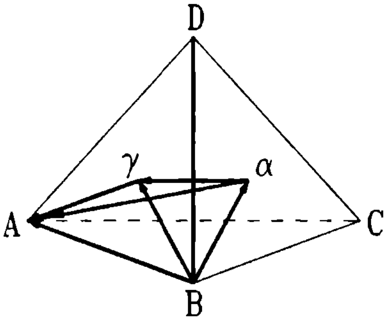

Figure 6.9 Schematic representation in a Thompson tetrahedron of the formation process of a Frank dislocation αA (eq. (6.15)).

is enhanced when the layer thickness is increased. Thus the hillocks are manifestations of the stacking fault areas, caused by the dislocation reaction of the leading partials.

The above described hillock growth process occurs at relatively low growth temperatures, as a result of cross slip. The Ga(g) dislocations are not mobile enough to nucleate and to expand towards the interface. At higher temperatures, above *ca.* 950 K, the mobility of the Ga(g) dislocations has become higher and the dislocations move through the epitaxial layers. The cross-slip process is not necessary anymore for strain relaxation. The observed cross-hatched pattern at the surface of samples grown at 970 K support these considerations. Because no cross slip is necessary at high temperatures, no hillock growth will be found. All dislocation lines in the $[01\bar{1}]$ direction are indications for the presence of Ga(g) dislocations. On the PL mappings of the samples, grown at 970 K, the dark lines in both the directions are accompanied with bright regions, indicating pure material, whereas at samples grown at lower temperatures bright regions were found only along the As(g) dislocations (fig. 5.2). When the dislocations are nucleated at the surface and propagate through the layer, as is the case with both the As(g) and the Ga(g) dislocations in samples grown at 970 K, they are subject to strong and long-lasting interactions with the epilayer material. The dislocations act as a sink for impurities and point defects, leaving a region of pure material around them. In samples grown at lower temperatures the Ga(g) dislocations are formed by cross slip at the interface, hence only interaction with the material in the regions near the interface has occurred. Along these dislocations no bright regions are found.

6.4.5 The non-parallel dislocation lines

As is shown earlier, the misfit dislocations in mismatched (100) oriented epilayers form a cross-hatched pattern, where the dislocations run along the ⟨011⟩ directions and cross each other at right angles. However, on vicinal surfaces this is not true anymore, as can be seen from figure 6.3b, where an epilayer is shown with a misorientation in the [011] direction. In this direction non-parallel groups of dislocations are observed. This can be explained as follows. The lines of intersection of the (100) surface and the four possible {111} slip planes are the two ⟨011⟩ directions. The intersecting lines of the {111} planes coincide two by two. By a misorientation of the (100) substrate surface, the orientation of the intersecting lines changes too, breaking up the coincidence of the intersecting lines of two different {111} planes. This is illustrated in fig. 6.10. It appears from this

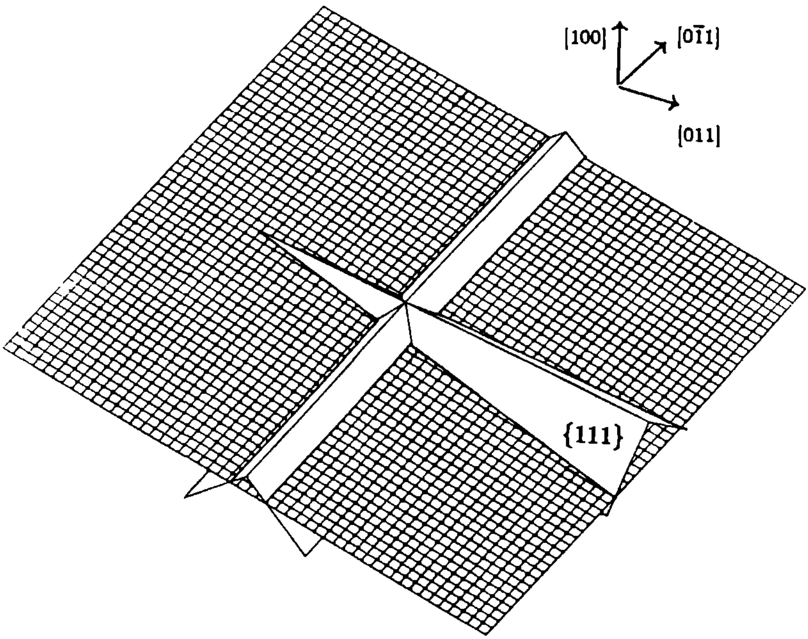

Figure 6.10 Intersection of the (100) surface, misoriented in the [011] direction (cross-hatched plane), with the four {111} planes. In the [01$\bar{1}$] direction the intersecting lines of the two {111} planes with the surface are parallel. In the [011] direction the intersecting lines make a slight angle with each other

Table 6.4 Comparison between the calculated and the observed angle ϕ on substrates with different orientations

Substrate orientation	Line direction	θ	Calculated angle ϕ (±0.7°)	Observed angle ϕ (±0.2°)
(100)2°(011)	[011]	2°	2.8°	3.1°
	[01$\bar{1}$]	0°	0°	0°
(100)2°(01$\bar{1}$)	[011]	0°	0°	0°
	[01$\bar{1}$]	2°	2.8°	3.0°
(100)2°(110)	[011]	1.4°	2.0°	2.2°
	[01$\bar{1}$]	1.4°	2.0°	2.1°

figure that if the substrate surface is misoriented in one of the dislocation directions, only in this direction the dislocation traces on the surface are not parallel. If the surface is misoriented in another than one of these two directions, like the [110] in fig. 6.3d, in both the dislocation directions non-parallel groups can be observed.

The above can be verified by comparing the measured and calculated angle ϕ between the non parallel lines. With the aid of fig. 6.10 one obtains the relation for ϕ

$$\tan\frac{\phi}{2} = \frac{\sin\theta}{\sqrt{2}} \tag{6.16}$$

where θ is the misorientation of the substrate surface in the direction of the non-parallel dislocation groups, between which the angle ϕ is determined. In table 6.4 the results of the calculated and observed angles are given. The error in the calculated values of ϕ is the consequence of the inaccuracy of substrate orientation as is given by the manufacturer. It appears that the observed angles are in good agreement to the calculated ones. This shows that the presence of non-parallel dislocation groups can be used to determine and to check the direction and the magnitude of the misorientation.

6.5 Summary and conclusions

It has been shown that the difference in mobilities between the As(g) and the Ga(g) dislocations in GaAs based heterostructures is the origin of asymmetric strain relieve in

(100) oriented epitaxial layers at low growth temperatures. It has been found that in layers under tensile stress the nucleated V-shaped As(g) dislocations are not able to cross slip in order to relieve the strain in the orthogonal direction, since the dissociation width of the screw dislocation is increased by the shear stress. In compressively strained layers the dissociation width has been found to be decreased by the shear stress, enabling the dislocation to cross slip. An energy barrier analysis has shown that the energetically most favourable cross-slip process proceeds by the formation of a sessile $\frac{a}{6}\langle 011\rangle$ stair-rod dislocation.

Hillock growth, observed in layers under tensile stress, grown at relatively low temperatures, has been found to be originated by the cross slip of the leading partial of a 60° dislocation. This reaction is followed by a reaction of the trailing partial with the stair-rod dislocation to form a Frank partial. At higher growth temperatures the described cross-slip process, is not active anymore, since then the mobility of the Ga(g) dislocations is sufficiently high to relieve the strain.

It further has been demonstrated that the cross-hatched pattern reveals the (mis)-orientation of the substrate surface by the non-parallel groups of dislocation lines at the surface.

Finally, it can be concluded that the relaxation phenomena, as observed in epitaxial layers under tensile as well as under compressive stress are reasonably well understood.

Acknowledgements

The authors would like to thank Dr. F.W. Schapink of the Delft University of Technology for the helpful discussions.

References

[1] J.W. Matthews and A.E. Blakeslee, J. Cryst. Growth **27** (1974) 118

[2] J.W. Matthews, S. Mader and T.B. Light, J. Appl. Phys. **41** (1970) 3800.

[3] P.M.J Marée, J.C. Barbour, J F. van der Veen, K.L. Kavanagh, C W.T. Bulle-Lieuwma and M.P.A Viegers, J. Appl. Phys. **62** (1987) 4413.

[4] R.H M. van de Leur, A.J.G. Schellingerhout, F. Tuinstra and J.E. Mooij, J.Appl. Phys **64** (1988) 3043.

[5] B W. Dodson and J.Y. Tsao, Appl. Phys. Lett. **51** (1987) 1325

[6] R. People and J.C. Bean, Appl. Phys. Lett. **47** (1985) 322, Erratum, Appl. Phys. Lett **49** (1986) 229.

[7] F.C. Frank and J.H. van der Merwe, Proc. Roy. Soc. London, Ser. **A198** (1949) 205.

[8] Y. Fukuda, Y. Kohama and Y. Ohmachi, Jap. J. Appl. Phys **29** (1990) L20.

[9] B.A Fox and W.A. Jesser, J. Appl. Phys. **68** (1990) 2739.

[10] M S. Abrahams, J.Blanc and C.J Buiocchi, Appl. Phys. Lett **21** (1972) 185.

[11] H. Nagai, J. Appl. Phys. **43** (1972) 4254

[12] G H. Olsen, M.S Abrahams and T.J. Zamerowski, J. Electrochem. Soc. **121** (1974) 1650.

[13] G.A. Rozgonyi, P.M. Petrol and M B. Panish, J. Cryst. Growth **27** (1974) 106.

[14] W.J. Bartels and W. Nijman, J. Cryst. Growth **37** (1977) 204.

[15] E.A. Fitzgerald, G.P. Watson, R.E. Proano, G D Pettit, J M. Woodall and D G. Ast, Appl Phys. Lett. **52** (1988) 1496

[16] P.J. van der Wel, J. te Nijenhuis, E.R.H. van Eck and L.J. Giling, Semicond Sci. Technol **7** (1992) A63, this thesis, chapter 5.

[17] E. Molva, Ph. Bunod, F. Roturier, A. Chabli, F. Bertin, J.P. Leludec and P. Lamaudie, in: Semi-insulating III-V Materials, Malmo, 1988, Eds G. Grossmann and L Ledebo (Hilger, Bristol, 1988), p. 565.

[18] J.L. Weyher and J. van de Ven, J. Cryst. Growth **63** (1983) 285.

[19] D.B. Holt, J. Phys. Chem. Solids **27** (1966) 1053

[20] J. Hornstra, J. Phys. Chem. Solids **5** (1958) 129

[21] D.B. Holt, J. Phys. Chem. Solids **23** (1962) 1353.

[22] J.P. Hirth and J Lothe, Theory of Dislocations, 2nd. ed. (Wiley, New York, 1982).

[23] Convention, made at the International Symposium on Dislocations in Tetrahedrally Coordinated Semiconductors, Hunfeld (1979), J. Phys. (Paris) **40** (1979) Colloq. C6, Foreword.

[24] H. Alexander, J. Phys. (Paris) Colloq. **40** (1979) C6-1.

[25] R. Jones, S. Oberg and S. Marklund, Phil. Mag. B **43** (1981) 839.

[26] N. Burle-Durbec, B. Pichaud and F. Minari, Phil. Mag. Lett. **59** (1989) 121.

[27] H. Steinhardt and P. Haasen, Phys. Stat Sol. (a) **49** (1978) 93.

[28] Y. Fukuda, Y. Kohama, M. Seki and Y. Ohmachi, Jap. J. Appl. Phys. **28** (1989) L19.

[29] K. Wessel and H. Alexander, Phil. Mag. **35** (1977) 1523.

[30] Y. Androussi, G. Vanderschaeve and A. Lefebvre, Phil. Mag. **A59** (1989) 1189.

[31] H. Alexander and C. Kisielowski-Kemmerich, Proceedings 8th International School on Defects in Crystals, Szczyrk, Poland (1988).

[32] J. Petruzello and M.R. Leys, Appl. Phys. Lett. **53** (1988) 2414.

[33] C.S. Hartley and D.L.A. Blachon, J. Appl. Phys. **49** (1978) 4788.

[34] P. Pirouz, Scripta Metall. **21** (1987) 1463.

[35] H. Fujita and T Mori, Scripta Metall. **9** (1975) 631.

[36] C.G. Tuppen, C.J. Gibbings, M. Hockly and S.G. Roberts, Appl. Phys. Lett. **56** (1990) 54.

[37] R. Gleichmann, M.D. Vaudin and D.G. Ast, Phil. Mag **A51** (1985) 449.

[38] R. Gleichmann, C. Frigieri and C. Pelosi, Phil. Mag. **A62** (1990) 103.

[39] A.S. Jordan, J. Crystal Growth **49** (1980) 631.

[40] A. Djemel, J. Castaing, N. Burle-Durbec and B. Pichaud, Revue Phys. Appl. **24** (1989) 779.

[41] W. Hagen and H. Strunk, Appl. Phys. **17** (1978) 85.

[42] R.H. Dixon and P.J. Goodhew, J. Appl. Phys. **68** (1990) 3163.

[43] A. Lefebvre, C. Herbeaux, C. Bouillet and J. Di Persio, Phil. Mag. Lett. **63** (1991) 23.

[44] L.J. Giling and B. Dam, J. Crystal Growth **67** (1984) 400.

[45] J. van de Ven, J.L. Weyher, H. Ikink and L.J. Giling, J. Electrochem. Soc. **134** (1987) 989.

Chapter 7

Dissociated V-shaped dislocation model for the relaxation of strained single heterostructures

Abstract

An energy equilibrium model for the prediction of the critical layer thickness of strained single heterostructures, based on relaxation by generation of dissociated V-shaped dislocations, is derived. In this model the dislocations in the layers under tensile as well as under compressive stress are assumed to be extended. The theoretical relation between the thickness and the lattice mismatch is compared with experimental results and with other equilibrium models as proposed in the literature. It is found that a good description of the critical thickness is given by the models assuming nucleation of semicircular perfect dislocation loops and nucleation of dissociated V-shaped dislocations. From kinetic and energetic considerations it is made clear that the model for dissociated V-shaped dislocations is preferred to the model for semicircular perfect loops.

7.1 Introduction

It is well known that the misfit stress in epitaxial layers only can be accomodated elastically up to a certain limit, the critical layer thickness. Above this thickness misfit dislocations will be formed. Generally, these misfit dislocations will degrade the material properties [1]. So in order to fabricate high quality devices, it is important to avoid the generation of dislocations. In the literature several models have been proposed, giving a relation between the lattice mismatch and the critical layer thickness in strained single and multiple heterostructures Frank and Van der Merwe [2]-[4] were the first to calculate the interfacial energy and its dependence on the fit of atomic planes. The value of the critical thickness is found by minimizing the total Gibbs free energy of an epitaxial layer, containing a square grid of two perpendicular and noninteracting arrays of edge dislocations.

Another approach has been reported by Jesser and Matthews [5] and Matthews and Blakeslee [6]. In this model the critical layer thickness is derived from force balance equations on threading dislocations. These dislocations are formed during the growth of the epilayer and expand along the interface to release the strain. Recently, Hu [7, 8] has shown that the critical thickness relation of Matthews and Blakeslee may also be derived from energy equilibrium calculations It can be stated that the mechanical equilibrium model of Matthews and Blakeslee yields the minimal thickness at which misfit dislocation formation can be expected, since in the derivation of this model the dislocations are assumed to be straight and no nucleation and kinetic barriers are taken into account [9] However, in dislocation free material the experimentally observed critical thicknesses of semiconductor epilayers in the diamond or zincblende structure is found to be much higher than the theoretically predicted one by the above models [10].

Addition of Peierls-Nabarro frictional forces in the mechanical equilibrium model increases the theoretical critical layer thickness for short relaxation times [11] However, in the case of long relaxation times and high dislocation mobilities the dislocations are able to attain their equilibrium positions, and therefore the dislocation velocity and the frictional force become zero This reduces the kinetic model to the mechanical equilibrium model.

Another effect which increases the critical layer thickness is the crystallographic perfection of semiconductor substrates. The density of threading dislocations is low and spontaneous nucleation at the top surface and propagation towards the interface of half loop dislocations is necessary for strain relaxation [11]. This relaxation mechanism has been elaborated by several authors for perfect semicircular [12], dissociated semicircular [13] and perfect V-shaped [14] dislocation half loops The accuracy with which the critical layer thickness (the thickness at which the first misfit dislocation appears) is determined depends upon the sensitivity of the measuring technique used to detect the lattice relaxation [15]. However, it is not necessary to determine the change in strain caused by the formation of the first misfit dislocation, since it has been shown that the theoretical curves can also be considered as critical-strain-thickness relations [16].

In chapter 6 the relaxation mechanism of strained $In_xGa_{1-x}As$ and GaAs epitaxial layers is discussed [17] on the basis of the dislocation types [18] and the dislocation mobilities [19]. It has been shown that the relaxation of strained layers starts by the nucleation of As(g) dislocations, which are in the $[01\bar{1}]$ direction for layers under tensile stress and in the [011] direction for layers under compressive stress. The nucleated dislocations expand as V-shaped dislocations towards the interface. It was revealed that the dissociation of dislocations influences the relaxation process strongly. This relaxation mechanism differs from those in the aforementioned critical thickness models [12]-[14].

In this chapter a relation is derived between the layer thickness and the lattice mismatch for both layers under tensile and under compressive stress, based on relaxation by the formation of dissociated V-shaped dislocations. Calculations of the critical thickness and the activation energy are presented and compared to the previous models and experimental observations of dislocation formation in GaAs epitaxial layers under tensile stress and $In_xGa_{1-x}As$ (100) epitaxial layers under compressive stress. The model of People and Bean [20] is not mentioned in the discussion, because of the physical imperfections in this model, discussed by Hu [8].

7.2 Theory of equilibrium models

The equilibrium theories for the critical layer thickness are based on the assumption that the first misfit dislocation will nucleate when the total Gibbs free energy of the epitaxial layer containing one misfit dislocation at the interface becomes lower than that of the completely strained, pseudomorphic layer [12]. At the critical thickness these two configurations possess the same energy. In that case the formation energy of the dislocation line is as large as the elastic strain energy, released by this dislocation [12]. All the equilibrium theories, as are discussed in this chapter, follow a similar derivation approach, they only differ from each other in the configuration of the nucleated dislocation. Therefore first a general review of the equilibrium theory is given, which is followed by the subsequent treatment of the specific models. In order to obtain a good comparison of the models, the same expressions for the dislocation line energy and for the elastic strain energy are used in all the models; consequently the critical layer thickness relations may be slightly different from those derived in the original papers.

The strain in the epitaxial layers is assumed to be distributed uniformly. The assumption of elastic isotropy of the crystals does not apply for GaAs and $In_xGa_{1-x}As$. The anisotropy ratio for GaAs at the growth temperature, defined as $2c_{44}/(c_{11} - c_{12})$ [21], in which c_{ij} are the elastic constants, is *ca.* 1.8 [22]. Since the use of anisotropic constants would make the problem complex, they are estimated in the calculations by the Voigt averages. These constants give average values over all possible orientations of the coordinate system, relative to the crystal axes. They are most appropriate in cases of uniform strain around dislocations. For the case of cubic crystals the Voigt averages of the Lamé constant λ_v, the shear modulus μ and the Poisson's ratio ν as a function of the anisotropic constants are given in the appendix.

The elastic force F on a straight dislocation line with length L and Burgers vector b is given by:

$$F = L\tau b = L\sigma b \cos\phi \cos\lambda, \qquad (7.1)$$

in which τ is the shear stress on an $\{111\}$ glide plane, σ is the misfit stress, $\cos\phi\cos\lambda$ is the Schmid factor [23], which relates the shear stress τ to the misfit stress σ. ϕ is the angle between the normal to the slip plane and σ, which is perpendicular to the growth direction and the intersection line of the surface and the glide plane, and λ is the angle between σ and the Burgers vector. In the isotropic elasticity theory [24] the relation between the biaxial stress σ and the strain ϵ is given by:

$$\sigma = 2\mu \left(\frac{1+\nu}{1-\nu}\right) \epsilon. \qquad (7.2)$$

When a dislocation with length L nucleates at the surface of an epitaxial layer and moves towards the interface over a distance ds, perpendicular to the dislocation line, it releases the strain energy in an area A, which is the integral of the product $L\mathrm{d}s$. In this case the total released elastic energy E_ϵ is expressed by:

$$E_\epsilon = 2\mu A \left(\frac{1+\nu}{1-\nu}\right) \epsilon b \cos\phi \cos\lambda. \qquad (7.3)$$

The area A depends on the assumed configuration of the dislocation half loop When the first dislocation nucleates, no relaxation has taken place yet, and therefore the strain ϵ equals the lattice mismatch f [16].

The line energy of a dislocation depends on the crystallographic orientation as well as on the angle β between the Burgers vector and the dislocation The general expression for the line energy E_{d} of a straight dislocation line of infinitesimal length dl is given by [21]

$$E_{\mathrm{d}} = \mathrm{d}l\left(\frac{K_{\mathrm{e}}\sin^2\beta + K_{\mathrm{s}}\cos^2\beta}{4\pi}\right)b^2\left\{\ln\left(\frac{\alpha R}{b}\right) - 1\right\} \tag{7 4}$$

In this expression K_{e} and K_{s} are the energy coefficients of the edge and the screw component respectively, α is the core parameter and R is the smallest distance from the dislocation core to the surface. For straight dislocations in $\{111\}$ planes parallel to the $\langle 011\rangle$ directions in the face-centred-cubic (FCC) structure the energy coefficients are known exactly [21] and given in the Appendix For curved dislocations, like the semicircular dislocation loop, the character of the dislocation changes continuously with orientation In this case the values of the Voigt averages for μ and ν are used Other contributions to the total energy of an epilayer containing a misfit dislocation line, like the energy of a new surface step, created by the nucleation of a dislocation, may be ignored for layer thicknesses above 5 nm [11]

The change in the Gibbs free energy, resulting from the nucleation and expansion of a misfit dislocation, is given by

$$\Delta G = E_{\mathrm{d}} - E_{\epsilon} \tag{7 5}$$

When a dislocation nucleates and propagates as far as the interface, first the Gibbs free energy increases to a maximum value and then decreases, provided that the layer thickness is large enough. This will be discussed more in detail in section 7 3 At a certain critical point the Gibbs free energy of the epilayer becomes as large as in the initial state, *i e* ΔG becomes zero The critical thickness of an epitaxial layer is defined as the thickness, at which the change in the Gibbs free energy ΔG is exactly zero, when the dislocation has just reached the interface [12] At lower thicknesses ΔG is larger than zero, which

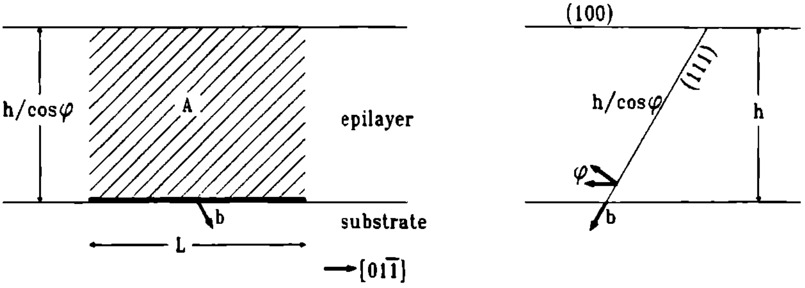

Figure 7.1 Projection and side view on the {111} plane of the equilibrium dislocation configuration of a single heterostructure of the model of Hu [7]. The hatched area represents the slipped material, the dark line at the interface is the dislocation line, the arrow represents the Burgers vector of the dislocation.

means that a nucleated dislocation brings the epilayer in a metastable state. Therefore it is not likely that in this case dislocations will nucleate. The described criterion for the critical layer thickness was first considered by Van de Leur *et al.* [12] and is used in the derivations of the relations throughout this chapter.

7.2.1 Mechanical equilibrium model

In the model of Hu [7, 8] the misfit dislocation is assumed to be a 60° dislocation lying along the ⟨011⟩ direction at the interface between the substrate and the epitaxial layer. It will elongate, when the increase of the line energy is smaller than the released elastic energy. The nucleation process (from the surface or from threading dislocations) is not taken in account.

The projection on the {111} plane of the configuration is given in fig. 7.1. In an epilayer of height h with orientation (100), the area A in which the strain energy is released, is given by $A = Lh/\cos\phi$. From eqs. (7.3), (7.4) and (7.5) the following relation for the critical layer thickness is obtained:

$$h_c = \frac{(3K_e + K_s)}{16\pi f \cos\lambda} \frac{b}{2\mu} \left(\frac{1-\nu}{1+\nu}\right) \left\{ \ln\left(\frac{\alpha h_c}{b}\right) - 1 \right\}. \tag{7.6}$$

This relation is the same as the one derived by Matthews and Blakeslee [6] from the force balance approach, except for the -1 term at the right hand side. This discrepancy is the result of a different approximation of the dislocation core energy [8].

7.2.2 Nucleation model for semicircular dislocation loops

The relaxation process, on which the equilibrium model of Van de Leur *et al.* [12] is based, starts by the nucleation of a semicircular perfect dislocation loop at the surface. This is schematically given in fig. 7.2a. The half loop expands as far as the interface (fig. 7.2b), continued by the elongation of the dislocation line along the interface (fig. 7.2c). The line energy of a semicircular dislocation loop with radius R is given by [25]:

$$E_{\mathrm{d}} = \frac{\pi R \mu b^2}{8\pi}\left(\frac{2-\nu}{1-\nu}\right)\left\{\ln\left(\frac{8\alpha R}{b}\right) - 2\right\}. \tag{7.7}$$

The area in which strain release has taken place is $\pi R^2/2$. At the critical thickness h_{c}, the largest loop which just fits in the film has a radius R_{c}, which is related to h_{c} by:

$$h_{\mathrm{c}} = R_{\mathrm{c}} \cos\phi. \tag{7.8}$$

Using eqs. (7.3), (7.5), (7.7) and (7.8), results in the relation for the critical layer thickness to be:

$$h_{\mathrm{c}} = \frac{b}{8\pi f \cos\lambda}\left(\frac{2-\nu}{1+\nu}\right)\left\{\ln\left(\frac{8\alpha h_{\mathrm{c}}}{b\cos\phi}\right) - 2\right\}. \tag{7.9}$$

7.2.3 Nucleation model for dissociated semicircular dislocations

A variant on the half loop nucleation model is proposed by Marée *et al.* [13]. In this model, which has been derived for relaxation in layers under tensile stress originally, the dislocation half loop is assumed to be dissociated into a 30° and a 90° Shockley partial. Inbetween these partials a stacking fault area is formed, which adds another energy term to

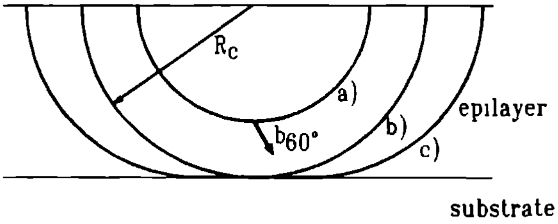

Figure 7.2 Projection on the $\{111\}$ plane of the nucleation and propagation of a semicircular dislocation loop at various stages of the relaxation process a) shows the dislocation as a subcritical half loop In b) the half loop just has reached the interface and has the critical radius R_c In c) the dislocation is elongated along the interface to form a dislocation line The arrow represents the Burgers vector *b*

the equation of ΔG In order to be able to make a good comparison between this model and the other equilibrium theories, in the following a derivation is given using the approach of Van de Leur *et al* [12] The final result is therefore different from the original relation of Marée *et al* [13].

The dislocation generation process is the same as in the case of the perfect half loops, except for the fact that the dislocation is now dissociated, this is schematically depicted in fig 7 3. Since the half loop exists in this case of two partials, in line energy calculations these two are both taken into account Using eqs (7 7) and (7 8) this results in·

$$E_{\mathrm{d}} = 2\frac{\pi h}{\cos\phi}\frac{\mu b_{\mathrm{p}}^2}{8\pi}\left(\frac{2-\nu}{1-\nu}\right)\left\{\ln\left(\frac{8\alpha h}{b_{\mathrm{p}}\cos\phi}\right)-2\right\} \tag{7 10}$$

The mean dissociation distance d of the extended dislocation is determined by the repulsive force of the partials and the attractive forces of the stacking fault γ and the misfit stress τ [13]

$$d = \frac{\mu b_{\mathrm{p}}^2}{8\pi}\left(\frac{2-\nu}{1+\nu}\right)\frac{1}{\gamma+\tau b_{\mathrm{pt}}}, \tag{7 11}$$

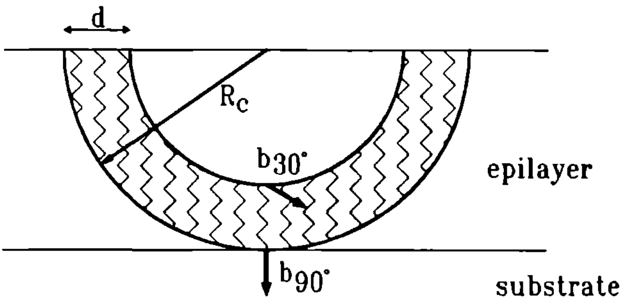

Figure 7.3 Projection on the {111} plane of the configuration of a critical dissociated semicircular dislocation loop a layer under tensile stress. The dissociation distance of the partials is indicated as *d*. The shaded region is the stacking fault area between the partial dislocations. The arrows represent the Burgers vectors of the Shockley partials.

in which $b_{p(t)}$ is the Burgers vector of the (trailing) Shockley partial. The extra energy term E_γ of the stacking fault area, caused by the dissociation, is for small values of d with respect to R [13]:

$$E_\gamma = (\gamma + \tau b_{pt})\,\pi R d = \frac{\mu b_p^2 R}{8}\left(\frac{2-\nu}{1+\nu}\right). \tag{7.12}$$

At large misfit stresses the dissociation distance can become as large as the layer thickness.

With the aid of eq. (7.3), (7.5), (7.10) and (7.12), the result for the critical layer thickness is:

$$h_c = \frac{b_p^2}{4\pi b f \cos\lambda}\left(\frac{2-\nu}{1+\nu}\right)\left\{\ln\left(\frac{8\alpha h_c}{b_p\cos\phi}\right) - \frac{3}{2}\right\}. \tag{7.13}$$

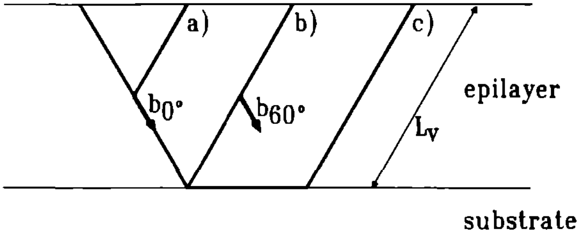

Figure 7.4 Projection on the $\{111\}$ plane of the nucleation and propagation of a V-shaped dislocation loop at various stages of the relaxation process. The 60° segment of the subcritical loop, shown in a), moves towards the interface. In b) the critical V-shaped dislocation loop is shown, which expands as a semihexagonal dislocation loop to form a dislocation line along the interface (c). L_v is the length of a segment of the V-shaped dislocation. The arrows represent the Burgers vectors of the screw and the 60° dislocations.

7.2.4 Nucleation model for V-shaped dislocations

Based on transmission electron microscopy (TEM) observations of misfit dislocations in strained layers [26, 27], Fukuda *et al.* have reported a model for the critical layer thicknes, in which the nucleated misfit dislocation is V-shaped, as is shown in fig. 7.4. The two segments of this dislocation lie in the $\langle 011\rangle$ directions of a $\{111\}$ glide plane. One of them is a screw dislocation, whereas the other is a 60° dislocation. The critical V just fits in the epilayer (fig. 7.4b) and expands farther along the interface, forming a hexagonal dislocation half loop (fig. 7.4c). The dislocation along the interface is a 60° dislocation. The relation between the thickness h and the segment length L_v is:

$$h = L_v \cos\psi, \tag{7.14}$$

in which ψ is the angle between the dislocation line direction and the surface normal. The area enclosed by the V-shaped dislocation is an equilateral triangle with length L_v:

$$A = \frac{\sqrt{3}}{4}L_v^2 = \frac{\sqrt{3}h^2}{4\cos^2\psi}. \tag{7.15}$$

The dislocation line energy, as is given by eq. (7.4), is dependent on the shortest distance from the position on the dislocation line to the surface. Along a V-shaped dislocation this distance varies from 0 at the surface to h at the interface. Therefore the line energy has to be integrated over the total length L_v of the segments. This is given by:

$$E_d = \frac{K_t b^2}{4\pi} \int_0^{L_v} \left\{ \ln\left(\frac{\alpha l \cos\psi}{b}\right) - 1 \right\} dl = \frac{K_t b^2 h}{4\pi \cos\psi} \left\{ \ln\left(\frac{\alpha h}{b}\right) - 2 \right\}, \qquad (7.16)$$

in which K_t is the energy coefficient of the specific dislocation type t (60° or screw), and $l\cos\psi$ is the distance from the dislocation to the surface. The total line energy of a V-shaped dislocation of height h is given by the summation of the energies of the individual screw and the 60° parts. Using eqs. (7.3), (7.5), (7.15) and (7.16), the resulting relation for the critical layer thickness is calculated to be:

$$h_c = \frac{(5K_s + 3K_e)b}{16\pi f} \left\{ \ln\left(\frac{\alpha h_c}{b}\right) - 2 \right\} \frac{\cos\psi}{\cos\phi \cos\lambda} \frac{4}{2\mu\sqrt{3}} \left(\frac{1-\nu}{1+\nu}\right). \qquad (7.17)$$

7.2.5 Nucleation model for dissociated V-shaped dislocations

In chapter 6 a relaxation mechanism is proposed, which is valid for epilayers both under tensile and under compressive stress [17]. The relaxation process is initiated by the nucleation of arsenic glide (As(g)) dislocations, which lie in the $[01\bar{1}]$ and in the $[011]$ direction for layers under tensile and under compressive stress respectively [28]. These dislocations will expand as dissociated V-shaped dislocations. The projections on the $\{111\}$ of the configurations are shown in fig. 7.5. The screw part of the V is dissociated into two 30° Shockley partials; the 60° part is dissociated into a 90° and a 30° partial. In the case of tensile stress the 30° As(g) of the 60° dislocation (at the right hand side of fig. 7.5a) is the first partial to nucleate [17], in the case of compressive stress this is the 90° As(g) partial of the 60° dislocation (fig. 7.5b). The dissociation width of the dislocations is dependent on the orientations of the Burgers vectors with respect to the shear stress [29]. In the following a new model for the critical layer thickness in layers both under tensile and under compressive stress is presented, based on the above described relaxation mechanism.

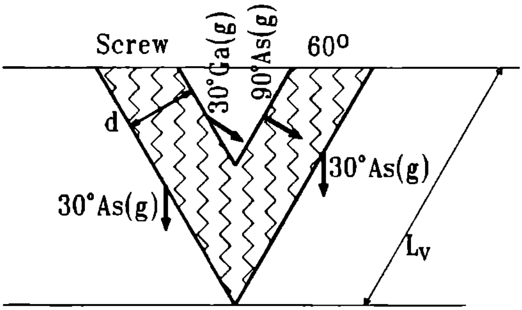

a) Tensile system

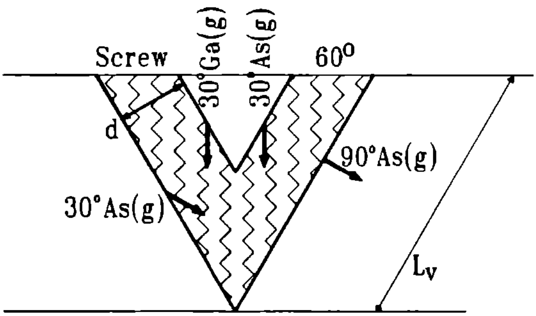

b) Compressive system

Figure 7.5 Projection on the {111} plane of a critical dissociated V-shaped dislocation loop in a) a layer under tensile stress and b) a layer under compressive stress. *d* is the dissociation distance between the two Shockley partials. The left hand side of the V is the dissociated screw dislocation, the right hand side the dissociated 60° dislocation. The stacking fault area is the shaded region. The Burgers vectors of the specific Shockley partials are represented by the arrows.

The line energy of a dissociated V-shaped dislocation is the summation of the four partials, which constitutes this dislocation. The relation for inclined dislocations, derived in the previous section (eq. (7.16)), can be used. Substitution of the appropriate values for the individual parts and summation results in the total line energy for dissociated V-shaped dislocations of height h:

$$E_d = \frac{(9K_s + 7K_e)}{16\pi} \frac{b_p^2 h}{\cos\psi} \left\{ \ln\left(\frac{\alpha h}{b_p}\right) - 2 \right\}. \tag{7.18}$$

The stacking fault energy in the area enclosed by the partial dislocations E_γ is the sum of the area between the screw and the 60° parts:

$$E_\gamma = (\gamma + \tau b_{pt})\,(d_{60^\circ} + d_s)\,L_v, \tag{7.19}$$

in which the dissociation widths of the 60° and the screw dislocation under tensile and compressive stress respectively are given by [17]:

$$d_{60^\circ} = \frac{d_{60^\circ,o}}{1 + (g - \rho)\,b\tau/2\gamma}, \tag{7.20}$$

$$d_{st} = \frac{d_{s,o}}{1 - (1 - g/\rho)\,b\tau/2\gamma}, \tag{7.21}$$

$$d_{sc} = \frac{d_{s,o}}{1 - (1 + g/\rho)\,b\tau/2\gamma}. \tag{7.22}$$

In these relations $d_{t,o}$ is the dissocation width of the specific dislocation type t in stress free conditions [21], g is a geometrical factor [17, 29] and ρ is $(1 - r)/(1 + r)$ with r the ratio of the mobilities of the partial dislocations [29, 30]. If the released elastic energy is taken from the perfect V-shaped dislocation (eqs. (7.3) and (7.15)), together with eqs. (7.5), (7.18) and (7.19) the following critical thickness relation for relaxation by dissociated V-shaped dislocations is obtained:

$$h_c = \left(\frac{(9K_s + 7K_e)\,b_p^2}{16\pi} \left\{ \ln\left(\frac{\alpha h_c}{b}\right) - 2 \right\} + (\gamma + \tau b_{pt})\,(d_{60^\circ} + d_s) \right) \times$$

$$\frac{\cos\psi}{2\mu f b \cos\phi \cos\lambda} \frac{4}{\sqrt{3}} \left(\frac{1 - \nu}{1 + \nu}\right). \tag{7.23}$$

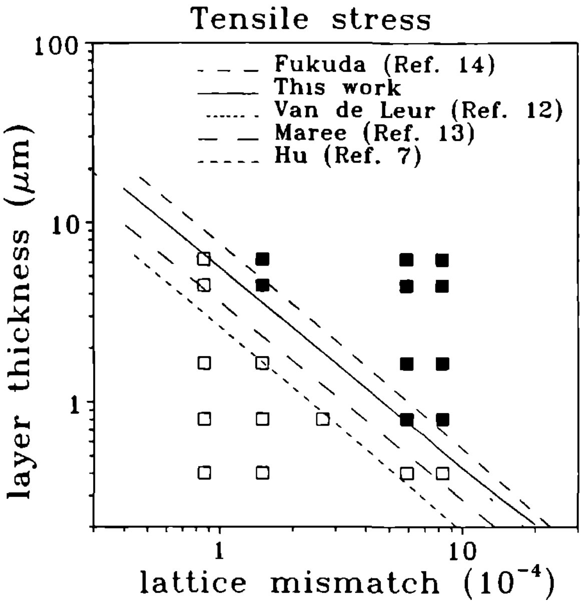

Figure 7.6 Calculated critical layer thickness h_c as a function of the lattice mismatch f in the case of tensile stress according to the V-shaped dislocation nucleation model (eq. (7.17)), the dissociated V-shaped dislocation nucleation model (eq. (7.23)), the semicircular dislocation nucleation model (eq. (7.9)), the dissociated semicircular dislocation nucleation model (eq. (7.13)) and the mechanical equilibrium model (eq. (7 6)). The filled and open symbols indicate experimental data of GaAs layers grown on $In_xGa_{1-x}As$ substrates with and without misfit dislocations respectively

7.3 Discussion

In figs. 7.6 and 7.7 the results of the calculations of the critical layer thickness as a function of the lattice mismatch are presented for tensile and compressive stress respectively. As it was already mentioned, it has been shown that the model of Hu (eq.(7.6)) yields the lowest critical layer thickness at a certain lattice mismatch. The curves of the dissociated half loop nucleation models (eqs. (7.13) and (7.23)), lie under those of the corresponding perfect half loop models (eqs. (7.9) and (7.17)), proving that strain relaxation by extended dislocations proceeds in an energetically more favourable way than by perfect dislocations. It is further noticed that the curves for the semicircular models always lie under those of the V-shaped models, both in the case of dissociated and of perfect dislocations. This may be explained as a consequence of the fact that the area to periphery ratio of a semicircle is higher than that of an equilateral triangle by a factor 2. A semicircular dislocation loop releases more strain energy at the cost of the formation of a dislocation line than a V-shaped dislocation in an epilayer of the same thickness.

In fig. 7.6 the experimental results are shown of epitaxial GaAs layers, grown by metalorganic vapour phase epitaxy (MOVPE) on $In_xGa_{1-x}As$ substrates. The details of the growth experiments have been described in chapter 4. In this heteroepitaxial system the GaAs layers are under tensile stress. It has been shown that these layers already have reached the equilibrium state during growth, post growth annealing has hardly changed the amount of residual strain [16]. Experimental results of compressively strained layers are shown in fig. 7.7. Here the results of $In_xGa_{1-x}As$ epilayers, grown by MOVPE on GaAs [28] are shown. It follows for both the stress types that the critical thickness calculations of the V-shaped dislocation model yield higher values than the experimental results, whereas the predictions of the mechanical equilibrium model and the dissociated semicircular loop give lower values. A good description of the critical layer thickness is given by both the semicircular half loop model of Van de Leur *et al.* [12] and the dissociated half loop model of this work. In the following a discrimination between these two models is possible by looking at their propagation mechanisms and at the resultant morphology and by considering the required activation energies.

A dislocation slips in the direction of the Burgers vector. For a V-shaped dislocation it is shown in fig. 7.4 that the 60° segment propagates towards the interface, thereby reducing the strain in the interior of the V. The dislocation line remains V-shaped under the movement of the 60° part. On the other hand, in the case of a dislocation loop which expands as a circle (fig. 7.2) from a certain point at the surface, each point of the dislocation line propagates into the direction normal to the circle, to keep the dislocation circularly shaped, and not into the direction of the Burgers vector. It is therefore more likely that the dislocations propagate as V-shaped dislocations than as semicircular dislocation loops.

Another argument for the strain relaxation by V-shaped dislocations is obtained from calculations of the activation energy of the critical dislocation loops. In fig. 7.8 the Gibbs free energy ΔG as a function of the height h of the loop is presented for both theories. The lattice mismatch f is taken 7.2×10^{-4}, corresponding to an indium content of 1% in the $In_xGa_{1-x}As$/GaAs system. It is demonstrated that the maximum energy is higher for the semicircular dislocation loop (17.1 keV, 15.1 eV/nm) than for the dissociated V-shaped

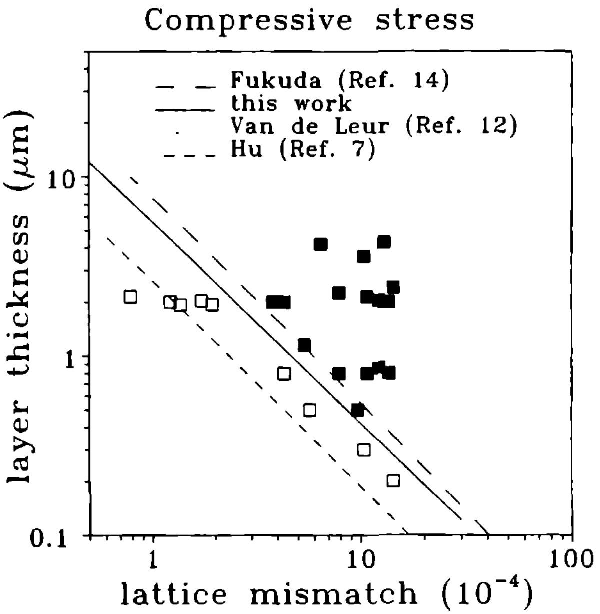

Figure 7.7 Calculated critical layer thickness h_c as a function of the lattice mismatch f in the case of compressive stress according to the V-shaped dislocation nucleation model (eq. (7.17)), the dissociated V-shaped dislocation nucleation model (eq. (7.23)), the semicircular dislocation nucleation model (eq. (7.9)) and the mechanical equilibrium model (eq. (7.6)). The filled and open symbols indicate experimental data of In_xGa_{1-x} As layers grown on GaAs substrates with and without dislocations respectively.

dislocation (7.2 keV, 7.9 eV/nm), which means that the latter loop will be formed more easily than the first one.

In addition, in chapter 6 it has been demonstrated that the morphology of partially relaxed strained layers under compressive and under tensile stress could be explained by assuming relaxation by dissociated V-shaped dislocations and not by semicircular loops [17].

Based on these considerations, it has become clear that the model, describing the relaxation by dissociated V-shaped dislocations is to be preferred.

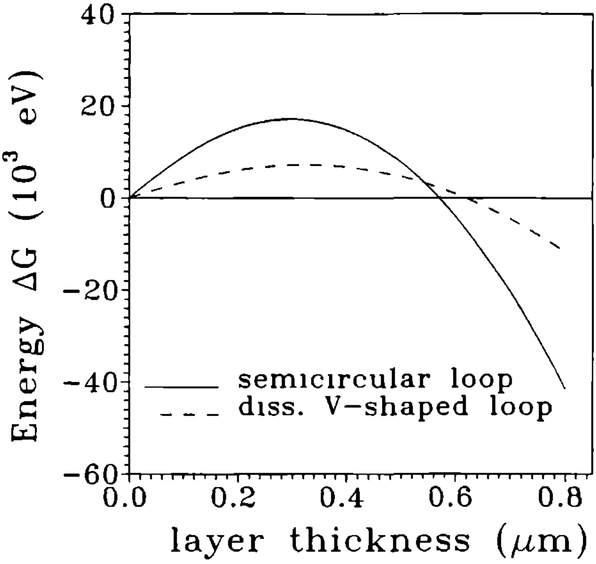

Figure 7.8 Gibbs free energy ΔG of a semicircular dislocation loop and of a dissociated V-shaped dislocation as a function of the height h of the loop The lattice mismatch f is taken to be $7\ 2 \times 10^{-4}$

7.4 Summary and conclusions

A model for the prediction of the critical layer thickness based on the relaxation by dissociated V-shaped dislocations generated at the surface is presented The theoretical relation between the lattice mismatch and the thickness is compared to experimental results, obtained from layers under tensile stress and under compressive stress in the $In_xGa_{1-x}As/GaAs$ system, and to other equilibrium models It was found that the present model and the perfect semicircular model match the experimental results well, both in the case of tensile stress and in the case of compressive stress. Kinetic and energetic arguments have made it plausible that the dissociated V-shaped dislocation model is to be preferred

7.A Appendix

Approximations for isotropic constants expressed in terms of anisotropic constants provide possibilities to apply the more simple isotropic theories on anisotropic crystals, thereby reducing the problem complexity. The Voigt aproximation gives values for the elastic constants, averaged over all possible orientations of the coordinate system relative to the crystal axes. In the case of cubic crystals the Voigt averages are given by [21]:

$$\begin{aligned} \lambda_v + 2\mu &= c_{11} + 2/5H, & (7.A.1) \\ \lambda_v &= c_{12} - 1/5H, & (7.A.2) \\ \mu &= c_{44} - 1/5H, & (7.A.3) \\ \nu &= \frac{c_{12} - 1/5H}{c_{11} + c_{12} + 1/5H}, & (7.A.4) \end{aligned}$$

in which H is the anisotropy factor, defined as

$$H = 2c_{44} + c_{12} - c_{11}. \qquad (7.A.5)$$

For the calculation of the energy coefficients K_s and K_e for screw and edge dislocations in

$$\frac{W}{L} = \frac{K_s \cos^2\beta + K_e \sin^2\beta}{4\pi} \left\{ \ln\left(\frac{\alpha R}{b}\right) - 1 \right\} \qquad (7.A.6)$$

the more exact anisotropic theory can be used [21]. For straight dislocations along the $\langle 011 \rangle$ directions in FCC-crystals they are given by:

$$K_s = (c'_{44} c'_{55})^{1/2} \qquad (7.A.7)$$

and

$$K_e = \frac{1}{3}\left(2 + \frac{c'_{22}}{\bar{c}'_{11}}\right)(\bar{c}'_{11} + c'_{12}) \left[\frac{c'_{55}(\bar{c}'_{11} - c'_{12})}{c'_{22}(\bar{c}'_{11} + c'_{12} + 2c'_{55})}\right]^{1/2}, \qquad (7.A.8)$$

in which c'_{ij} are the elastic constants for cubic crystals in a coordinate system which is rotated over 45° about one of the cubic axes. They are expressed in the cubic coordinate system by:

$$\begin{aligned} c'_{11} &= c_{11}, & (7.A.9) \\ c'_{12} &= c_{12}, & (7.A.10) \\ c'_{55} &= c_{44}, & (7.A.11) \\ c'_{22} &= c_{11} + 1/2H, & (7.A.12) \\ c'_{23} &= c_{12} - 1/2H, & (7.A.13) \\ c'_{44} &= c_{44} - 1/2H & (7.A.14) \end{aligned}$$

and

$$\bar{c}'_{11} = (c'_{11}c'_{12})^{1/2}. \tag{7.A.15}$$

In the isotropic case K_s and K_e are given by the well known relations:

$$\begin{aligned} K_s &= \mu, & (7.A.16) \\ K_e &= \frac{\mu}{1-\nu}. & (7.A.17) \end{aligned}$$

References

[1] J.M. Woodall, G.D. Pettit, T.N. Jackson, C. Lanza, K.L. Kavanagh and J.W. Mayer, Phys. Rev. Letters **51** (1983) 1783.

[2] F.C. Frank and J.H. van der Merwe, Proc. Roy. Soc. London Ser. **A198** (1949) 205.

[3] F.C. Frank and J.H. van der Merwe, Proc. Roy. Soc. London Ser. **A198** (1949) 216.

[4] F.C. Frank and J.H. van der Merwe, Proc. Roy. Soc. London Ser. **A200** (1949) 125.

[5] W.A. Jesser and J.W. Matthews, Phil. Mag. **15** (1967) 1097.

[6] J.W. Matthews and A.E. Blakeslee, J. Cryst. Growth **27** (1974) 118.

[7] S.M. Hu, J. Appl. Phys. **69** (1991) 7901, erratum J. Appl. Phys. **70** (1991) 4009.

[8] S.M. Hu, J. Appl. Phys. **70** (1991) R53.

[9] M.R. Leys, in: Low-Dimensional Structures in Semiconductors, Eds. A.R. Peaker and H.G. Grimmeis (Plenum Press, New York, 1991).

[10] E. Kasper and H.J. Herzog, Thin Solid Films **44** (1977) 357.

[11] J.W. Matthews, S. Mader and T.B. Light, J. Appl. Phys. **41** (1970) 3800.

[12] R.H.M. van de Leur, A.J.G. Schellingerhout, F. Tuinstra and J.E. Mooij, J. Appl. Phys. **64** (1988) 3043.

[13] P.M.J. Marée, J.C. Barbour, J.F. van der Veen, K.L. Kavanagh, C.W.T. Bulle-Lieuwma and M.P.A. Viegers, J. Appl. Phys. **62** (1987) 4413,

[14] Y. Fukuda, Y. Kohama and Y. Ohmachi, Jap. J. Appl. Phys. **29** (1990) L20.

[15] I.J. Fritz, Appl. Phys. Lett. **51** (1987) 1080.

[16] J. te Nijenhuis, P.J. van der Wel, R.W.F. van Asten, P.R. Hageman and L.J. Giling, J. Cryst. Growth **107** (1991) 496, this thesis, chapter 4.

[17] J. te Nijenhuis, P.J. van der Wel, E.R.H. van Eck and L.J. Giling, J. Appl. Phys. (submitted), this thesis, chapter 6.

[18] D.B. Holt, J. Phys. Chem. Solids **23** (1962) 1353.

[19] H. Steinhardt and P. Haasen, Phys. Stat. Sol. (a) **49** (1978) 93.

[20] R. People and J.C. Bean, Appl. Phys. Lett. **47** (1985) 322, Erratum **49** (1986) 229

[21] J.P. Hirth and J. Lothe, Theory of dislocations, 2nd. ed. (Wiley, New York, 1982) ch. 13.

[22] A.S. Jordan, J. Crystal Growth **49** (1980) 631.

[23] See *e.g.* D. Hull and D.J. Bacon, Introduction to dislocations, 3rd. ed. (Pergamon Press, Oxford, 1984).

[24] See *e.g.* J.F. Nye, Physical properties of crystals (Oxford University Press, Oxford, 1967).

[25] Ref. [21], ch. 3.

[26] Y. Fukuda, Y. Kohama, M. Seki and Y. Ohmachi, Jap. J. Appl. Phys. **28** (1989) L19.

[27] Y. Fukuda, J. Crystal Growth **99** (1990) 269.

[28] P.J. van der Wel, J. te Nijenhuis, E.R.H. van Eck and L.J. Giling, Semicond. Sci. Technol. **7** (1992) A63, this thesis, chapter 5.

[29] K. Wessel and H. Alexander, Phil. Mag. **35** (1977) 1523.

[30] Y. Androussi, G. Vanderschaeve and A. Lefebvre, Phil. Mag. A **59** (1989) 1189.

Chapter 8

Relaxation slip systems in (110) oriented epitaxial layers in the zincblende structure

Abstract

The slip systems for the relaxation of lattice mismatched (110) oriented $In_xGa_{1-x}As$ epitaxial layers have been investigated. From a theoretical study of the glide systems in the zincblende structure it appears that three dislocation types are able to relax strain in these layers. Experimentally two of these types have been observed. The first misfit dislocations nucleate in the $[1\bar{1}0]$ direction, gliding along the $\{111\}$ planes. At higher thicknesses or indium concentrations dislocations also nucleate in the $\langle 112 \rangle$ directions and glide along the $\{311\}$ planes. The critical layer thickness for relaxation by misfit dislocations of these types has been calculated, using the equilibrium theory for V-shaped dislocations. A comparison with the experimentally observed critical thickness shows that the theory is in good agreement with the experiments in the case of $[1\bar{1}0]$ oriented dislocations, whereas a large discrepancy exists for the case of the $\langle 112 \rangle$ dislocations. This discrepancy is explained by (*i*) the low mobility and (*ii*) the high activation energy of the perfect $\langle 112 \rangle$ dislocations. From a comparison of the surface morphologies of $In_xGa_{1-x}As$ with those of Ge_xSi_{1-x} and diamond (110) oriented epilayers, it could be concluded that the relaxation pattern is strongly dependent on the mobilities of the dislocations.

8.1 Introduction

Mechanisms for the relaxation of strain by the nucleation and propagation of misfit dislocations in (100) oriented epitaxial layers in the zincblende [1]-[5] as well as in the diamond structure [6]-[10] have been studied extensively. In chapter 6 the relaxation mechanisms in (100) strained layers in the $In_xGa_{1-x}As/GaAs$ system under tensile and compressive stress have been described [11]. It appeared that the relaxation starts by the nucleation of dissociated V-shaped dislocations at the surface, which propagate along the $\{111\}$ glide planes towards the interface between the epitaxial layer and the substrate. The segments of the dislocations all belong to the screw and 60° $\langle 110\rangle\{111\}$ type. When the dislocations have reached the interface, they elongate along the [011] and the $[01\bar{1}]$ directions, which are the lines of intersection between the glide planes and the substrate surface. The orientation of the four $\{111\}$ planes with respect to the (100) surface is equivalent. However, it has been shown [11]-[13] that due to the zincblende structure of GaAs the dislocations along the two $\langle 110\rangle$ directions show a different electric and kinetic behaviour.

Based on the reported relaxation mechanism [11] an energy balance model for the calculation of the critical layer thickness has been derived [14]. This model equates the line energy of the nucleated dislocations with the released elastic energy. The resulting theoretical relation between the lattice mismatch and the layer thickness matches well with the experimentally observed critical layer thickness for both layers under compressive and under tensile stress.

From these investigations it may be concluded that the relaxation process in the (100) system is clearly understood. Relaxation in strained layers with other orientations than (100) has attracted much less attention. Experimentally, the critical layer thickness for (111)B oriented $In_xGa_{1-x}As$ epilayers grown on GaAs has been determined [15]. In this case the misfit dislocations glide along the other three $\{111\}$ planes which are inclined to the surface [16]. The surface morphology shows a triangular pattern of dislocations along the $\langle 110\rangle$ directions [17].

Relaxation in (110) oriented strained layers has been reported for Ge_xSi_{1-x} alloys under compressive stress grown on silicon [18]. It has been found that the strain is relieved mainly uniaxially along the $[1\bar{1}0]$ direction by the formation of partial dislocations. In this chapter the relaxation of (110) $In_xGa_{1-x}As$ epilayers grown under compression on GaAs is described. The relaxation slip systems are determined on the basis of theoretical conditions for a slip system and compared with the experimentally observed surface morphologies. The critical layer thickness in the different glide systems is calculated and

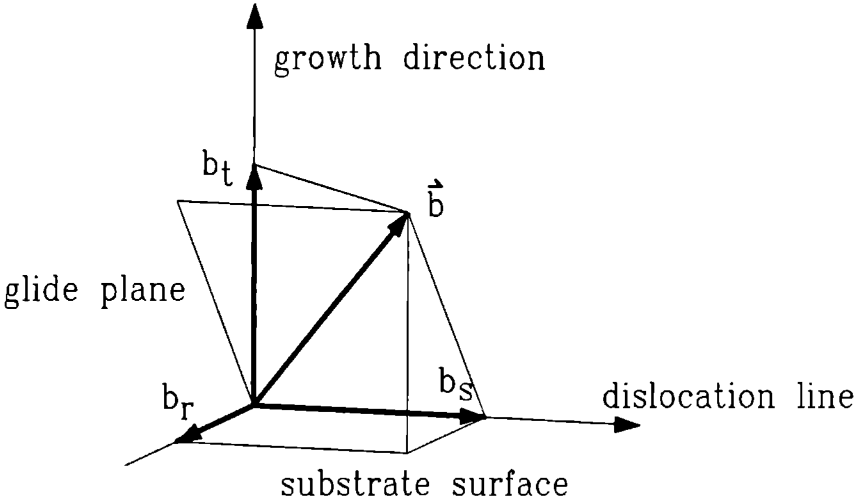

Figure 8.1 The decomposition of the Burgers vector into the three orthogonal components. b_s is the screw component. b_r is the edge component, responsible for relaxation. b_t is the edge component, necessary for the motion of the dislocation towards the interface and responsible for the tilt in the epilayers. The glide plane is the plane containing the Burgers vector b and the dislocation line.

compared with the experimental results. Finally, the relaxation patterns of $In_xGa_{1-x}As$, Ge_xSi_{1-x} and diamond epilayers are discussed, based on the dislocation mobilities.

8.2 Slip systems in (110) epitaxial layers.

In a strained epilayer the Burgers vector of a misfit dislocation can be divided into three components [19]: (*i*) a screw component b_s, which is parallel to the misfit dislocation line, lying in the interface, (*ii*) an edge component b_r, perpendicular to the growth direction and the line of intersection of the substrate surface and the glide plane, and (*iii*) an edge component b_t in the growth direction, normal to the interface. This is schematically given in fig. 8.1. The component b_r gives rise to strain relaxation, whereas the screw component b_s does not contribute to relaxation. The component of the Burgers vector b_t can cause a misorientation (tilt) of the epitaxial layer [19] and is also responsible for the propagation

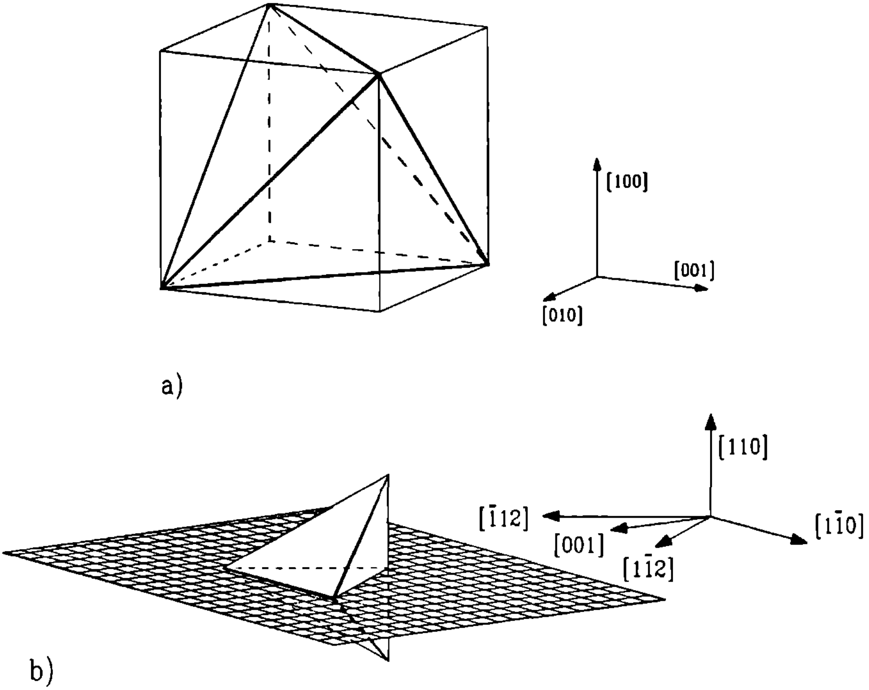

Figure 8.2 Orientation of the {111} planes in the zincblende structure in a) (100) and b) (110) layers. In b) also the four dislocation directions are given.

of the dislocation line from the surface towards the interface. Without this component a dislocation can only glide along planes parallel to the interface. In order to reach the interface in this case the less favourable dislocation climb process is required. Therefore it can be stated that for a good relaxation slip system it is necessary that the Burgers vector at least can be divided into a relaxation and a tilt component.

In (100) epilayers in the zincblende structure, the ⟨110⟩{111} slip systems satisfy this condition. In fig. 8.2a the four {111} glide planes (the tetrahedron planes) are shown. On each of these planes there are possible orientations present for the Burgers vectors (parallel to the edges of the tetrahedron) which possess both the components b_r and b_t.

For (110) epilayers the situation is different. The orientation of the {111} planes with respect to the (110) surface is shown in fig. 8.2b. In this case only two of the four {111} planes are inclined to the surface. The Burgers vectors of misfit dislocations which glide along these two planes can be divided into the three distinguished components. The lines of intersection of the glide planes and the surface are in the $[1\bar{1}0]$ direction. The two other $\{111\}$ glide planes are perpendicular to the (110) surface. In this case none of the possible Burgers vectors has a component b_r and therefore no strain can be released by slip of dislocations along these planes. From this it follows that in (110) oriented epilayers not only $\langle 110\rangle\{111\}$, but also other glide systems are necessary in order to release the misfit stress in other directions.

Hornstra [20] has described nine different dislocation types in the diamond structure with Burgers vector $\frac{a}{2}\langle 110\rangle$, which is the shortest lattice vector allowed as Burgers vector. As is shown by Holt [21] these models may also be applied on dislocations in crystals in the zincblende structure. According to Hornstra [20], the misfit dislocations in the (110) plane can lie along four different directions: $[1\bar{1}0]$, $[1\bar{1}2]$, $[\bar{1}12]$ and $[001]$. By combining each of these dislocation directions with the six possible $\langle 110\rangle$ orientations of the Burgers vectors, 24 glide systems are obtained. In table 8.1 they are classified according to the dislocation types, reported by Hornstra [20]. From this table it becomes clear that only three of these dislocation types, II with $\{111\}$ glide planes, VI with $\{311\}$ glide planes and IX with $\{001\}$ glide planes, may be considered as relaxation slip systems, since in these systems the Burgers vectors both have a relaxation and a tilt component. Slip system II is the system which is commonly observed in relaxed (100) and (111) epilayers. Dislocations of type VI are assumed to be instable in the diamond structure [20], but glide of these dislocations has been observed in (100) oriented horizontal Bridgman (HB)-grown GaAs [22]. Dislocations directed along the [001] axis are also found in GaAs [23], but no discrimination between the types VIII and IX has been made. In the next section a closer analysis of the nucleation and the propagation of the misfit dislocations in these three systems is given.

8.2.1 Nucleation of misfit dislocations in (110) epitaxial layers

In chapter 6, a relaxation mechanism for (100) strained layers in the zincblende structure is proposed [11]. In this model the misfit dislocations are assumed to be semihexagonal. These dislocations nucleate spontaneously at the surface and propagate as V-shaped dislocations through the epitaxial layer. When they have reached the interface, they elongate parallel to the interface, thereby forming a semihexagonal loop. In this section this model is used to describe the relaxation process in (110) strained layers. The projections on the glide planes of the semihexagonal loops of the dislocation types II, VI and IX are shown

Table 8.1 The 24 possible dislocation slip systems in (110) oriented epilayers. The Roman symbols in the first column refer to the dislocation types, reported by Hornstra [20]. β is the angle between the dislocation line and the Burgers vector In the last column the components are given into which the Burgers vector can be divided are indicated.

Dislocation type	Line direction	Burgers vector	β	Glide plane	$b_r + b_s + b_t$
I	$[1\bar{1}0]$	$[1\bar{1}0]$	0°	-	b_s
II	$[1\bar{1}0]$	$[101]$	60°	$(\bar{1}\bar{1}1)$	$b_r + b_s + b_t$
	”	$[10\bar{1}]$	”	(111)	”
	”	$[011]$	”	$(\bar{1}\bar{1}1)$	”
	”	$[01\bar{1}]$	”	(111)	”
III	$[1\bar{1}0]$	$[110]$	90°	(001)	b_t
IV	$[\bar{1}12]$	$[10\bar{1}]$	30°	$(\bar{1}1\bar{1})$	$b_s + b_t$
	”	$[011]$	”	$(\bar{1}1\bar{1})$	”
	$[1\bar{1}2]$	$[101]$	30°	$(1\bar{1}\bar{1})$	$b_s + b_t$
	”	$[01\bar{1}]$	”	$(1\bar{1}\bar{1})$	”
V	$[\bar{1}12]$	$[110]$	90°	$(\bar{1}1\bar{1})$	b_t
	$[1\bar{1}2]$	$[110]$	90°	$(1\bar{1}\bar{1})$	b_t
VI	$[\bar{1}12]$	$[101]$	73.22°	$(13\bar{1})$	$b_r + b_s + b_t$
	”	$[01\bar{1}]$	”	(311)	”
	$[1\bar{1}2]$	$[10\bar{1}]$	73.22°	(131)	$b_r + b_s + b_t$
	”	$[011]$	”	$(31\bar{1})$	”
VII	$[\bar{1}12]$	$[1\bar{1}0]$	54.74°	(110)	$b_r + b_s$
	$[1\bar{1}2]$	$[1\bar{1}0]$	54.74°	(110)	$b_r + b_s$
VIII	$[001]$	$[110]$	90°	$(1\bar{1}0)$	b_t
	”	$[1\bar{1}0]$	”	(110)	b_r
IX	$[001]$	$[011]$	45°	(100)	$b_r + b_s + b_t$
	”	$[01\bar{1}]$	”	(100)	”
	”	$[101]$	”	(010)	”
	”	$[10\bar{1}]$	”	(010)	”

in fig. 8.3. All the segments of the dislocations are along one of the four possible line orientations. The dislocation loop of type II is represented in an extended state, since in {111} glide planes the dislocations are known to dissociate into Shockley partials. No dissociation possibilities exist for the dislocations in other glide systems and therefore they are shown as perfect dislocations. It should be noticed that from the Thompson tetrahedron construction it follows that for relaxation of compressive strain in (110) epilayers the 30° Shockley partial (at the right hand side of fig. 8.3a) is the first partial to nucleate, whereas in (100) layers under compressive stress the 90° is the leading partial [11, 18]. Further, dislocations on {111} glide planes belong either to the As(g) or the Ga(g) type. In (100) epilayers these different dislocation types run along the two different ⟨011⟩ directions [24]. In (110) layers, where only one ⟨011⟩ direction is present at the surface, both types nucleate along this direction, although they glide along different {111} planes. In compressively strained layers As(g) and Ga(g) dislocations glide along (111) and $(\bar{1}\bar{1}1)$

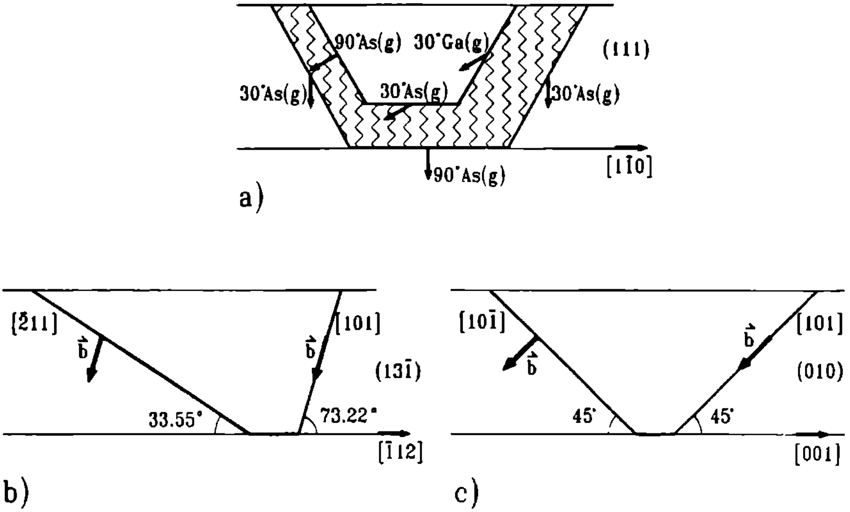

Figure 8.3 Projections of the semihexagonal dislocation loops of a) type II on the (111) plane, b) type VI on the $(13\bar{1})$ plane and c) type IX on the (010) plane. The dislocation of type II is shown in the dissociated state. The dislocations of type VI and IX cannot dissociate into partials and are shown as perfect dislocations. The right hand side of all the dislocation loops is the screw dislocation.

respectively. In layers under tensile stress these dislocation types are interchanged with respect to the glide planes. Since the As(g) dislocations are observed to be the most mobile types and the first dislocations to nucleate, in fig. 8.3a the configuration of a dissociated semihexagonal As(g) dislocation is given.

8.2.2 Critical layer thickness model for (110) epitaxial layers

The critical layer thickness h_c of the strained layers, containing one of the dislocation configurations of fig. 8.3, can be calculated by using the expressions obtained from the equilibrium models for perfect and dissociated dislocations [14], with some adaptations for the (110) geometry. In these models the critical layer thickness of a strained epitaxial layer with a certain lattice mismatch is defined as that thickness at which the line energy of the V-shaped dislocation loop which has just reached the interface equals the strain released by the dislocation loop [7, 14]. For perfect dislocations the expression for the critical layer thickness is given by [14, 25]:

$$h_c = \left\{ \frac{K_1}{\cos\psi_1} + \frac{K_2}{\cos\psi_2} \right\} \frac{b}{4\pi f} \left\{ \ln\left(\frac{\alpha h_c}{b}\right) - 2 \right\} \frac{\cos\psi_1 \cos\psi_2}{\cos\phi \cos\lambda} \left(\frac{2}{\sin\xi}\right) \frac{1}{2\mu} \left(\frac{1-\nu}{1+\nu}\right), \tag{8.1}$$

in which

K_i	the dislocation energy coefficient of dislocation segment i, given by $K_e \sin^2\beta + K_s \cos^2\beta$,
K_e, K_s	the energy coefficients of edge and screw dislocations respectively,
β	the angle between the Burgers vector and the dislocation line,
b	the length of the Burgers vector,
f	the lattice mismatch,
α	the dislocation core parameter,
ψ_i	the angle between the dislocation line i and the growth direction,
ϕ	the angle between the normal to the slip plane and the misfit stress σ, which is perpendicular to the growth direction and to the intersection line of the substrate surface and the glide plane,
λ	the angle between the misfit stress and the Burgers vector,
ξ	the angle between the two segments of the V-shaped loop,
μ	the shear modulus,

ν the Poisson's ratio.

If the crystal is assumed to be isotropic the edge and screw energy coefficients are given by $K_e = \mu/(1-\nu)$ and $K_s = \mu$ [26].

Type II dislocations are dissociated during the relaxation process. Due to the stacking fault area between the partial dislocations, an extra energy term has to be taken into account in the critical thickness calculations. In the (110) geometry the critical thickness relation of the dislocation configuration of type II in the dissociated state is calculated to be given by:

$$h_c = \left((9K_s + 7K_e) \frac{b_p^2}{16\pi} \left\{ \ln\left(\frac{\alpha h_c}{b}\right) - 2 \right\} + (\gamma + \tau b_{pt})(d_{60^\circ} + d_s) \right) \times \frac{\cos\psi}{\cos\phi\cos\lambda} \left(\frac{2}{\sin\xi}\right) \frac{1}{2\mu b f} \left(\frac{1-\nu}{1+\nu}\right), \tag{8.2}$$

in which in addition

b_p	the Burgers vector of the Shockley partials,
γ	the stacking fault energy density,
τ	the shear stress, defined as $\sigma \cos\phi \cos\lambda$ [27],
d_{60° and d_s	the dissociation widths of the 60° and the screw dislocation [11, 14].

Here it should be kept in mind that the dissociation width of the screw dislocation under compressive stress in the (110) geometry is given by the relation for the dissociation width of the screw dislocation under tensile stress in the (100) geometry, due to the orientation of the Burgers vector of the Shockley partials. In table 8.2 for each of the three relaxation slip systems the angles, used in the eqs. 8.1 and 8.2, are given.

8.3 Experimental details

For the determination of the misfit dislocation patterns and the critical layer thickness in the (110) geometry, a number of $In_xGa_{1-x}As$ epitaxial layers have been grown by metalorganic vapour phase epitaxy (MOVPE) on GaAs substrates. The substrates were (110)2°(001) orientated, chromium-doped, semi-insulating (SI), horizontal Bridgman grown (HB) and chemo-mechanically polished on one face.

Table 8.2 Overview of the angles β, ψ, ϕ, λ and ξ, as appearing in eqs (8 1) and (8 2) for the relaxation slip systems II, VI and IX

slip system	β_1	β_2	ψ_1	ψ_2	ϕ	λ	ξ
II	0°	60°	60°	60°	54 74°	45°	60°
VI	0°	73 22°	60°	73 22°	58 52°	35 26°	73 22°
IX	0°	90°	60°	60°	45°	60°	90°

Upon these substrates undoped $In_xGa_{1-x}As$ epitaxial layers have been grown in a low pressure MOVPE reactor. Trimethylgallium (TMG), trimethylindium (TMI) and arsine (AsH_3) have been used as source materials The growth temperature was 923 K The concentration of TMI in the gasphase, relative to the total concentration of group III precursors was between 0 4 % and 2 3% The thicknesses of the epilayers have been measured using a scanning electron microscope (SEM) after cleaving and etching

The indium concentration in the epilayers has been calculated from the lattice constants, determined from high-resolution X-ray diffraction (HRXRD) experiments [28, 29] The indium concentration in completely strained epilayers has also been determined from photoluminescence (PL) spectra The relation between the band gap shift, caused by the misfit stress, and the indium concentration is given by the deformation potential theory [30] The photoluminescence spectra have been recorded at 4K

The morphology of the epilayers has been observed with an interference-contrast (IC) microscope In order to make the misfit dislocations more clearly visible, the samples have been etched with the defect revealing diluted Sirtl-like etch with the use of light (DSL) [31]

8.4 Results and discussion

8.4.1 Morphology

The surface morphologies of the (110) strained layers grown beyond the critical layer thickness can be divided into three groups, which are shown in fig 8 4 In layers which

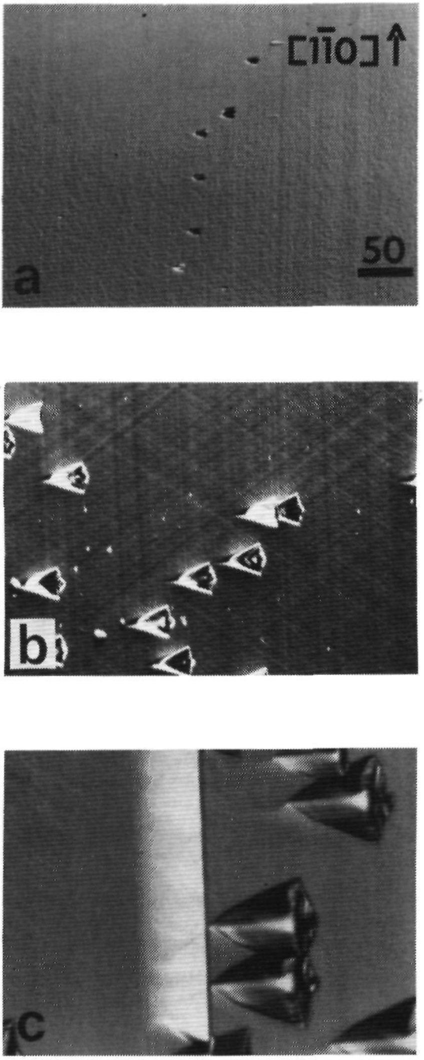

Figure 8.4 Optical micrographs of surface morphologies of $\mathrm{In_{0.012}Ga_{0.988}As}$ epilayers grown on (110) GaAs substrates, with thicknesses of a) 0.6 μm, b) 2.2 μm and c) 3.7 μm. All samples have been DSL treated. The dislocations run parallel to the a) $[1\bar{1}0]$, b) $[1\bar{1}0]$ and $\langle 112 \rangle$. In c) a crack is observed in the $[1\bar{1}0]$ direction. All micrographs show growth hillocks. The bar indicates 50 μm for all the micrographs. The vertical direction is $[1\bar{1}0]$.

are slightly thicker than the critical thickness, the first appearing misfit dislocation lines lie parallel to the $[1\bar{1}0]$ direction, as is shown in fig. 8.4a. Then, at larger thicknesses or higher indium concentrations in the layers, also misfit dislocations are seen along the two $\langle 112 \rangle$ directions parallel to the (110) surface (fig. 8.4b). Finally, for still thicker layers, cracks parallel to the $[1\bar{1}0]$ direction are formed, as is shown in fig. 8.4c. No misfit dislocation lines have been found parallel to the [001] direction.

By comparing these relaxation patterns with the proposed relaxation slip systems in (110) layers, it has been demonstrated that the relaxation process proceeds by the nucleation and propagation of dislocations of the types II and VI. No evidence has been found for relaxation by type IX dislocations.

The formation of cracks may be explained by the presence of partial dislocations along the $[1\bar{1}0]$ direction. The dissociation width of the screw part of the V-shaped dislocation, gliding in the $\{111\}$ plane, (fig. 8.3a) increases with the misfit stress. At high stresses the separation distance of the partials may become as large as the layer thickness [32], resulting in a stacking fault plane throughout the whole epilayer. At high concentrations of these stacking fault planes the stacking fault energy is released by the formation of a crack (fig. 8.4c).

The onset of crack formation was also observed by Hull *et al.* [18], who have demonstrated the presence of stacking faults at the inclined $\{111\}$ planes and 90° Shockley partials at the interface of compressively strained Ge_xSi_{1-x} layers and the Si substrate on cross-sectional transmission electron microscopy (TEM) images.

8.4.2 Critical layer thickness

Once the relaxation slip systems have been determined from the surface morphologies, the experimentally observed critical layer thickness can be compared with the calculated values, as obtained from the equilibrium models. In fig. 8.5 the results of the calculations of the critical layer thickness as a function of the lattice mismatch for the slip systems II, VI and IX are shown. The dislocations in system II are assumed to be dissociated (eq. (8.2)), whereas the dislocations in the other two systems only can be perfect (eq. (8.1)). It is shown that the theory predicts the highest values for the critical layer thicknesses for slip system IX. The curves for the systems II and VI lie very close to each other and are below the curve for system IX.

The experimental results are also shown in fig. 8.5. In this figure the samples on which only dislocation lines in the $[1\bar{1}0]$ direction and those on which in two or more directions dislocation lines have been observed are represented by different symbols. As it

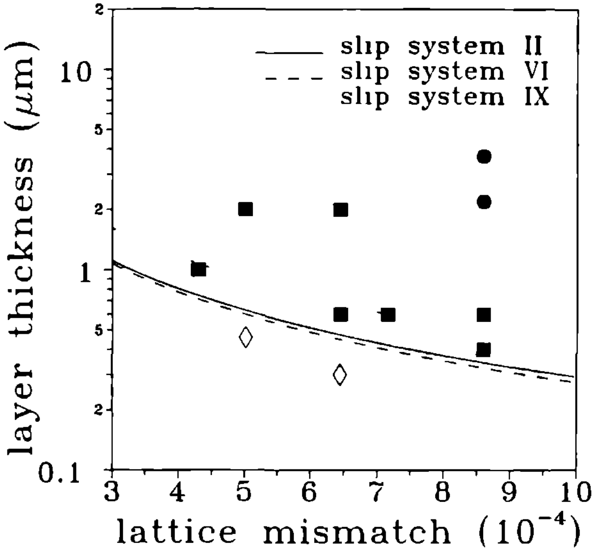

Figure 8.5 Calculated critical layer thickness h_c as a function of the lattice mismatch f for the dislocation loops of the types II, VI and IX. The symbols represent $In_xGa_{1-x}As$ epitaxial layers grown on GaAs. The open diamonds represent epilayers without misfit dislocations, the filled squares represent epilayers with only misfit dislocations in the $[1\bar{1}0]$ direction and the filled circles represent epilayers with misfit dislocations in the $[1\bar{1}0]$ and in the $\langle 112\rangle$ directions

was already mentioned before, the dislocations parallel to the $\langle 112\rangle$ directions are formed at a later stage of the growth process than the $[1\bar{1}0]$ lines.

It appears that the experimentally found critical layer thickness for dislocation lines in the $[1\bar{1}0]$ direction matches well with the theoretical curve for relaxation slip system II. On the other hand, the dislocations along the $\langle 112\rangle$ directions are only seen in samples, grown far beyond the theoretical critical thickness.

These results may be explained by the following arguments. The activation energy of the formation processes [14] of the type II and type VI dislocations as a function of the height h of the dislocation loop are represented in fig 8.6. The lattice mismatch f is taken 7.2×10^{-4}, which corresponds to an indium concentration in the epilayer of 1%. It is demonstrated that, although the two systems nearly have the same critical thickness, the maximum Gibbs free energy for type VI dislocations (11.2 keV, 9.8 eV/nm) is higher

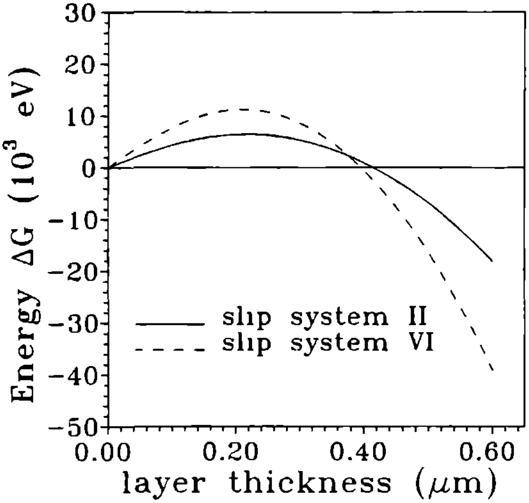

Figure 8.6 Gibbs free energy ΔG of a V-shaped dislocation loop of type II and type VI as a function of the height h of the loop The lattice mismatch f is taken to be 7 2 × 10^{-4}, corresponding to an indium concentration of 1% in the epilayer

than for type II dislocations (6 4 keV, 7 4 eV/nm). From an energetic point of view the nucleation of a dislocation of the latter type is easier.

Furthermore, it is known that dislocations in the ⟨110⟩{111} slip system have high mobilities at the growth temperatures [33] It is also known that the layers in which the relaxation process proceeds by type II dislocations, already obtain their equilibrium state during the growth process [34]. On the other hand, no dislocation mobilities are known for the type VI dislocation in the ⟨110⟩{311} system However, since these dislocations do not have the possibility to dissociate into partials and therefore move in a perfect state, it is assumed that these dislocations have a much lower mobility than type II dislocations From these two arguments it is concluded that the relaxation process by type VI dislocations proceeds in a much lower rate, so that the equilibrium state is not reached during growth, as is also the case in (100) Ge_xSi_{1-x} epilayers [7].

Type VI as well as type IX dislocations can relax the strain perpendicular to the direction of strain relaxation of the type II dislocations Since of those two types the

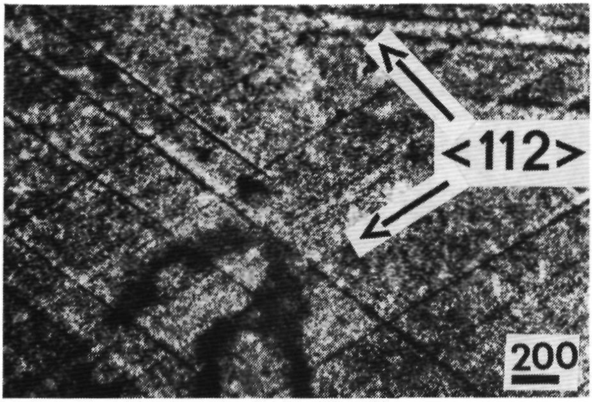

Figure 8.7 Optical micrograph of an (110) diamond epitaxial layer. The cracks are parallel to the ⟨112⟩ directions. The bar indicates 200 μm.

type IX dislocations have the highest critical layer thickness, no nucleation of dislocations along the [001] direction is found.

8.4.3 Comparison with strained Ge_xSi_{1-x} and diamond (110) epitaxial layers

In this section the $In_xGa_{1-x}As$ relaxation patterns are compared with those of Ge_xSi_{1-x} [18] and of flame-deposited diamond epitaxial layers [35]. The results are discussed on the basis of the dislocation mobility. It is known that dislocations in Ge_xSi_{1-x} alloys are less mobile than in GaAs based materials. In diamond the dislocations are assumed to be not mobile at all, at least not at temperatures below 2200 K [36].

In Ge_xSi_{1-x} alloys, Hull *et al.* [18] have only observed misfit dislocations, parallel to the $[1\bar{1}0]$ direction. This is different from the morphology of $In_xGa_{1-x}As$ epilayers, where the misfit dislocations are observed in the $[1\bar{1}0]$ and two ⟨112⟩ directions. From the absence of relaxation along the ⟨112⟩ direction it is concluded that in these layers the mobility of the type VI dislocations is not high enough as is required for the nucleation process.

On (110) flame-deposited diamond homoepitaxial layers [35] cracks are observed along the ⟨112⟩ directions, as shown in fig. 8.7. The origin of these defects may be the misfit stress, resulting from the difference in lattice constant between the flame-deposited layers and the substrate [37]. From transmission optical microscopy observations it was found that the crack planes were the {111} planes which are perpendicular to the (110) surface. These cracks are comparable with the cracks, observed in (111) oriented epitaxial diamond layers, grown by thermal chemical vapour deposition [38]. It is assumed that, because of the low dislocation mobility in diamond, the relaxation process does not proceed by the nucleation of dislocations. It is more likely that the strain in the epilayer is released by cleavage along the {111} planes, since in diamond these are the lattice planes with the lowest cleavage energy [39].

From this discussion, it is concluded that the surface morphology depends strongly on the misfit dislocation mobility.

8.5 Summary and conclusions

The relaxation process in (110) oriented compressively strained epitaxial $In_xGa_{1-x}As$ layers on GaAs is described. From the condition that in a relaxation slip system the Burgers vector at least possesses a relaxation and a tilt component, three possible glide systems have been identified. Two of these three dislocation systems have been observed on (110) epilayers. The relaxation process is started by the formation of misfit dislocations in the $[1\bar{1}0]$ direction, gliding along the {111} planes. At a later stage of the growth process also dislocations are formed along the $\langle 112 \rangle$ directions on the surface. These dislocations glide along the {311} planes. The equilibrium theory, in which the dislocations are assumed to nucleate as V-shaped dislocations at the surface and propagate through the layer, matches well with the experimentally observed critical layer thickness for the $[1\bar{1}0]$ oriented dislocations. The large difference between the theoretically predicted and the experimentally found critical layer thickness for the $\langle 110 \rangle\{311\}$ dislocations (type VI) is explained by the high activation energy of the V-shaped dislocation loop in the {311} planes and the expected low dislocation mobility. From a comparison with strained Ge_xSi_{1-x} and diamond (110) epitaxial layers it is concluded that the relaxation pattern depends strongly on the dislocation mobilities.

Acknowledgement

Dr. W.J.P. van Enckevort is gratefully acknowledged for providing the micrograph of the diamond.

References

[1] G.H. Olsen, M.S. Abrahams and T.J. Zamerowski, J. Electrochem. Soc. **121** (1974) 1650.

[2] W.J. Bartels and W. Nijman, J. Crystal Growth **37** (1977) 204.

[3] A. Gustafsson, M.-E. Pistol, M. Gerling, L. Samuelson, M.R. Leys and H. Titze, J. Appl. Phys. **70** (1991) 1660.

[4] A. Lefebvre, C. Herbeaux and J. Di Persio, Phil. Mag. A **63** (1991) 471.

[5] B.A. Fox and W.A. Jesser, J. Crystal Growth **109** (1991) 252.

[6] P.M.J. Marée, J.C. Barbour, J.F. van der Veen, K.L. Kavanagh, C.W.T. Bulle-Lieuwma and M.P.A. Viegers, J. Appl. Phys. **62** (1987) 4413.

[7] R.H.M. van de Leur, A.J.G. Schellingerhout, F. Tuinstra and J.E. Mooij, J. Appl. Phys. **64** (1988) 3043.

[8] B.W. Dodson, J. Crystal Growth **111** (1991) 376.

[9] Y. Fukuda, Y. Kohama, M. Seki and Y. Ohmachi, Jap. J. Appl. Phys. **28** (1989) L19.

[10] D.C. Houghton, J. Appl. Phys. **70** (1991) 2136.

[11] J. te Nijenhuis, P.J. van der Wel, E.R.H. van Eck and L.J. Giling, J. Appl. Phys., submitted, this thesis, chapter 6.

[12] P.J. van der Wel, J. te Nijenhuis, E.R.H. van Eck and L.J. Giling, Semicond. Sci. Technol. **7** (1992) A63, this thesis, chapter 5.

[13] B.A. Fox and W.A. Jesser, J. Appl. Phys. **68** (1990) 2739.

[14] J. te Nijenhuis, H.F.J.M. van Well, M.M.G. Bongers and L.J. Giling, J. Appl. Phys., submitted, this thesis, chapter 7.

[15] T. Anan, K. Nishi and S. Sugou, Appl. Phys. Lett. **60** (1992) 3159.

[16] D.B. Holt, J. Phys. Chem. Solids **27** (1966) 1053.

[17] A. Gustafsson, M.-E. Pistol, M. Gerling, L. Samuelson and H. Titze, J. Appl. Phys. **70** (1991) 1667.

[18] R. Hull, J.C. Bean, L. Peticolas and D. Bahnck, Appl. Phys. Lett. **59** (1991) 964.

[19] G.H. Olsen, J. Crystal Growth **31** (1975) 223.

[20] J. Hornstra, J. Phys. Chem. Solids **5** (1958) 129.

[21] D.B. Holt, J. Phys. Chem. Solids **23** (1962) 1353.

[22] J.L. Weyher and L.J. Giling, in: Defect Recognition and Image Processing in III-V Compounds, Ed. J.P. Fillard (Elsevier, Amsterdam, 1985) p.63.

[23] J.L. Weyher and J. van de Ven, J. Crystal Growth **78** (1986) 191.

[24] M.S. Abrahams, J. Blanc and C.J. Buiocchi, Appl. Phys. Lett. **21** (1972) 185.

[25] Y. Fukuda, Y. Kohama and Y. Ohmachi, Jap. J. Appl. Phys. **29** (1990) L20.

[26] J.P. Hirth and J. Lothe, Theory of dislocations, 2nd. ed. (Wiley, New York, 1982).

[27] See *e.g.* D. Hull and D.J. Bacon, Introduction to dislocations, 3rd. ed. (Pergamon Press, Oxford, 1984).

[28] W J Bartels, J Vacuum Sci Technol **B1** (1983) 338

[29] J Hornstra and W J Bartels, J Crystal Growth **44** (1978) 513

[30] See *e g* F H Pollak, in Semiconductors and Semimetals, Eds R K Willardson and A C Beer, Vol 32, Strained-Layer Superlattices Physics, Vol Ed T P Pearsall, Ch 2

[31] J L Weyher and J van de Ven, J Crystal Growth **63** (1983) 285

[32] Y Androussi, G Vanderschaeve and A Lefebvre, Phil Mag A **59** (1989) 1189

[33] H Steinhardt and P Haasen, Phys Stat Sol (a) **49** (1978) 93

[34] J te Nijenhuis, P J van der Wel, R W F van Asten, P R Hageman and L J Giling, J Cryst Growth **107** (1991) 496, this thesis, chapter 4

[35] J J Schermer and G Janssen, unpublished results

[36] J Evans and R K Wild, Phil Mag **12** (1965) 479

[37] L M Hanssen, W A Carrington, J E Butler and K A Snail, Mater Lett **7** (1988) 289

[38] W J P van Enckevort, G Janssen, W Vollenberg, M Chermin, L J Giling and M Seal, Surface and Coatings Technology **47** (1991) 39

[39] J E Field, The properties of diamond (Academic Press, London,1979)

General conclusions

The growth of epitaxial layers in the $In_xGa_{1-x}As/GaAs$ system by metalorganic vapour phase epitaxy and the relaxation of strained layers under compressive and tensile stress have been investigated.

Growth by MOVPE of $In_xGa_{1-x}As$ epitaxial layers at misoriented surfaces is found to be dependent on the dangling bond configuration of the steps. At steps which are kinked according to the PBC-theory the incorporation of indium is found to be more efficient than at stable steps.

The system $In_xGa_{1-x}As/GaAs$ is very well suited to study relaxation in thin epitaxial layers, since it appeared that the mobility of the dislocations at the growth temperatures (*ca.* 900 K) is high enough to obtain the equilibrium configuration of elastic and plastic deformation already during the growth process. This is in contrast to the system $Si_{1-x}Ge_x/Si$, in which the relaxation process proceeds in a much lower rate. In this system post-growth annealing is necessary to obtain the equilibrium configuration, whereas it has been shown that in the $In_xGa_{1-x}As/GaAs$ system the residual strain is hardly changed by annealing. The strain in a layer will be relaxed, until it has reached the value of the lattice mismatch for which the thickness of the layer is critical. Therefore in this system the curve, which gives the critical layer thickness as a function of the lattice mismatch, can also be considered as a critical-strain-thickness curve.

Misfit dislocations in (100) oriented layers are mainly 60° $\langle 110\rangle\{111\}$ As(g) and Ga(g) dislocations. The direction of the As(g) and the Ga(g) types depends on the stress type (tensile or compressive).

A difference in opto-electronic behaviour between As(g) and Ga(g) dislocations is revealed by photoluminescence imaging and defect selective etching. It appears that the As(g) and the Ga(g) act like donors and acceptors respectively. This difference originates from the difference in the dislocation core configuration. The results are in agreement with the theoretical considerations on dislocation cores in GaAs described in the literature.

A difference in the mobilities of the As(g) and the Ga(g) dislocations gives rise to asymmetric dislocation patterns on layers grown under tensile stress at relatively low growth temperatures. The As(g) dislocations are the most mobile dislocations and nucleate first to form misfit dislocations. At higher growth temperatures (*ca.* 970 K) the Ga(g) dislocations are mobile enough to nucleate and propagate toward the interface. The dislocation patterns are symmetric on layers grown at these temperatures. Compressively strained layers do not show morphological asymmetry.

The model for the relaxation mechanism, in which it is assumed that misfit dislocations nucleate as dissociated V-shaped dislocations at the surface, gives a good description of the observed relaxation phenomena in layers under tensile and compressive stress. Nucleation of V-shaped dislocations is more realistic than nucleation of semicircular dislocation half loops, since the dislocations tend to form long straight dislocations in the Peierls valleys along the $\langle 110 \rangle$ directions. It has been shown that cross slip of the screw part of the V-shaped dislocation from one $\{111\}$ glide plane to another is only possible in compressively strained layers. This model explains that the asymmetric relaxation pattern in layers under tensile stress is caused by (*i*) the low mobility of the Ga(g) dislocations and (*ii*) the absence of cross-slip possibilities for the As(g) dislocations. Hillock growth on these layers at low growth temperatures is explained by the formation of sessile Frank dislocations.

The critical layer thickness model which is derived from this description of the relaxation process, gives a good description of the observed transition from coherent to incoherent growth, both in layers under tensile and compressive stress.

During relaxation of (110) oriented strained layers two dislocation glide systems are active. The relaxation is started by the nucleation of $\langle 110 \rangle \{111\}$ dislocations along the $[1\bar{1}0]$ direction. In thicker layers also $\langle 110 \rangle \{311\}$ dislocations along the $\langle 112 \rangle$ directions are observed. The critical layers thickness theory in which the dislocations are assumed to nucleate as V-shaped dislocations gives a good description of the experimentally found critical thickness in the case of $\langle 110 \rangle \{111\}$ dislocations. The large difference between the theoretical and experimentally observed critical layer thickness for $\langle 110 \rangle \{311\}$ dislocations is due to the high activation energy and the low dislocation mobility of these dislocations.

Summary

In this thesis the growth of heteroepitaxial strained layers of III-V semiconductors from the vapour phase and their relaxation is described. As a result of the lattice mismatch, caused by the difference in lattice constant between the substrate and the epitaxial layer, a mechanical stress in the layer is present This stress will be relaxed by the formation of misfit dislocations at the interface between the substrate and the epitaxial layer, if the elastic energy, stored in the layer, exceeds a certain critical value This critical value is determined by the geometry of the formation process of the dislocations, the thickness of the epitaxial layer and the lattice mismatch. In this study the growth of $In_xGa_{1-x}As$ epitaxial layers on GaAs substrates with different (mis-)orientations and the formation processes of misfit dislocations in epitaxial layers of GaAs under tensile stress and of $In_xGa_{1-x}As$ under compressive stress are investigated.

In chapter 1 an introduction is given on the growth of III-V semiconductors from the vapour phase by Metalorganic Vapour Phase Epitaxy (MOVPE) and on the relaxation of strained layers by the formation of misfit dislocations.

In the chapters 2 and 3 the influence of the direction of the misorientation of the substrate on the amount of silicon and indium incorporated during the growth of GaAs is discussed Silicon is incorporated on both the group III and the group V sublattice sites at the monatomic steps at the surface, whereas indium is only incorporated at the group III sublattice sites. The experimentally found trends are explained by considering the reconstruction possibilities under arsenic rich conditions in the gas phase at the steps and the incorporation possibilities of silicon and indium thereon. It appears that the incorporation of silicon and indium on the group III sublattice sites is higher at the fully kinked steps than at the stable steps at the (100) surface On the (111)A surface no difference in incorporation of silicon on the fully kinked and on the stable steps is observed, whereas for indium a higher incorporation at the fully kinked steps is observed From this it appears that the incorporation possibilities for silicon on the group III and on the group V sublattice sites at both the steps are the same.

In chapter 4 the relaxation of (100) oriented GaAs epitaxial layers grown under tensile stress on $In_xGa_{1-x}As$ substrates is studied. The experimentally observed critical layer thickness for the formation of misfit dislocations appears to match well with theoretical calculations of the change of the Gibbs free energy of an epitaxial layer, in which a dislocation half loop is nucleated, which has released a certain amount of elastic energy It further appears that the mechanical stress in the layer is not released completely The residual stress in the layer is determined by the equilibrium between the amount of energy,

necessary for the formation of a dislocation half loop, and the residual elastic energy

In chapter 5 the opto-electronic behaviour of misfit dislocations in (100) oriented epitaxial layers under compressive as well as under tensile stress is investigated In both the systems dislocation lines along the ⟨011⟩ directions are observed Using spatially resolved photoluminescence the presence of many non-radiative deep levels along the dislocation lines is shown The opto-electronic asymmetry of the dislocations along the two different ⟨011⟩ directions, observed both on photoluminescence mappings and on photo-etch patterns, is explained from the differences in composition of the core of the dislocations, causing a different depletion behaviour

In chapter 6 a closer analysis of the relaxation mechanism in (100) oriented epitaxial layers under tensile as well as under compressive stress by the formation of misfit dislocations is given In epitaxial layers under tensile stress in the first instance only dislocations along the $[01\bar{1}]$ direction are observed, whereas in layers under compressive stress dislocations along the $[01\bar{1}]$ as well as along the [011] direction are observed It appears that the difference in mobilities between the As(g) (arsenic glide) and the Ga(g) (gallium glide) dislocations is the origin of this asymmetry The As(g) dislocations are the first to appear due to their higher mobilities The dislocations move in an extended state through the layer It appears that the cross-slip process is only possible in layers under compressive stress, so only in these layers dislocations in two directions are observed From energetic considerations it is shown that the cross-slip process proceeds most easily by the formation of stair-rod dislocations In layers under tensile stress a sessile Frank dislocation can be formed by the cross-slip process, leading to the formation of growth hillocks At higher growth temperatures the dislocation patterns becomes symmetric, due to the higher mobility of the Ga(g) dislocations

In chapter 7 a model for the calculation of the critical layer thickness for the formation of misfit dislocations is derived from the relaxation mechanism described in chapter 6 In this model the Gibbs free energy of a completely elastically deformed epitaxial layer is balanced with that of an epitaxial layer, in which a misfit dislocation is nucleated, thereby releasing a certain amount of elastic energy The model is compared with experimental observations of the formation of misfit dislocations in both layers under tensile and under compressive stress and with other equilibrium models, described in the literature It appears that a good description of the critical layer thickness is given by the models in which the dislocations are assumed to nucleate as semicircular or as dissociated V-shaped dislocations Energetic and kinetic considerations have shown that the latter model is to be preferred

In chapter 8 the relaxation of (110) oriented epitaxial layers under compressive stress is investigated Of the three theoretically possible misfit dislocation types only two have been observed, in the $[1\bar{1}0]$ and in the $\langle 112 \rangle$ directions The equilibrium model, derived in chapter 7, gives a good description of the critical layer thickness for the formation of dislocations along the $[1\bar{1}0]$ direction The discrepancy between the theory and the observations of the dislocations in the $\langle 112 \rangle$ directions is explained by the low mobility and the high activation energy for the formation of the misfit dislocations in the $\langle 112 \rangle$ directions

In general it can be concluded that the model for the formation and propogation of dissociated hexagonal half loop misfit dislocations gives a good description of the relaxation processes in (100) and (110) oriented strained layers

Samenvatting

In dit proefschrift worden de groei van heteroëpitaxiale dunne lagen van III-V halfgeleiders vanuit de gasfase en de relaxatie ervan beschreven. Ten gevolge van de roostermispassing, veroorzaakt door een verschil in roosterconstante tussen het substraat en de epitaxiale laag, ontstaat er in de epilagen een mechanische spanning. Deze spanning wordt gerelaxeerd door middel van de vorming van mispassingsdislocaties (Eng: *misfit dislocations*) in het grensvlak tussen het substraat en de epitaxiale laag, wanneer de in de laag opgeslagen elastische energie een bepaalde kritische waarde overschrijdt. Deze kritische waarde wordt bepaald door de geometrie van het vormingsproces van de dislocatie, de dikte van de epitaxiale laag en de roostermispassing. In dit onderzoek is aandacht besteed aan de groei van $In_xGa_{1-x}As$ epitaxiale lagen op GaAs substraten met verschillende (mis-) oriëntaties en aan het vormingsproces van mispassingsdislocaties in epitaxiale lagen van GaAs onder trekspanning en van $In_xGa_{1-x}As$ onder drukspanning.

In hoofdstuk 1 wordt een inleiding gegeven op de groei van III-V halfgeleiders vanuit de gasfase door middel van Metaalorganische Gasfase Epitaxie (Eng: *Metal-organic Vapour Phase Epitaxy*) en op de relaxatie van *strained layers* door middel van de vorming van mispassingsdislocaties.

In de hoofdstukken 2 en 3 komt de invloed van de richting van de misoriëntatie van het substraat op de hoeveelheid silicium en indium die ingebouwd worden gedurende de groei van GaAs aan de orde. De inbouw van silicium vindt plaats op de groep III en de groep V roosterplaatsen aan monatomaire stappen op het oppervlak, terwijl indium alleen op de groep III roosterplaatsen ingebouwd wordt. De gevonden tendensen kunnen verklaard worden door de reconstructiemogelijkheden onder arseenrijke condities in de gasfase aan de stappen en de inbouwmogelijkheden van silicium en indium daaraan te beschouwen. Het blijkt dat de inbouw van silicium en indium op de groep III roosterplaatsen hoger is aan de volledige gekinkte stappen dan aan de stabiele stappen op het (100) oppervlak. Op het (111)A oppervlak wordt geen verschil in inbouw van silicium aan de volledig gekinkte en aan de stabiele stappen waargenomen, terwijl voor indium juist wel een verhoogde inbouw aan de volledig gekinkte stappen wordt gemeten. Hieruit blijkt dat de inbouwmogelijkheden voor silicium op de groep III en de groep V roosterplaatsen aan beide stappen hetzelfde zijn.

In hoofdstuk 4 wordt de relaxatie van (100) georiënteerde GaAs epitaxiale lagen gegroeid onder trekspanning op $In_xGa_{1-x}As$ substraten behandeld. De experimenteel bepaalde kritische laagdikte voor de vorming van mispassingsdislocaties blijkt goed beschreven te worden door de theoretische berekeningen voor de verandering van de

Gibbs vrije energie van een epitaxiale laag waarin zich een halve dislocatielus heeft gevormd, die een bepaalde hoeveelheid elastische energie heeft vrijgelaten. Het blijkt dat de mechanische spanning in de laag niet volledig wordt gerelaxeerd. De restspanning in de laag wordt bepaald door het evenwicht tussen de benodigde hoeveelheid energie om een halve dislocatielus in de epitaxiale laag te vormen en de resterende hoeveelheid elastische energie.

In hoofdstuk 5 wordt het opto-elektronische gedrag van mispassingdislocaties in (100) georiënteerde epitaxiale lagen zowel onder druk- als onder trekspanning beschreven. In beide systemen zijn dislocatielijnen in de $\langle 011 \rangle$ richtingen waargenomen. Met behulp van plaatsopgeloste fotoluminescentie is de aanwezigheid van veel diepe, niet-stralende, niveaux langs de dislocatielijnen aangetoond. De opto-elektronische asymmetrie van de dislocaties in de twee verschillende $\langle 011 \rangle$ richtingen, die zowel met behulp van fotoluminescentie als met behulp van fotoëtsen wordt waargenomen, is verklaard uit de verschillen in samenstelling van de kern van de dislocaties, die een verschillend depletiegedrag veroorzaken.

In hoofdstuk 6 wordt het relaxatiemechanisme in (100) georiënteerde epitaxiale lagen onder druk- en trekspanning door middel van de vorming van mispassingsdislocaties nader bestudeerd. In epitaxiale lagen onder trekspanning worden in eerste instantie slechts dislocaties in de $[01\bar{1}]$ richting waargenomen, terwijl in lagen onder drukspanning zowel in de $[011]$- als in de $[01\bar{1}]$ richting dislocaties worden gezien. Het blijkt dat het verschil in mobiliteiten tussen de As(g) (arsenic glide) dislocaties en de Ga(g) (gallium glide) dislocaties verantwoordelijk is voor deze asymmetrie. Door de hogere mobiliteit van de As(g) dislocaties zullen deze het eerst verschijnen. De dislocaties bewegen zich gesplitst in Shockley partiëlen door de laag. Het blijkt dat het *cross-slip* proces is alleen mogelijk in lagen onder drukspanning, zodat slechts in deze lagen in twee richtingen mispassingsdislocaties worden waargenomen. Uit energetische beschouwingen blijkt dat het *cross-slip* proces het eenvoudigst verloopt via de vorming van *stair-rod* dislocaties. In lagen onder trekspanning kan door middel van het *cross-slip* proces een (niet mobiele) Frank dislocatie gevormd worden, wat aanleiding geeft tot de vorming van groeiheuvels. Bij hogere groeitemperaturen wordt het dislocatie patroon symmetrisch door de hogere mobiliteit van de Ga(g) dislocaties.

In hoofdstuk 7 wordt aan de hand van het in hoofdstuk 6 beschreven model voor de nucleatie van mispassingsdislocaties aan het oppervlak een model voor de berekening voor de kritische laagdikte afgeleid. In dit model wordt de Gibbs vrije energie van een volledig elastisch gedeformeerde epitaxiale laag vergeleken met die van een epitaxiale laag waarin zich een mispassingsdislocatie gevormd heeft, waarbij een bepaalde hoeveelheid elastische energie is vrijgekomen Het model is vergeleken met experimentele waarnemingen van dislocatievorming in zowel lagen onder druk- als onder trekspanning en met andere evenwichtsmodellen, eerder beschreven in de literatuur Het blijkt dat een goede beschrijving van de kritische laagdikte wordt gegeven door de modellen waarin wordt aangenomen dat de dislocaties nucleeren als halfcirkelvormige en als gesplitste V-vormige dislocaties Energetische en kinetische beschouwingen maken duidelijk dat het laatstgenoemde model de voorkeur verdient.

In hoofdstuk 8 wordt een studie naar de relaxatie van (110) georienteerde lagen onder drukspanning beschreven. Van de drie theoretisch mogelijke mispassingsdislocatietypes worden er twee waargenomen, in de $[1\bar{1}0]$- en in de $\langle 112\rangle$-richtingen Het in hoofdstuk 7 afgeleide evenwichtsmodel blijkt een goede beschrijving te geven voor de kritische laagdikte voor de vorming van dislocaties in de $[1\bar{1}0]$-richting De discrepantie tussen theorie en waarnemingen voor dislocaties in de $\langle 112\rangle$-richtingen wordt verklaard door de lage mobiliteit en de hoge activeringsenergie voor de vorming van de dislocaties in de $\langle 112\rangle$-richtingen

Tot slot kan geconcludeerd worden dat het model dat de nucleatie en beweging van gedissocieerde hexagonale halve-lusvormige mispassingsdislocaties een goede beschrijving geeft van de relaxatie processen in (100) en (110) georienteerde *strained layers*

Curriculum Vitae

Johannes te Nijenhuis
Geboren op 5 april 1964 te 's-Gravenhage

1976 - 1982 VWO, Christelijke Scholengemeenschap "Melanchthon" te Rotterdam.

1982 - 1987 Studie Technische Natuurkunde aan de Technische Universiteit te Delft.
Propaedeutisch examen : 28 februari 1984.
Doctoraal examen : 26 mei 1987.
Afstudeerrichting: Vaste Stof, Fysische Kristallografie.

1987 - 1991 Als Onderzoeker in Opleiding (OIO) in dienst van de Stichting voor Fundamenteel Onderzoek der Materie (FOM), werkgemeenschap Halfgeleiders, werkzaam op de afdeling Vaste Stof Fysica III van de Faculteit Natuurwetenschappen van de Katholieke Universiteit te Nijmegen.
Thema onderzoek: Defectstudies aan vanuit de gasfase gegroeide III-V halfgeleiders.

1992 - heden Als toegevoegd onderzoeker in dienst van de Technische Universiteit te Delft, werkzaam in de vakgroep Fysica en Chemie van de Materiaalkunde van de Faculteit der Scheikundige Technologie en der Materiaalkunde.

Stellingen

I

De door Gustafsson *et al.* gegeven verklaring voor de ongelijke dichtheid van de mispassingsdislocaties langs de $\langle 110 \rangle$ richtingen in een (111)B georienteerde GaAsP epitaxiale laag onder trekspanning berust op een verkeerde interpretatie van de kristalstructuur van deze laag.
A. Gustafsson, M.-E. Pistol, M. Gerling, L. Samuelson and H. Titze, J. Appl. Phys. 70 (1991) 1667.

II

Het relaxatieproces in *strained layers* in de zinkblendestructuur kan beschreven worden aan de hand van de vorming en beweging van V-vormige dislocaties, waarvan het 60° segment zowel voor de relaxatie van de spanning in de laag als voor de uitbreiding van de dislocatie zorgt.
Dit proefschrift.

III

In het model voor de berekening van de kritische laagdikte van Marée *et al.* wordt ten onrechte de maximale vormingsenergie van een halfcirkelvormige dislocatie vergeleken met de elastische-energiedichtheid van de epitaxiale laag
P.M.J. Marée, J.C Barbour, J F van der Veen, K L Kavanagh, C W.T. Bulle-Lieuwma and M.P.A. Viegers, J. Appl. Phys 62 (1987) 4413,
dit proefschrift.

IV

De misoriëntatie tussen een monokristallijn saffieren substraat en de daarop opgedampte epitaxiale niobium-, vanadium- en tantaallagen kan verklaard worden uit de aanwezigheid van mispassingsdislocaties aan het grensvlak, waarvan de burgersvector een component evenwijdig aan de groeirichting bezit.
R.H M. van de Leur, Artificial superlattices, proefschrift Technische Universiteit Delft, 1988.

V

Bij de met behulp van röntgendiffractie bepaalde spanning in polykristallijne dunne lagen dienen de gebruikte waardes voor de röntgenelastische constanten vermeld te worden

VI

De elastische spanning in een epitaxiale laag met een dikte boven de kritische laagdikte zal gerelaxeerd worden door middel van de vorming van dislocaties totdat in de laag een dislocatieconfiguratie aanwezig is, waarbij de hoeveelheid energie die benodigd is voor de vorming van een volgende dislocatie in evenwicht is met de hoeveelheid elastische energie die hierbij vrijkomt In het geval dat de vorming van nieuwe dislocaties nog niet gehinderd wordt door de al aanwezige dislocaties, geeft het model voor de berekening van de kritische laagdikte een goede beschrijving van het verband tussen de dikte van de epitaxiale laag en de erin resterende rek
Dit proefschrift.

VII

Gasfasedepositie van III-V halfgeleiders behoort tot het "pointilisme" van de kristalgroei

VIII

Gegeven het feit dat de ångström geen SI-eenheid is, dient het gebruik ervan vermeden te worden
R.J Bolt, Nijmegen, 16 november 1992

IX

De uitspraken van religieuze aard tijdens de promotieplechtigheid van de Katholieke Universiteit Nijmegen, winnen aan betekenis, als ze alleen op verzoek van de betrokkenen in de plechtigheid worden opgenomen

X

Het omslaan van de kosten van de ontslaguitkering voor uit dienst getreden onderzoekers in opleiding (OiO's) over de betrokken werkgroepen komt niet overeen met de opvatting van deze voorziening als collectieve verzekering

J te Nijenhuis,
9 februari 1993